UNIVERSITY CAMPUS BIO-MEDICO

DEPARTMENT OF ENGINEERING

UNIT OF COMPUTER SYSTEMS AND BIOINFORMATICS

DIRECTOR: PROF. GIULIO IANNELLO

Signal Processing techniques and brain imaging in TMS EEG signals

Dissertation for the Doctoral Degree in Biomedical Engineering

XXVIII Edition Year 2013

Sara Petrichella

Rome, 14/12/2015

Academic dissertation

Signal Processing techniques and brain imaging in TMS EEG signals

Author: **Eng. Sara Petrichella**
Department of Engineering
Unit of Computer Systems and Bioinformatics
University Campus Bio-Medico
Rome, Italy

Co-Tutor: **Dr. Florinda Ferreri**
Department of Medicine
Unit of Neurology, Neurophysiology, Neurobiology
University Campus Bio-Medico
Rome, Italy

Co-Tutor: **Prof. Bin He**
Department of Biomedical Engineering
University of Minnesota
Minneapolis, Minnesota

Tutor: **Prof. Luca Vollero**
Department of Engineering
Unit of Computer Systems and Bioinformatics
University Campus Bio-Medico
Rome, Italy

Preliminary examiners: **Dr. Sara Maatta**
Department of Clinical Neurophysiology,
Kuopio University Hospital,
University of Eastern Finland,
Kuopio, Finland

Dr. Filippo Zappasodi,
Dipartimento di Neuroscienze, Imaging e Scienze Cliniche,
Università degli Studi G. D'Annunzio,
Chieti - Pescara,

Index

3 TMS and TMS EEG: Clinical applications and experimental studies

Acronyms

TMS	Transcranial Magnetic Stimulation
EEG	Electroencephalography
EMG	Electromiography
MEP	Motor Evoked Potential
TEPs	Transcranial Evoked Potentials
VLo	Ventral lateral nucleus pars oralis
SMA	Supplementary Motor Area
M1	Motor Area
S2	Secondary somatosensory areas
PV	Parietal ventral somatosensory areas
PET	Postron Emission Tomography
fMRI	Funtional Magnetic Resonance Image
rTMS	Repetitive Transcranial Magnetic Stimulation
NIRS	Near Infrared Spettroscopy
MRS	Magnetic Resonance Spettorscopy
rCBF	Regional Cerebral Blood
CMRglc	Cerebral Metabolic Rate for Glucose
BOLD	Blood Oxygen level Dependent Contrast
tDCS	Transcranial Direct Current Stimulation
MEG	Magnetoencephalography
CC	Corpus Callosum
FA	Fractional Anisotropy
DTI	Diffusion Tensor Imaging
EP	Evoked Potential

LTP	Long Term Potentiation
AD	Alzheimer's Disease
PD	Parkinson's Disease
MCI	Mild Cognitive Impairment
FDI	First Dorsal Interosseous
ppTMS	Paired Pulse TMS
IHI	Interhemispheric Balance
FES	Functional Electric Stimulation
BMI	Brain Machine Interface
ERP	Event Related Potential
ICA	Indipendent Compenent Analysis
PCA	Principal Component Analysis
CAW	Classification and Weight Method
CAD	Classifiction and Dropping Method
EA	Ensemble Averaging
ERA	Event Related Activity
ECG	Electrocardiography
RMT	Resting Motor Threshold
DBS	Deep Brain Stimulation
FEM	Finite Element Model
BA	Brodmann Area
NIBS	Non Invasive Brain Stimulation
MVAAR	Multivariate Adaptive Autoregressive Model
DTF	Directed Transfer Function
SBC	Schwarz Bayesian Criterion
RLS	Recursive least Squares
ADTF	Adaptive Directed Transfer Function

GMFP	Global Mean Field Power
PCI	Perturbational Complexity Index
TSE	Temporal Spectral Evolution
ERSP	Event Related Spectral Perturbation
ITC	Inter-trial Coherence
CT	Computed Tomography
ADM	Abductor Digiti Minimi
MT	Motor Threshold
TS	Test Stimulus
ISI	Interstimulus Interval
ICF	Intracortical Faciliation
CSP	Cortico Spinal Period
CS	Conditioning Stimulus
ECD	Extensor digitorum Communis
LH	Left Hemisphere
RH	Right Hemisphere
MMSE	Mini Mental State Examination
SIVD	Subcortical Ischemic Vascular Dementia
MRC	Medical Resarch Council
MDB	Mental Deterioration Battery
CO	Controls
PPI	Presentpain Scale
VAS	Pain visual Analogue Scale
GEE	General Estimated Equations
VOI	Volume of Interest

Acknowledgments

I would like to thank Professor Giulio Iannello for the opportunity he gave me in starting this experience of work and professional growth in the Computer Systems and Bioinformatics Laboratory at University of Campus Bio-Medico. I also would like to thank my advisor Prof. Luca Vollero for the extraordinary availability and useful advices. I would like to acknowledgment Dr. Florinda Ferreri for all the scientific insights she gave me in these years. I also would like to thank Dr. Andrea Guerra for the useful collaboration. A special acknowledgment goes to all the group of Neurologists of the University of Campus Bio-Medico because with their great efforts in the research field they showed me that it is possible to provide better life's conditions for patients. I also thank all the PhD students that worked with me in the Laboratory in these years: Roberto D'Ambrosio, Leonardo Onofri, Ludovica Acciai, Ermanno Cordelli and Mario Merone.

It was an honour and my great pleasure to have spent an year as Visiting PhD Student in the Department of Biomedical Engineering at University of Minnesota under the supervision of Prof. Bin He. I would like to thank Prof. Bin He for supervising a part of my graduate studies and for immersing me into the world of multimodal assessment of brain imaging. I also like to thank all the Biomedical Functional Imaging and Neuroengineering Laboratory's members Nessa Johnson, Bryan Baxter, Chris Cline, Brad Edelman, Abhrajeet Roy, Abbas Sohrabpour, Huishi (Clara) Zhang, Ting Yang, Yicun (Eason) Wang, Long Yu, Kai Yu, Michelle Case, Jiaen Liu, Xiaotong Zhang, James Stieger, Jianjun (Steve) Meng for friendship and collaboration.

I would like to thank the reviewers for the valuable comments Dr. Sara Maatta and Dr. Filippo Zappasodi. I also thank all the coauthors for the precious scientific contributions.

My special acknowledgment goes to my family for support and to my friends and brothers and sisters in faith for being part of my life.

To my uncle Eraldo

List of publications:

Petrichella Sara, Johnson Nessa, He Bin, "The Influence of Corticospinal Activity on TMS-Evoked Activity and Connectivity in Healthy Subjects: A TMS-EEG Study''. *Plos One*, 2017.

Ferreri, F., Vecchio, F., Vollero, L., Guerra, A., **Petrichella, S.**, Ponzo, D., Määttä, S., Mervaala E., Könönen, M., Ursini F., Pasqualetti P., Iannello G., Rossini P.M., & Di Lazzaro V., (2016). Sensorimotor cortex excitability and connectivity in Alzheimer's disease: A TMS-EEG Co-registration study. *Human brain mapping*. 37:2083–2096

Vollero, Luca, **Sara Petrichella**, and Giulio Innello. "Optimal weighted averaging of event related activity from acquisitions with artifacts." *38th Annual International Conference of the IEEE Engineering in Medicine and Biology Society (EMBC'16)*, Orlando, Florida, USA on August 17-20.

Guerra, Andrea, **Sara Petrichella**, Luca Vollero, David Ponzo, Patrizio Pasqualetti, Sara Määttä, Esa Mervaala, Mervi Könönen; Federica Bressi; Giulio Iannello, Paolo Maria Rossini, Florinda Ferreri. "Neurophysiological features of motor cortex excitability and plasticity in Subcortical Ischemic Vascular Dementia: a TMS mapping study." *Clinical Neurophysiology* (2014).

Ferreri F., D. Ponzo, L. Vollero, Guerra, A, G. Di Pino, **S. Petrichella**, A. Benvenuto, M. Tombini, L. Rossini, L. Denaro, S. Micera, G. Iannello, E. Guglielmelli, V. Denaro, P.M. Rossini. "Does an intraneural interface short-term implant for robotic hand control modulate sensorimotor cortical integration? An EEG-TMS co-registration study on a human amputee." *Restorative neurology and neuroscience* 32, no. 2 (2014): 281-292.

Petrichella, **Sara**, Luca Vollero, Florinda Ferreri, Vincenzo Di Lazzaro, and Giulio Iannello. "TRS-TMS: An EEGLAB plugin for the reconstruction of onsets in EEG-TMS datasets." In *Bioinformatics and Bioengineering (BIBE), 2013 IEEE 13th International Conference on*, pp. 1-4. IEEE, 2013.

Petrichella S., Vollero L., Ferreri F., Guerra A., Määtta, S., Könönen M., Di Lazzaro V., Iannello G., Channel interpolation in TMS EEG: a quantitative study towards an accurate topographical representation, *38th Annual International Conference of the IEEE Engineering in Medicine and Biology Society (EMBC'16)*, Orlando, Florida, USA on August 17-20.

Guerra, A., G. Curcio, P. Pasqualetti, F. Bressi, **S. Petrichella**, F. Scrascia, D. Ponzo, M. Könönen, F. Bressi, G. Iannello, P. M. Rossini, F. Ferreri. "Unilateral cortical hyperexcitability in congenital hydrocephalus: A TMS study." *Neurocase* 20, no. 4 (2014): 456-465.

Introduction

Transcranial magnetic stimulation (TMS) is a unique tool that utilizes magnetic fluxes to noninvasively stimulate the human cortex.

TMS is based on Faraday's principle of electromagnetic induction and features the application of rapidly changing magnetic field pulses to the scalp via a copper wire coil connected to a magnetic stimulator. These brief pulsed magnetic fields painlessly pass through the skull and can create electric currents of sufficient magnitude in discrete brain regions that depolarize neurons. When applied to the motor cortex, this depolarization results in a series of descending (direct and indirect) cortico-spinal waves that can sum-up at the spinal segmental level, depolarize alpha motor neurons, and lead to the contraction of contralateral muscles. This contraction, known as a motor evoked potential (MEP), can be measured using electromyography (EMG). Applied to cortical regions, the TMS evokes a local field potential that can be recorded via EEG, and represents a measure of cortical reactivity to TMS (Pascual Leone et al 2011).

The focus of this thesis is on TMS EEG techniques, with a special focus on signal processing methodologies and clinical applications. The thesis collects the contribution produced during the three years spent in the PhD and covers methodological aspects related to the definition of innovative signal processing techniques and personal contributions in the characterization of motor functions in healty and non-healty subjects.

The first part of chapter one introduces notions of neurophysiology and neuroanatomy of the motor control, focusing on the applications of TMS in neuroimaging. Then an overview of benefits and drawbacks in using concurrent TMS and EEG are discussed. Eventually the chapter ends up discussing the state-of-the-art of TMS-EEG in some relevant clinical applications.

Chapter two focuses on signal processing techniques. The first part of the chapter presents the steps needed in the pre-processing of EEG-TMS signals. It introduces a specific and innovative technique for artifacts rejection in the extraction of event related potentials, and a thorough characterization of the effects that the interpolation of artifacted channels introduces. Eventually, the main indexes taken into account for time and frequency evaluation of Transcranial Evoked Potentials (TEPs) are presented and discussed.

Chapter three lists the personal contributions brought to different clinical studies. A TMS study on the excitability evaluation in a hydrocephalus subject is presented, followed by a study on subjects affected by Subcortical Ischemic Vascular Dementia. Then, two studies focusing on the excitability

of Alzheimer's Disease subjects and that of an amputee before and after the implantation of 4 intra-fascicular electrodes in the stump are presented.

Chapter four presents a TMS EEG cortico-cortical evaluation of the connectivity between areas activated during TEPs in healthy subjects. Eventually, Chapter five ends this thesis with conclusions and presenting future works.

1 TMS and Neuroimaging: from motor control to clinical applications

This Chapter discusses two topics: the neurophysiology of the motor loop and some relevant applications of TMS and EEG TMS, in general and in relation to the motor loop.

1.1 Neurophysiology and neuroanatomy of the motor control

The cerebrum can be divided into four lobes:

(1) the **frontal lobe** is largely concerned with planning future action and with the control of movement;
(2) the **parietal lobe** is responsible of somatic sensation, with forming the body image, and with relating one's body image with extrapersonal space;
(3) the **occipital lobe** is concerned with vision and
(4) the **temporal lobe** with hearing; and through its deep structures—the hippocampus and the amygdaloid nuclei—with aspects of learning, memory, and emotion.

Each lobe (shown in figure 1) has several characteristic deep infoldings, which represent a favored evolutionary strategy for packing in more cells in a limited space. The crests of these convolutions are called *gyri*, while the intervening grooves are called *sulci* or *fissures*. The more prominent gyri and sulci are quite similar in everyone and have specific names and functions. For example, the *central sulcus* separates the *precentral gyrus*, which is concerned with motor function, from the *postcentral gyrus*, which is concerned with sensory function. Similarly, the motor areas in the right hemisphere exert control over the movements of the left half of the body. Although the hemispheres are similar in appearance, they are neither completely symmetrical in structure nor equivalent in function.

The cerebellum is an important movement control center, and it has extensive connections with the spinal cord and the cerebrum. The spinal cord provides the information about the body's position in space. The cerebellum compares the informations related to the goals of willed movements and

calculates the sequence of muscle contractions that are required to achieve these goals. Damage to the cerebellum results in uncoordinated and inaccurate movements.

The spinal cord can be divided into (i) **dorsal** and (ii) **ventral** horns (see figure 2). Cells in the dorsal horn receive sensory inputs from the dorsal root fibers, ventral horn cells project axons into the ventral toots that innervate muscle and, intermediate zone cells are interneurons that shape motor outputs in response to sensory inputs and descend the commands from the brain. The large dorsal column contains axons that carry somato sensory (touch) information up the spinal cord toward the brain. It's like a superhighway that speeds information from the ipsilateral side of the body up in the nuclei. The postsynaptic neurons in the medulla give rise to axons ascending to the thalamus on the contralateral side. The lateral column contains the axons of the descending corticospinal tract. These axons innervate the neurons of the intermediate zone and ventral horn and communicate the signals that control voluntary movement.

The spinal cord is the major conduit of information from the skin, the joints, and muscles to the brain and vice versa. The neurons of the spinal gray matter begin the analysis of sensory information and play a critical role in coordinating the movement and orchestrating simple reflexes.

There are three regions of the cerebral cortex involved with sensorimotor actions: the first is composed of sensory areas, which are first to receive signals from the ascending sensory pathways. The second consists in the secondary sensory areas, so designated because of their heavy connections with the primary sensory areas. The third is composed by motor areas, which are intimately involved in the control of voluntary movement. These cortical areas receive input from the thalamic nuclei that relay information from the basal telenchephamum and cerebellum and send outputs to the motor neurons in the brain stem and spinal cord.

The cerebral cortex plays an important role in the control of voluntary movement. The major motor control areas are the primary motor cortex (Brodmann area 4), the supplementary motor area and the premotor area. In the human brain, large parts of the cortex cannot be simply assigned to sensory or motor functions. For instance, an important role in the brain is covered by the association areas of the cortex. Some of the more important areas are in the prefrontal cortex, the posterior parietal cortex and the inferotemporal cortex.

The internal capsule is a large collection of axons that connect the white matter with the thalamus and the corpus callosum is an enormous sling of axons that connect the cerebral cortex. Three important collections of neurons in the basal telencephalon are the caudate nucleus, the putamen, and the globus

pallidus. Collectively these structures are called the basal ganglia and are an important part of the brain systems that control the movement.

The thalamus provides much of the input to the cerebral cortex with different thalamic nuclei that project axons to diffent brain areas. The ventral posterior nucleus, a part of the somatic sensory system, projects to the cortex of the postcentral gyrus. The ventral lateral nucleus and closely related ventral anterior nucleus are parts of the motor system: they project to the motor cortex of the precentral gyrus. The lateral pathways are involved in voluntary movement of the distal musculature and are under direct cortical control, and the ventromedial pathways are involved in the control of posture and locomotion and are under brain stem control. The most important part of the lateromedial pathway is the corticospinal tract. The ventromedial tract contains four descending tracts that originate in the brain stem and terminate among the spinal interneurons controlling proximal and axial muscles (Bear, Neuroscience: exploring the brain).

1.1.1 The motor loop

The motor loop (shown in figure 3) is the circuit of the brain that is involved in every voluntary movement and its primary function is to select, initiate and coordinate any willed movement. In the motor loop, the basal ganglia are involved in regulating any voluntary movements through the balance of the direct pathway and the indirect pathway. The direct pahway increases the excitatory drive from the thalamus to the cortex, ultimately increasing motor activity. The indirect pathway decreases the excitatory drive from the thalamus to the cortex, ultimately decreasing motor activity.

The most direct path in the motor loop through the basal ganglia originates with an excitatory connection from the cortex to cells in the *putamen*. The *putamen* cells make inhibitory synapses on neurons in the *globus pallidus*, which in turn make inhibitory connections with the cells in *ventral lateral nucleus pars oralis* (VLo). The thalamocortical connection is excitatory and facilities the discharge of movement related cells in the *Supplementary Motor Area* (SMA).

SMA is heavily interconnected with *motor area* (M1), the cortical Brodmann area 4 in the *precentral gyrus*. The pathway by which motor cortex activates lower motor neurons originates in cortical layer V. Layer V is populated by pyramidal neurons. The layer V pyramidal cells in M1 receive their input primarily from two sources: other cortical areas and the thalamus. The major cortical input originates from the area adjacent to Brodmann area 4: Brodmann area 6, 3, 2 and 1. The thalamic input to M1

arises from another part of the ventral lateral nucleus, which relays on information from the cerebellum. Besides projecting directly to the spinal cord, layer V pyramidal cells also send axon collaterals to many subcortical sites involved in sensorimotor processes.

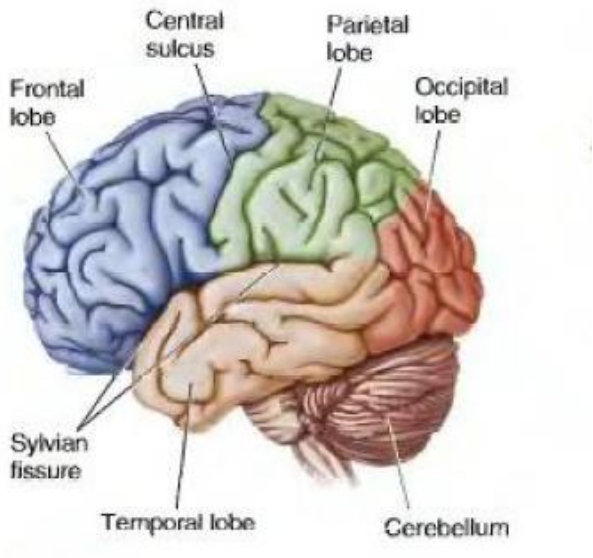

Figure 1 The lobes of the cerebrum (Paradiso, Michael A., Mark F. Bear, and Barry W. Connors. "Neuroscience: exploring the brain." *Hagerstwon, MD: Lippincott Williams & Wilkins* (2007): 718)

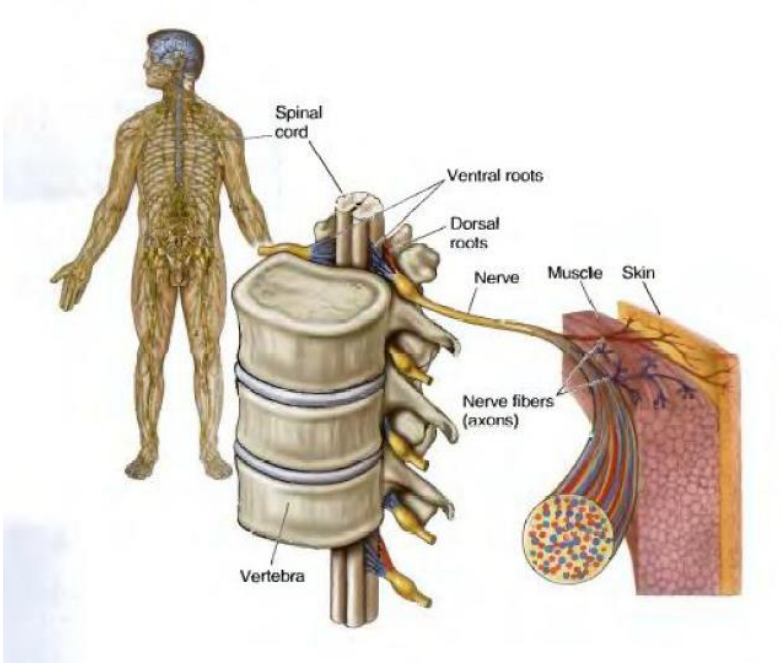

Figure 2 Spinal nerve and spinal nerve roots (Paradiso, Michael A., Mark F. Bear, and Barry W. Connors. "Neuroscience: exploring the brain." *Hagerstwon, MD: Lippincott Williams & Wilkins* (2007): 718).

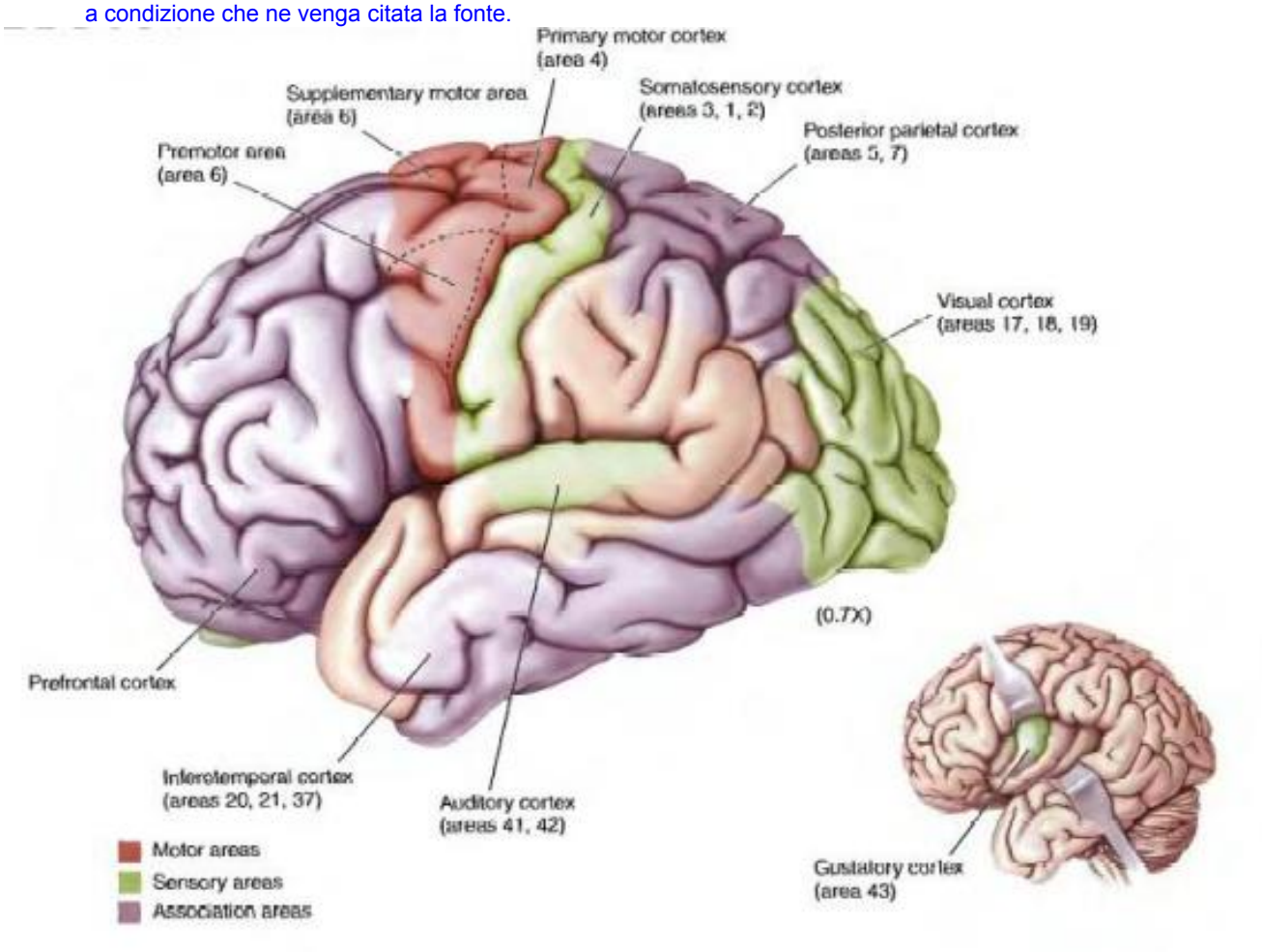

Figure 3 Major sensory, motor, and association areas of the cortex (Paradiso, Michael A., Mark F. Bear, and Barry W. Connors. "Neuroscience: exploring the brain." *Hagerstwon, MD: Lippincott Williams & Wilkins* (2007): 718).

1.1.2 Functional modulation of M1 through TMS: new insights in models of motor control

Transcranial Magnetic Stimulation (TMS) involves the application of a focused magnetic field that generates an electric field in the nervous tissue. This electric field produces a current flow, which is able to depolirize the membrane of neurons, stimulating or interrupting for a few milliseconds the brain activity. A coil administers a magnetic field with high intensity. This pulse passes through the scalp and, the cranium, arriving to induce an electric current in the brain tissue.

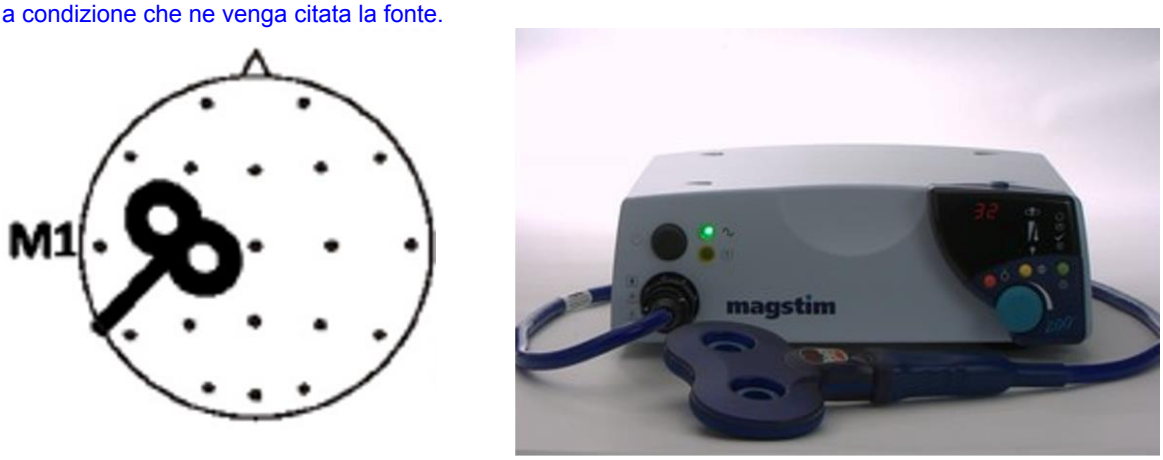

Figure 4: TMS Magstim coil applied to M1.

There are three types of stimulation:

Single pulse TMS: a single impulse is dispensed in a precise moment during the execution of a task or at rest. The minimum time interval between two successive impulses is three seconds;

Paired pulse TMS: paired pulses with a duration of different time interval between stimuli (Interstimulus interval, ISI) can be delivered: ISI between 1-6 ms produce inhibition, ISI between 8-20 ms produce facilitation;

Repetitive TMS: the target brain area of interest is stimulated via repetead pulses at regular interval with a frequency that can be chosen between 1 and 20 Hz. The effects lasted up from minutes to hours depending on the type of stimuation paradigm.

TMS provides a tecnhique to examine computational processes that the brain may use to implement actions in real time, and their influence on output stage. TMS can thus be used to read-out the functional state of motor system during action preparation and selection, and thus provide insights into their physiological underpinnings in an unprecedented way.

TMS can reveal the dynamic changes in the functional state of M1 during and prior to actions, and how these relate to our prior expectations. However, these findings themselves do not yet provide a mechanistic account that can explain the functional role of such modulations and influences, nor how such signals actually reach the motor system. It is now established that M1 exhibits responses to sensory signals in a variety of modalities including vision and somatosensation (Hatsopoulos and Suminski 2011), and thus is likely to integrate such signals for the selection and preparation of appropriate movements.

Two recent theories provide architectures and mechanistic accounts on how this may actually happen—the affordance competition hypothesis and active inference. The key point of the affordance competition hypothesis is that sensory information is continuously used to specify potentially available, and competing actions, whilst other kinds of information (such as motivation, reward expectation, new sensory information) will be accumulated and provide evidence that ultimately leads to selecting one action from the available set of actions. Potential actions therefore 'compete' with one another, and internal representations influence this competition. As initially introduced by (Gibson 1979), the concept of affordances reflects the idea that these internal representations are opportunities, or affordances, for action defined by the environment. The competition at the level of Dorsal Premotor Area (PMd)/M1 is driven by inputs from other regions, such as parietal and prefrontal cortex and the basal ganglia that contain information or evidence about the most appropriate action, given the context. These regions therefore bias the competition among actions until some (unspecified) threshold is reached and a commitment to an action is made. These affordances for action are based on incoming sensory information and internally represented decision variables (e.g. subjective reward, motivation, wakefulness, hunger), which are continuously transformed into parameters of action.

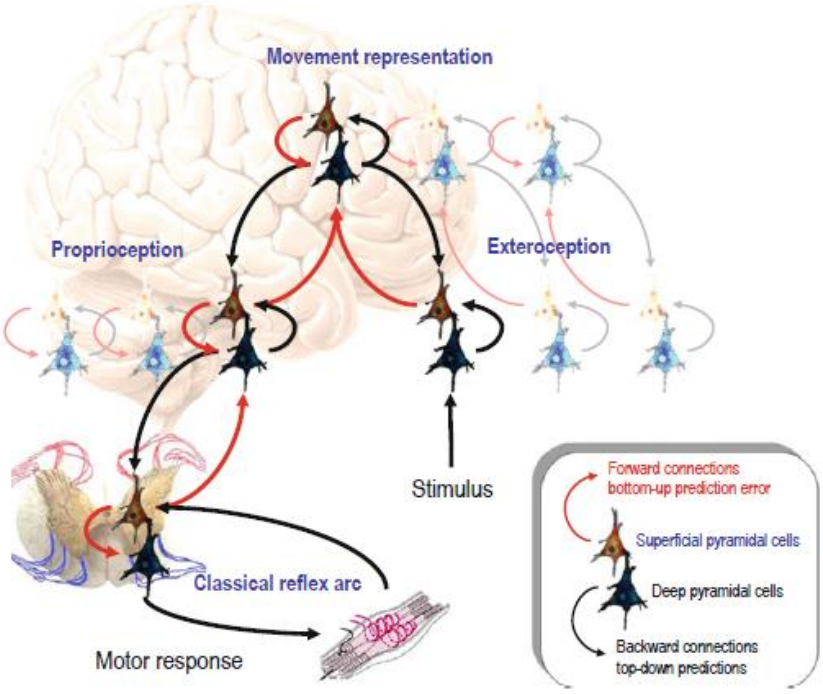

Figure 5: Active inference and predictive coding (Chen, Robert, ed. *Cortical Connectivity: Brain Stimulation for Assessing and Modulating Cortical Connectivity and Function*. Springer Science & Business Media, 2012).

Active inference is a generalisation of predictive coding that covers motor behaviours and itself is a special instance of the principle of free energy minimisation (cf. Friston et al. 2011). Free energy is a statistical quantity that bounds the surprise (self-information) associated with sensory signals. This surprise is quantified in relation to a generative model of how those signals were caused. As shown in figure 5 predictive coding uses prediction error as a proxy for free energy and rests on a hierarchical model, in which prediction errors are passed up the hierarchy (red arrows) to optimize high-level representations that provide top-down predictions (black arrows). In this schematic, prediction error units are portrayed in red and units encoding the conditional expectations of the hidden causes of sensory input are shown in blue. During perception, the best explanation for sensory input emerges when the top-down predictions can explain as much of the prediction error (at each hierarchical level) as possible. Active inference takes this one step further and notes that certain sensory modalities can use prediction errors to drive motoneurons to eliminate prediction error directly (through classical motor reflex arcs). This is shown schematically on the lower left, using units in the dorsal and ventral horns of the spinal cord.

Under active inference, a movement just fulfils the predictions afforded by percepts that predict both exteroceptive (e.g. visual) and interoceptive (e.g. stretch receptor) consequences. This high-level (sensorimotor) percept is activated by an exteroceptive (sensory) cue, and the ensuing top-down predictions propagate to both sensory cortex (to suppress exteroceptive prediction error) and the motor system. However, in the motor system, the predictions engender a prediction error that is eliminated by movement (adapted from Brown et al. 2011) (Bestmann cap. 10 Functional Modulation of Primary Motor Cortex in Chen, Robert, ed. *Cortical Connectivity: Brain Stimulation for Assessing and Modulating Cortical Connectivity and Function*. Springer Science & Business Media, 2012).

Descending (corticospinal) signals are not motor commands in the traditional sense per se, but predictions of the proprioceptive signals that arise from movement. The peripheral motor system, through movement, therefore tries to fulfil its predictions about proprioceptive signals. This framework provides a unifying account for the organizational principles underpinning sensory perception and action: if ascending sensory signals are prediction errors and descending motor commands are predictions, then the optimisation of predictions (and the resulting movements) should depend on optimising precision (i.e. reliability) in exactly the same way as in sensory processing.

1.2 TMS and Neuroimaging

The off-line approach, in which TMS and neuroimaging are separated in time, is technically easier to implement than the "online" approach, in which TMS and neuroimaging overlap in time with TMS having the possibility to adversely affect data acquisition. TMS may be performed during neuroimaging (i.e., online TMS, perturb and measure approach). In this case, neuroimaging provides a spatiotemporal assay of the immediate effects of TMS on neuronal activity (Siebner et al 2009).

The value of the online approach is the ability to test via TMS perturbation how focal cortex stimulation acutely modifies the activity and connectivity in the stimulated neural circuits (see Driver et al., 2009 for a review). If the goal of the experiment is to investigate the spatial pattern of TMS-induced changes in the brain activity, an online combination of TMS with Positron Emission Tomography (PET) or functional Magnetic Resonance Image (fMRI) allows one to visualize the causal impact of target neural interference on connected brain structures. Conversely, if temporal aspects of neuronal processing are the main focuses, the combination of TMS with EEG provides a methodology to investigate causal and dynamic relations between brain areas. (Kobayashi and Pascual-Leone 2003; Wagner et al. 2007; Horvath et al. 2011, Pascual-Leone et al 2011).

Neuroimaging can be performed before a TMS experiment to reveal the temporal (e.g. with EEG) or spatial (e.g. with fMRI) brain activation pattern during the performance of an experimental task. Then, the spatiotemporal information of task-related activity can be used to define the optimal time spot for the application of TMS during a task and to guide the placement of the coil over the cortical target. This a-priori knowledge is of particular value when designing experiments in which TMS is used to interfere with task performance.

This "map-and-perturb" approach can be used to make causal interferences about the contribution of a cortical area or its interconnected network to a distinct brain function. TMS can be applied over the area of interest to disrupt regular neuronal processing while participants perform the same experimental task. If TMS modulates task performance, it can be concluded that the stimulated cortical area or its closely interconnected areas make a relevant contribution to the task. This "condition-and-map" approach probes the changeability of functional brain networks. Among other possibilities, neuroimaging after Repetitive Transcranial Magnetic Stimulation (rTMS) conditioning can map the lasting functional impact of rTMS on task-related neuronal activity at a system level. Neuroimaging should start as quickly as possible after rTMS to ensure that short-lasting aftereffects

of rTMS are captured. The task specificity of functional reorganization can be shown contrasting the results with those in which participants perform an additional control task. (Siebner et al 2009).

In Zieman et al 2011 different neuroimaging technique are used in concurrent way with TMS (PET, fMRI, Near-infrared spectroscopy (NIRS), magnetic resonance spectroscopy (MRS), EEG) and combining TMS with the exposure to drugs (pharmacy-TMS).

TMS and PET allow measuring effective connectivity in neuronal networks by measuring rCBF (regional Cerebral Blood Flow) or CMRglc (cerebral metabolic rate for glucose) adjustments under TMS-induced modulation. TMS and fMRI allow measuring effective and state dependent effective connectivity in neuronal networks by means of BOLD imaging (Blood-oxygen-level dependent contrast imaging). TMS and NIRS allows measuring effective connectivity in neuronal networks by measuring the changes in oxy-Hb and deoxy-Hb. NIRS allows to measure rTMS- or Transcranial direct current stimulation (tDCS-induced) changes in brain neurotransmitters and metabolites.

Last but not least, Magnetoencephalography (MEG) and EEG allow measuring the magnetic fields and skull conductive potentials produced by the synchronous postsynaptic currents of neuronal populations and how there are modulated by TMS or rTMS protocols (Siebner et al 2009).

Each tecnhique has its potentiality and its weakness:

TMS-fMRI has the highest spatial resolution, whereas TMS EEG and MEG have the highest temporal resolution. The subcortical structures are accessible with TMS and fMRI; the neurotransmitter specific technique are TMS PET, TMS MRS and pharmaco TMS.

TMS NIRS measures the hemodynamic response, TMS and MRS measures GABA and glutammate levels. They allow measuring the metabolic consequences and those related to neurotransmitters.

These characteristics are used in several studies. For instance, in Fox et al 1997 the cerebral cortex (M1 for hand) was stimulated using TMS, and local and remote responses were recorded using PET. Specific aims of this experiment were to determine the location, intensity, extent, sense (increase or decrease) and time course of blood flow at the stimulated site, and to map intra-cerebral connectivity as remote co-variance with the stimulated site. In Premoli et al 2014 was studied the role of GABAA/B-ergic neurotransmission for TEPs in healthy subjects using a pharmaco-TMS-EEG approach. Alprazolam and diazepam increased the amplitude of the negative potential at 45ms after stimulation (N45) and decreased the negative component at 100ms (N100), whereas zolpidem increased the N45 only. In contrast, baclofen specifically increased the N100 amplitude. These results

provide strong evidence that the N45 represents activity of 1-subunit-containing GABAARs, whereas the N100 represents activity of GABABRs. These and other findings open a novel window of opportunity in the study of alteration of GABAA-/GABAB-related inhibition in disorders, such as epilepsy or schizophrenia.

In Bestmann et al 2008 the authors discuss the applications of TMS in producing a direct causal effect on brain activity and its study by new approaches that simultaneously combine TMS with neuroimaging methods, such as functional magnetic resonance imaging (fMRI). In this review, the authors highlight recent concurrent TMS–fMRI studies that illustrate how this novel combined technique may provide unique insights into causal interactions among brain regions in humans. They argue that combining TMS with neuroimaging techniques allows a step further in understanding the physiological underpinnings of TMS, as well as the neural consequences on perception and behaviour correlated with TMS-evoked activities. This can provide powerful new insights about causal interactions among brain regions, in both healthy and ill population of subjects, and may ultimately lead to the development of more efficient protocols for basic research and therapeutic TMS applications.

In Pascual Leone et al 2011, the authors argue that the combination of TMS with EEG or functional magnetic resonance imaging (fMRI) enables clinicians and researchers to directly study in vivo cortical plasticity in humans, and to characterize their changes across the age-span.

Combining Diffusion Tensor Imaging (DTI) with functional magnetic resonance imaging (fMRI) allows noninvasive quantitative *in vivo* analysis of anatomical connections between functionally defined brain regions (Conturo et al., 1999; Koch et al., 2002; Dougherty et al., 2005; Kim and Kim, 2005). Both TMS EEG and TMS fMRI tecniques could have benifits from DTI anatomical informations to achieve a more accurate evaluation of brain excitability and connectivity.

The corpus callosum (CC) is the principal white matter fiber bundle connecting neocortical areas of the two hemispheres (Innocenti, 1986; Gazzaniga, 2000). One step toward a refined understanding of the function of the human CC would be to identify its detailed topographical organization by novel MRI techniques. DTI allows quantification of the directionality of diffusion by the fractional anisotropy (FA) index. FA estimates the orientational coherence of white matter fiber bundles (Moseley et al., 1990; Le Bihan et al., 2001; Beaulieu, 2002; Le Bihan, 2003; Pfefferbaum et al., 2003).

1.3 TMS EEG: pros and cons

Transcranial Magnetic Stimulation co-registrated EEG has multiple advantages: given its exquisite temporal resolution and the provision of a direct measure of brain activity (rather than an indirect index).

During a typical TMS EEG session it is possible to:

(1) Measure the strength of the immediate response in the cortical target area of interest,

(2) Detect the spatiotemporal dynamics linked with the spread of activation,

(3) Calculate corticocortical conduction times

(4) Quantify complex dynamics such as phase locking or power modulation of EEG rhythms.

The main advantageous features of TMS EEG are, indeed:

(1) the ability to introduce perturbations on natural brain responses;
(2) the high temporal resolution,
(3) the direct cortical access,
(4) the high reproducibility at the subject level, which is ideal to study brain dynamics,

the main disantvantageous issues of TMS EEG are

(1) the partial brain coverage,
(2) the heavy logistic
(3) the needing of complex equipment and mesure procedures when performing group studies (Boly et al 2012).

The effects of TMS on the EEG signal have been studied both in the time domain (Paus et al.,2001; Iramina et al., 2002; Iwahashi et al., 2008; Lioumis et al., 2009; Casali et al., 2010) and in the frequency domain (Paus et al., 2001; Iramina et al., 2002; Fuggetta et al., 2005, 2008). Several studies have reported changes in coherence between electrodes associated with the stimulation (Fuggetta et al., 2005, 2008), suggesting that the stimulation induces a re-organization in interregional interaction.

Another potential drawback of the online approach is as shown in Hampson et al 2010, that the ordinary EEG amplifiers are saturated by TMS pulses. However, this difficulty can be overcome, as shown again in Hampson et al. 2010, by using a sample-and-hold circuit that pin the amplifier output to a constant level during the TMS pulse and release it after stimulation.

Eventually, electroencephalography has intrinsic limitations in terms of spatial resolution. Nonetheless, the very high temporal resolution of EEG allows the possibility of detecting differential effects of brain disturbance on conduction time or frequency-specific interregional oscillations that could have wide applicability in characterizing the functional networks underlying pathological conditions.

1.3.1 TMS EEG: directed measure of the brain responses

By means of TMS a physician can deliver a controllable input of known spatial and temporal characteristics to an identifiable brain region and by means of EEG he can study local responses and distant interactions between different brain regions (Thut et al 2009). Hence, TMS EEG can be used to study the longitudinal changes in the brain states not only between different populations as diagnostic tool (see Chapter 3 Section 3.3), but also in the same subject across different sessions. The aim could be the online evaluation of brain state, via indexes as the excitability measurable on Evoked Potentials (EPs), and the assessment of neuroplasticity in order to adapt the stimulation parameters to obtain the optimal motor response in the restoration of manipulative functions lost, for instance, in a stroke.

In TMS EEG are available three different experimental approaches (Miniussi et al 2010):

(1) **Inductive**: under this approach, brain excitability and connectivity are evaluated from stimulated sites and connected areas (activated by the TMS);

(2) **Interactive**: under this approach, the interaction between stimulation and a task is evaluated, allowing to study causal networks between stimulated site and areas typically involved in the considered task;

(3) **Rhythmic**: under this approach single pulse TMS can be used to identify the oscillatory state of the brain cortex and the brain response caused after the stimulus.

In details:

1) This approach allows to compare brain responses separated during TMS at rest and during task performance (Miniussi et al 2013). In Deslow et al 2004 the brain activations during the M1 stimulation measured during rest with TMS fMRI is compared with those activated by finger motor task. The same regions were activated. In Bestmann et al 2008 TMS-induced corticospinal excitability and connectivity during rest (TMS fMRI) was compared with those induced by TMS during grasp left hand task. The same regions were activated but the corticospinal volleys toward periphery

increased during the task and cortical activity in M1 and premotor area in the right hemisphere increased during the task perfomance.

2) TMS during task can be used to investigate if the stimulus can cause the enachment in performance during task (Miniussi et al 2013, Sandrini et al 2011, Siebner et al 2009) to validate one of the hypothesis (disrupting or enhancement). The study of the brain during a particular state or during task with Non Invasive Brain Stimulation (NIBS) allows to investigate the importance of one area related to its function during task and to investigate the functional role of single populations of neurons that belong to the stimulated area in the execution of the task. Stimulating before task is better to cause the intervention of pre-activated regions (Busan et al 2012).

3) Analysis in the frequency domain of TMS EEG signals to study spontaneous brain activity and how TMS EEG changes it is the basic for new rehabilitation techniques (Sandrini et al 2011, Miniussi et al 2008). Electric field of 120 V/m that induce activation of brain regions (occipital, parietal, frontal) causes different rhythmic response in different areas of the brain. The electrical oscillations evoked in the brain by directed stimulation of different cortical sites has never been studied. The only existing study is Rosanova et al 2009 about the electrophysiological properties of the cortex.

From a very deep review on studies between 1989 to 2009 about Repetitive Transcranial Magnetic Stimulation (rTMS) we learned that only 2 studies of 100 are about rTMS EEG. Very interesting is to investigate which is the frequency of stimulation during rTMS that could cause oscillations in phase in the stimulated area and investigate for which frequency the spontaneous activity could be resetted. A very interesting research topic in the neuroscience field is the study of the oscillatory activity: how the TMS can interfere with the ongoing activity in the brain and how TMS could generate an enhancement in the brain oscillations (Miniussi et al 2013).

1.3.2 TMS EEG: cortico-cortical interactions

EEG can be used to study cortico-cortical interactions by applying TMS to one area and observing responses in remote, but interconnected areas, or to study how the activity in one area affects the ongoing activity in other areas (Ilmoniemi and Kicic, 2010).

Perturbational approach to study cortical connectivity and excitability responses can be pursued using NIBS (Paus et al 2005). Using current neuroimaging methods, if a given stimulus 'activates' regions A, B and C in a coordinated fashion, is not known whether region A influences region B, or region C

drives both regions A and B with no direct interactions taking place between A and B. Several contributions in this issue address this problem at a mathematical level (Eichler 2005; Penny et al. 2005; Harrison et al. 2005). Many evoke so-called Granger causality, which is based on the notion that an effect cannot precede its cause in time (Granger 1969).

TMS EEG tool is suitable to investigate the causal involvement of brain regions during cortical information processing. In a connectivity perspective TMS could be used to evaluate the connection between areas stimulating by placing stimuli at different parts of the network activated during the TEPs. The combined TMS-neuroimaging approach is capable of tracing the spatiotemporal dynamics of causal interactions within functional brain networks (Siebner et al 2009).

Considering the studies that regard the TMS-induced excitability and connectivity in the brain areas that belong to the motor loop, in Zanon et al 2010: the left parietal cortex is stimulated via single pulse TMS. This region then activates a network of prefrontal regions in the contra-lateral hemisphere in a time range of 102–167 ms after the stimulus. Moreover, activation in the ipsilateral middle temporal and fusiform gyri is observed at 171–177 ms after delivery of TMS. Findings suggest the existence of late driven connections between parietal and prefrontal regions that could partially represent the neural pathway related to attention, even if, in this experiment, no attentional processing was requested. Late connections between dorsal and ventral streams were also observed, confirming previous evidence about interchange of information between them.

In several studies with single pulse TMS on the sensorimotor areas, Massimini et al. (2005, 2007 and 2009) found bilateral activations of brain areas in the frontal lobe in the later latencies.

Single pulse TMS on the premotor area generates activations in bilateral SMA and frontal areas, in particular Brodmann Area 8 contralaterally, 9 bilaterally.

TMS can also be used to activate and study mechanisms of acute cortical reorganization in healthy human brain. This is achieved by applying rTMS over a target area to produce effects on cortical circuits that outlast the duration of the rTMS session. The functional effects that can be elicited with rTMS depend on stimulation parameters such as intensity, frequency, total number of stimuli and the functional state of the cortex targeted by rTMS. These neuromodulatory effects have great potential for studies on adaptive neuroplasticity in the human brain (Siebner et al 2009).

As an example, using rTMS stimulation over premotor area with a frequency of 0.9 Hz, Chen et al 2003 found that coherence and power measurable during the finger tapping task decrease in motor areas and M1 has reduced excitability.

In Casula et al 2014 the authors used low frequency rTMS on M1 and visual cortex (V1) as test and single pulse TMS to evaluate TEPs. 1 Hz rTMS appears to increase the amount of inhibition following a TMS pulse, as demonstrated by the higher N100 and P60, which are thought to originate from GABAb-mediated inhibitory post-synaptic potentials. The results confirm the reliability of the TMS-evoked N100 as a marker of cortical inhibition and provide insight into the neuromodulatory effects of 1Hz rTMS. This finding is of relevance for therapeutic and diagnostic purposes.

As another example, in Esser et al 2006, the authors used 5 Hz rTMS as neuromodulatry paradigm and single pulse TMS co-registrated with EEG to evaluate TEPs before and after rTMS. They found that, after rTMS, EEG responses at latencies of 15–55ms were significantly potentiated. A topographic analysis revealed that this potentiation was significant at EEG electrodes located bilaterally over premotor cortex. Thus, these findings provide a direct demonstration in humans of Long Term Potentiation (LTP) induced by rTMS defined as changes in the amplitude of the population response to electrical stimulation (Esser et al 2006 and Huber et al 2012). This is the main index to evaluate brain plasticity during the application of neurorehabilitation techniques.

The time courses of activity in different regions can be used to access the causal relationship between them. By studying the distributed changes in brain activity produced by focal transcranial brain stimulation, the connectivity pathways identified by traditional network analysis techniques can be validated in both normal subjects and in different disease states (Shafi et al 2012).

One of the benefit of using TMS EEG is the possibility to examine the state of neural network without a priori assumption about the regions functionally connected to the stimulation site. In fMRI based effective connectivity analysis the network connectivity can be examined within a group of preselected regions while in TMS EEG functionally connected regions can be identified in an exploratory manner (Akaishi et al 2013).

Taking into account well known network dynamics, increased excitation in one particular network or brain region may necessary lead to inhibition of an opposing network (or viceversa). As a consequence observed behavioural improvements due to NIBS may emerge from shift in the balance between (competing) neural networks in the brain (Wokke et al 2015). In order to acquire more insights into the effects of NIBS on distribution of neural resources, research on NIBS should take interrelatedness of different *network dynamics* as a central starting point. Therefore, in order to move the field of NIBS and its (clinical) applications forward, it is essential to extend current studies on the

effects of NIBS towards investigating the effects of stimulation on task-relevant as well as task-irrelevant functional brain networks (Wokke et al 2015).

Nowadays no studies have been done in the evaluation of cortico-cortical connectivity in TMS EEG signals between brain areas activated during the time period of elicitation of TEPs (first 300 ms after the stimulation, Ilmoniemi et al 1997).

1.4 TMS EEG in clinical studies in Alzheimer's disease

Combined TMS–EEG has been used to examine a wide range of clinical conditions and several studies focused on Alzheimer's disease (AD), with the aim of better understanding this disease.

Alzheimer's disease as Parkinson's Disease (PD) is characterized by a progressive degeneration of specific neurons in the brain. Alzheimer's disease leads to dementia a state of confusion characterized by a loss of ability to learn new information and to recall previously acquired knowledge. It is estimated that dementia affects 50 % of people over age 85. The number of Americans with dementia totals over 4 million. Alzheimer's disease is a disruption of cytoskeleton of neurons in the cerebral cortex, a region of the brain crucial for cognitive function.

In Julkunen et al 2011 authors analysed a small sample data with the aim to test the sensitivity of the TMS-EEG characteristics to discriminate control subjects (n = 4) from MCI[1] (n = 5) and AD (n = 5) subjects. Furthermore, they investigated how the characteristics of the TMS-EEG response related to the scores of the dementia in rating scales used to evaluate the severity of cognitive decline in these subjects. They found that the P30 amplitude correlates with cognitive decline and shows good specificity and sensitivity in identifying healthy subjects from those with MCI or AD. Given the small sample size, the results of this study have to be considered highly preliminary.

In Julkunen et al. 2008 the authors found that TMS delivered to M1 is less effective in activating widespread regions in Alzheimer's patients compared with controls. This result is now explained saying that in patients with AD, the hyperexcitability on the sensorimotor cortex may represent a protective mechanism that counteracts the prominent loss of cortical volume. In Niskanen et al 2011 the authors found that the motor cortex excitability correlates negatively with cortical thickness on the sensorimotor cortex, the precuneus and the cuneus but the strength of the correlation varied

[1] Mild Cognitive Impairment, a stage that is an intermediate stage between the expected cognitive decline of normal aging and the more serious decline of dementia. It can involve problems with memory, language, thinking and judgment that are greater than normal age-related changes

between the study groups. On the sensorimotor cortex the correlation was significant only in MCI subjects. On the precuneus and cuneus the correlation was significant both in AD and MCI subjects. In healthy controls the motor cortex excitability did not correlate with the cortical thickness.

In healthy subjects the motor cortex excitability is not dependent on the cortical thickness, whereas in neurodegenerative diseases the cortical thinning is related to weaker cortical excitability, especially on the precuneus and cuneus. However, in AD subjects there seems to be a protective mechanism of hyperexcitability on the sensorimotor cortex counteracting the prominent loss of cortical volume since the motor cortex excitability did not correlate with the cortical thickness. Such protective mechanism was not found on the precuneus or cuneus nor in the MCI subjects. Therefore, these results indicate that the progression of the disease proceeds with different dynamics in the structure and function of neuronal circuits from normal conditions via MCI to AD.

Moreover, in Nardone et al 2014 authors also assert that the increased excitability to TMS in patients with AD may be a consequence of an abnormality within the glutamatergic system, and this hypothesis was supported demonstrating an abnormal response to rTMS in patients with AD. Indeed the cortical silent period duration in the First Dorsal Interosseous (FDI) after 5 Hz rTMS increase in the patients, where MEPs decrease in size.

Cortical hyperexcitability has also been found as associated with reduced cortical thickness and reduced learning ability in older adults (List et al 2013), consistently with previous neurophysiologic studies in AD patients reporting increased cortical excitability, brain atrophy and cognitive deficits. Furthermore, a crucial question regards rTMS rationale for treating AD arises: since cortical hyperexcitability is one of the most robust findings in AD, the employment of high-frequency stimulation, that usually aims at enhancing cortical excitability, may seem paradoxical (Pallanti et al 2015).

Other TMS studies have demonstrated that cortical excitability is enhanced in AD and primary motor cortex presents functional reorganization (Guerra et al 2011). At present, it is not clear if these motor cortex excitability changes might be the expression of an involvement of intracortical excitatory glutamatergic circuits or an impairment of cholinergic and/or gabaergic activity (Ferreri et al 2003). In fact, although the best hypothesis for the pathogenesis of AD remains the degeneration of cholinergic neurons in specific regions of the basal forebrain, the application of specific TMS protocols, such as the paired-pulse TMS (ppTMS) and the study of the short-latency afferent

inhibition, points out the role of other neurotransmitters, such as γ-aminobutyric acid (GABA), glutamate, and dopamine. (Guerra et al 2011).

The change in threshold (the AD population showed an hyperexcitability – a lower value in the resting motor threshold) did not seem to correlate with dysfunction of inhibitory intracortical cholinergic and GABAergic circuits, nor with the central cholinergic activity. In Di Lazzaro et al 2003 the authors argued that the hyperexcitability of the motor cortex is caused by an abnormality of intracortical excitatory circuits. This cortical hyperexcitability is believed to be a compensatory mechanism to execute voluntary movements, despite the progressive impairment of associative cortical areas. Thus, the pattern of cortical hyperexcitability in AD seems to be stage-dependent and might turn into a loss of excitability during further progression of the disease. In AD patients, the functional meaning of cortical hyperexcitability might be searched for in a compensatory mechanism to execute voluntary movements when assistance from associative cortical areas is impaired (Pepin et al. 1999). As subsequently hypothesized (Ferreri et al. 2003), precentral regions, including premotor and supplementary motor areas, may be recruited even for movements of low level of complexity, in order to preserve motor performance. Inhibitory gabaergic dysfunction may affect the complex balance of cortical excitability in AD patients. Biochemical investigations of biopsy brain tissues from patients in the early phases of AD have not shown significant alterations in the concentration of GABA (Lowe et al. 1988, 1990) and no disturbance of GABA transporters (Nagga et al. 1999; Ohyama et al. 1999). Although early TMS studies suggested cholinergic deficit as the main accepted hypothesis, recent results indicate that AD should be considered as a complex neurodegenerative disease involving different neurotransmitter systems. Moreover, increased excitability and cortical reorganization of the motor output that occur in the course of AD could explain the frontomedial shift of the excitable motor areas, interpreted as a compensatory mechanism allowing the preservation of motor programming and execution over a long period, despite the clinical progression of AD. (Pennisi et al 2011).

In the 3.2 and 3.3 paragraph will be presented a personal contribution in the field of TMS study on Subcortical Ischemic Vascular Dementia and of TMS EEG excitability study on Alzheimer's population. In the paragraph 3.5 will be presented a clinical study regarding a correlation analysis between FA and excitability measured as voltage level activation through TMS EEG on left M1 in an Alzhiemer's popolation.

1.5 TMS EEG in clinical applications: Stroke neurorehabilitation

Neuroimaging techniques as EEG and non-invasive brain stimulation (NIBS) techniques such as TMS have proven useful in predicting prognosis, recovery trajectories and response to rehabilitation in individuals with stroke. However, additional synergetic effects can be achieved by simultaneously combining both approaches (Sato et al 2015). Combined TMS-EEG is able to activate discrete cortical regions and directly assess local cortical reactivity and effective connectivity within the network independent of the integrity of descending fiber pathways and also outside the motor system.

TMS-EEG could be used to identify neurophysiologic biomarkers of stroke recovery and prospectively monitor changes in cortical excitability and/or connectivity in response to rehabilitation approaches, pharmacologic therapy, NIBS or spontaneous recovery. For example, TMS-EEG could be used to evaluate changes in sensorimotor cortical connectivity contributing to motor deficits and impairments including hemiparesis, dyscoordination, and spasticity.

Co-registrated EEG signals with the TMS gives the possibility to have a direct measurement of the electrical signals generated by the neural activity and allows researchers to derive inhibitory and excitatory connections and calculate cortical connections strength characterizing specific connectivity deficit as related to functional impairment of neural connectivity caused by neurotransmitter imbalances (Bortoletto et al 2015, Skudlarski et al. 2008).

The convergence of graph theory and TMS EEG gives us the ability to map the effective connectivity between brain areas and derive dynamic measures of the brain response when a specific node is affected (Bortoletto et al 2015). Connectivity-based analysis allows an investigation based on hypothesis of interactions between regions under physiological and pathological conditions. Connectivity models put us in a network perspective in which changes in neural activity in a given region is explained by interactions between regions. Showing how the damage to a certain region changes the entire connectivity we can learn something about the intrinsic architecture of cortical circuitry engaged in cognitive, sensory, motor skills. Longitudinal studies (from post stroke to chronic stroke) are needed for a better understanding of the pathological interactions between brain areas after the stroke and how they are connected with deficits and clinical results (Grefkes et al 2011).

Carey et al 2014 reports that to correct this maladaptation studies regarding the interhemispheric balance (IHI) have used suppressive low-frequency repetitive transcranial magnetic stimulation (rTMS) over contralesional M1 to disinhibit ipsilesional M1 and promote higher function in the paretic hand.

Other studies report, as Grefkes et al. 2008, that further investigation are needed to understand the mechanism underlying neural disorders from stroke in cortical networks and how this leads to functional and physiological recovery based on the monitoring of cortical reorganization for the design of new treatments.

The use of advanced neuroimaging techniques allows determining if residual functional organization can predict the outcome, giving life to the stratification of patients based on how they respond favorably to intervention. Understanding these influences is the route to a stratification of patients into clinical trials and leads to a personalized medicine (Grefkes et al 2014).

A main aim could be the study of the brain circuits alterations during repetitive TMS to better understand motor functionality, how to optimize clinical intervention in an individual way, how to set optimally TMS parameters.

Repetitive stimulation (rTMS) can also be used as a neuromodulatory tool. Low frequency rTMS can be used to transiently perturb the stimulated brain region inducing a so called 'virtual lesion'. This form of inhibitory rTMS represents an in-vivo non-invasive method available for demonstrating the causal influence of a given cortical region or its interconnected network on specific behaviours. Depending on the specific stimulation protocol used, the neuromodulatory effects of rTMS can outlast the stimulation period by several minutes to hours (Liew et al 2014).

Advances in sensor technology, development of non-invasive and implantable wireless Brain Machine Interface BMI-systems (figure 6) and their combination with brain stimulation, along with evidence for BMI systems' clinical efficacy suggest that BMI-related strategies will play an increasing role in neurorehabilitation of stroke (Soekadar et al 2014).

Optimal settings and algorithms for BCI training protocols with proprioceptive (haptic) feedback in patients with brain lesions are unknown.

More and larger clinical studies are needed to develop optimal protocols for both, assistive and restorative BCI applications. Due to the heterogeneity of patient populations, multimodal approaches to evaluate subject specific characteristics in terms of anatomy and function including e.g. fMRI, DTI, MEG and diagnostic TMS are an important pre-requisite for a better understanding of BCI related neuroplasticity and might help to develop new strategies for BCI use in neurorehabilitation (Soekadar et al 2011).

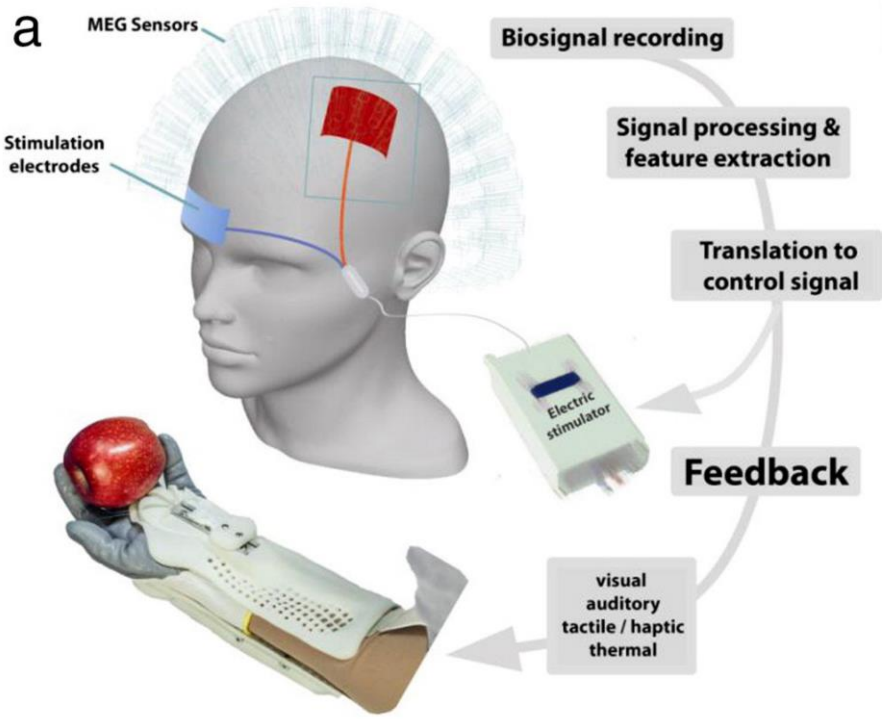

Figure 6: Illustration of Brain Machine Interface (BMI) system for stroke neurorehabilitation. Bio-signals associated with attempted movements of the paralyzed hand and fingers are translated into online feedback and/or brain-state dependent transcranial electric stimulation to agument neuroplasticity facilitating motor recovery (Soekadar, Surjo R., et al. "Brain–machine interfaces in neurorehabilitation of stroke." *Neurobiology of disease* (2014).

1.6 TMS EEG: Sensorimotor implication and prosthetis

The selective use of sensory feedback to correct deviations that interfere with task goals could account for several unexplained effects in motor control, such as the variability of task-irrelevant movement qualities. The concept that motor cortex could use sensory feedback contrasted with the earlier purely 'feed-forward' serial model of motor control. Optimal control needs an optimal estimate of the state of the system (state variables), which is generated from afferent feedback from sensors combined with efferent copy of motor signals. In humans, both afferent feedback and efferent copy are used to estimate on-going motor performance (Wolpert et al., 1995). Optimal state estimation is created by combining feedback signals and efferent copy of motor commands.

In Gandolla et al 2014 functional electrical stimulation (FES) is used to provide externally driven proprioceptive information during movement execution — in other words, to experimentally alter reafference. FES delivered to a mixed nerve trunk (i.e. nerve that contains both efferent motor and afferent sensory fibers) will synchronously depolarize motor and sensory axons that are bundled together, eliciting muscle contraction through two pathways. The first (direct descending pathway) conveys signals along the efferent motor fibers that generate muscle contraction by direct motoneuron

depolarization. The second (indirect ascending pathway) communicates signals via the afferent sensory fibers (Collins, 2007) that code proprioceptive signals frommuscle spindles, Golgi tendon organs and cutaneous receptors (Burke et al., 1983), but in particular Ia fibers responsible for muscle spindle information (Leis et al., 1995). This second pathway produces muscle contractions through a central mechanism, providing excitatory synaptic input to spinal neurons that recruit motor units in the natural order (Bergquist et al., 2011). Therefore, the proprioceptive signal elicited by the sensory fiber stimulation creates the impression that the muscle is extended (i.e.muscle spindles discharge), and leads to firing of the motor neurons in order to produce a contraction. During FES, it has been demonstrated that this information can be useful at the level of the spinal cord, inducing a reinforcement of the muscle contraction through themyotatic reflex circuit, however few notions about altered proprioceptive information sent up to the cortex are available in the literature.

Recently it has been shown that an upper limb robot-based rehabilitation improves motor performance in stroke patients, inducing brain reorganizations. Specifically, interhemispheric connectivity between primary somatosensory areas got closer to a 'physiological level' in parallel with the acquisition of more accurate hand control (Pellegrino et al 2012). In Di Pino et al 2012 the authors showed that the improvement in cybernetic hand prosthesis control is coupled with reorganization in sensorimotor cortical regions activity (Rossini et al. 2010; Tombini et al. 2012). In parallel with regional activation properties, it is well known that the motor abilities depend on intra- and inter-network functional connectivity (Hummel and Gerloff, 2006), and are anatomically related to the amount of transcallosal connections (Stancak et al. 2002).

Chapter 3 (paragraph 3.4) will show personal contribution on this topic, with the analysis of TMS EEG signals and the evaluation of brain plasticity before and after the implant of 4 intra-fascicular electrodes in the stump of an amputee subject.

2 TMS EEG Data Processing: From Signals to Brain Imaging

Introduction

This Chapter discusses the signal processing behind the extraction of biomarkers in EEG TMS signals. The chapter starts with a description of the standard processing pipeline and brain imaging in TMS EEG studies. The chapter, then, presents fourth original contributions in the field of TMS EEG signal processing. The paper ends with the description of principal biomarkers that can be extracted from TMS EEG signals.

2.1 TMS EEG: standard processing pipeline and brain imaging

The standard pre-processing pipeline used in the extraction of TMS evoked EEG-activity, i.e. TMS-evoked potentials (TEPs), is composed of the following steps:

1. Data is visually or automatically inspected and compromised channels are removed,
2. EEG signals are segmented around the stimulation onset;
3. Segments are automatically or visually classified and those contaminated by unremovable artifacts are dropped from the following analysis,
4. Signals are low pass filtered with a forward-backward zero phase low pass filer. A common cut-off frequency is 80 Hz in TMS EEG signals (physiological frequency to evaluate the brain responses in the frequency domain) as reported in other studies (Huber et al. 2013, Maki et al 2010, Casali et al 2010). The filtering is performed excluding a window around the TMS stimulus.
5. Signals are notch filtered (50Hz for EU signals and 60Hz for US signals). Again the filter works in a forward-backward zero phase way and it is applied excluding a window around the TMS stimulus.
6. To make data more computational manageable, signals are downsampled to achieve better computational performance.
7. All the data segments are pre-stimulus baseline corrected,
8. All the segments go re-referencing, usually to the average reference.
9. Ensemble averaging is performed in order to extract ERPs.

The brain imaging typically used in TMS EEG ERP applications is composed of the following steps:

1. Latencies of interest are inspected by means of topographic maps. Topographic maps can be evaluated at fixed latency or at peak values. In this case Semi-automatic amplitude/latency measurements of each component of the EEG evoked potentials (using Cz or GMFP as a reference to individualize the peak component latency) are computed to obtain the excitability results in all the scalp electrodes.
2. The Inverse problem solution is resolved to evaluate the current density distribution in the latencies of interest (with formulation in the paragraph 2.5).
3. Evaluation of different indices as connectivity (presented in paragraph 2.6), for population comparison in the time domain (as in paragraph 2.7) and in the frequency domain (as in paragraph 2.8)

2.2 Artifact rejection via an optimal two weights method for ERP data

Several biomedical applications TMS EEG and others require the signal processing of biological data, and have as standard procedure for noise reduction the ensemble averaging of multiple repeated acquisitions (trials). This method however is ineffective when artifacts are time-locked along epochs. In this section I present an innovative method, which is an original contribution of this thesis.

Every averaging method is based on the assumption that each trial recorded on an electrode is composed of two additive components:

(1) a time-locked activity related to some sensitive/stimulation phenomenon (ERA, Event Related Activity in the following) and

(2) a sum of several other non time-locked background activities.

The averaging aims at estimating the ERA activity from the background noise under very low Signal to Noise and Interference Ratio (SINR). Although averaging is a well-established tool, its performance can be improved in the presence of non-presistent time-locked artefacts by a trials classification (human or computer based) and removal stage. With our method we improve further the attainable performance by means of a weighted averaging method.

2.2.1 Signal Modeling

We assume that the signal recorded in a single epoch can be modelled as:

$$x_p = s + D_p\, a + \eta_p$$

where x_p is the measured p^{th} trial, s is the ERA activity to be estimated, a is the artifact that adds in the trial when D_p is equal to 1. D_p can be modelled as a Bernoulli random variable having success probability equal to q, and η_p is a random vector having zero mean and that models both acquisition noise and other physiological background activities. Under such a model the error adding up to every trial has an average power level equal to:

$$P_e = \frac{E\{\|e\|^2\}}{N} = \frac{\|a\|^2}{N} q + \frac{tr(\sum_\eta)}{N} = qP_a + P_\eta$$

Where $P_a = \|e\|^2$/N is the average artifact power and $P_\eta = tr(\sum_\eta)$ is the average of the noise power along the trial.

The ensable avereaging method ERA estimation is:

$$s_{ave} = \frac{1}{M}\sum_{p=1}^{M} x_p = s + \frac{1}{M}\sum_{p=1}^{M} D_p a + \frac{1}{M}\sum_{p=1}^{M} \eta_p.$$

Where M is the total number of recorded trials. This estimator introduce an error equal to:

$$e_{ave} = s_{ave} - s = \frac{1}{M}\sum_{p=1}^{M} D_p\, a + \frac{1}{M}\sum_{p=1}^{M} \eta_p$$

With an average power level equal to:

$$P_{e_{ave}} = \frac{E\{\|e_{ave}\|^2\}}{N} = \frac{tr(E\{e_{ave} e_{ave}^T\})}{N} = \left[q^2 + \frac{1}{M} q(q-1)\right] P_a + \frac{1}{M} P_\eta$$

The error power is composed of two components: an artifact component and a noise component. With respect to the single trial, the noise component exhibits a power reduction proportional to the number of trials that are averaged. The power of the artifact component has a different behavior. It is equal to 0, when q = 0, i.e. when all the trials are artifact-free. It increases up to P_a, when q increases up to 1. Hence, the EA estimator has an artifact mitiation effect that decreases with the increasing of the artifact occurrence rate across trials.

The CAD approach consists of the averaging only the trials that fit a well defined criterion. Generally, the CAD estimator averages all the trials selected by a classification process as not containing the artifact. The performance of such an approach can be easily modeled when classifier performance are known.

In the following we will denote by $O_p \in \{0, 1\}$ the classification outcome, where $O_p = 1$ is the outcome that corresponds to a trial classified as artifact-prone and that will be excluded from the average. We assume to know $p_{TP} = P\{O_p = 1 \,/\, D_p = 1\}$ the probability of the true positive (artifact prone trials), $p_{TN} = P\{O_p = 0 \,/\, D_p = 0\}$ the true positive and true negative rates of the classifier, i.e. the probability of correctly identifying an artifact affected and free trial, respectively.

We used C_P=1-O_p the flipped classification outcome, in order to simplify the models expressions. Cp can be modeled as a Bernoulli random variable having success probability equal to:

$$\mathbb{P}\{C_p = 1\} = p_{TN}\,(1-q) + (1-p_{TP})q = q^{\sim}$$

The Classification and Dropping Method has the following ERA estimation formula:

$$s_{cad} = \frac{\sum_{p=1}^{M} C_p x_p}{\sum_{t=1}^{M} C_t} = s + \sum_{p=1}^{M} A_p\, a + \sum_{p=1}^{M} B_p\, \eta_p$$

where the random variables $B_p = \frac{C_P}{\sum_{t=1}^{M} C_t}$ and $A_p = D_p B_p$ are the weights that the CAD estimator applies to the noise component, the former, and the artifact component, the latter, of the p^{th} trial. The CAD estimator produce an errore qual to:

$$e_{cad} = s_{cad} - s = \sum_{p=1}^{M} A_p\, a + \sum_{p=1}^{M} B_p \eta_p$$

With an average power level equal to:

$$P_{e_{cad}} = \frac{E\{\|e_{cad}\|^2\}}{N} = \frac{tr(E\{e_{cad} e_{cad}^T\})}{N} = M\left\{\left(E\{A_p^2\} + \,(M-1)E\{A_p A_t\}_{p\neq t}\right) P_a + E\{B_p^2\} P_\eta\right\}$$

The probability distributions of A_p and B_p are derived in the Appendix (see Vollero et al 2014) in conjunction with the computation of their squared average values and the cross-correlation term $E\{A_p A_t\}_{p\neq t}$. Also under such an estimator the error power is composed of two components, the former is artifact related and the latter is noise related. This time, however, the noise reduction factor is $ME\{B_p^2\}$ which is greater or at least equal to $\frac{1}{M}$ and hence the noise component reduction is not always greater than that of EA. Conversely depending on the statistical characterstics of the vector $A = [A_1, \ldots A_M]$ the artifact component can be signifincantly reduced.

The idea behind the CAW estimator is to extend the CAD averaging stage with the introduction of two weights, that we indicate in the following as w_L and w_H with $w_L \leq w_H$

These weights are applied to trials classified as artifact-prone, the former and artifact-free, the latter. We assume that in every reconstruction process, given h the number of trials classified as artifact free, the weights are chosen in order to deterministically cancel any contribution that the ERA has on the reconstruction error, i.e. they satisfy the condition

$$h\, w_H + (M - h)w_L = 1$$

The Classification and Weight Method has the following reconstruction formula:

$$s_{caw} = \sum_{p=1}^{M} W_p x_p = s + \sum_{p=1}^{M} F_p a + \sum_{p=1}^{M} G_p \eta_p$$

Where $W_p = C_p w_H + (1 - C_p) w_L$ is the weight associated to the p^{th} trial in the reconstruction process. Above the random variables $F_p = D_p\, W_p$ and W_p describe the weights used on the artefact, the former, and the noise, the latter, component of the p^{th} trial.

This estimator introduce an error equal to:

$$e_{caw} = s_{caw} - s = \sum_{p=1}^{M} F_p\, a + \sum_{p=1}^{M} W_p \eta_p$$

With an average power level equal to:

$$P_{e_{caw}} = \frac{E\{\|e_{caw}\|^2\}}{N} = \frac{tr(E\{e_{caw} e_{caw}^T\})}{N}$$
$$= M\left\{\left[E\{F_p^2(w_l)\} + (M-1)E\{F_p(w_l)F_t(w_l)\}_{p\neq t}\right] P_a + E\{W_p^2(w_L)\} P_\eta\right\}$$

Where in the expression above we made explicit the dependence of random variables from w_L alone, since w_H is linked to w_L by the classification outcome and the CAW reconstruction rule. The probability distribution of $F_p(w_l)$ and $W_p(w_L)$ are derived in the appendix (see Vollero et al 2014) in conjuction with the computation of their squared average values and the cross-correlation term $\{F_p(w_l)F_t(w_l)\}_{p\neq t}$. In the expression above it is possible to control the contribution that the artifact and the noise powers level have in the final signal reconstruction. Indeed., based on the above model we can choose:

$$w_L^* = argmin_\beta \left\{ E\{w_p^2(\beta)\} P_\eta + \left[E\{F_p^2(\beta)\}_{p \neq t} \right] P_a \right\}$$

in order to minimize the residual error power on the reconstructed signal.

In all the following experiment we obtain the optimal w_L by the application of the golden search algorithm to the expression above. This yields to an optimal configuration which is a function of both the dataset parameters (P_a, P_η, q) and the classifier performance (p_{TN}, p_{TP}) formally:

$$w_L^* = w_L\,(P_a, P_\eta, q, p_{TN}, p_{TP})$$

2.2.2 Model Validation

The simulator implements the generation of trials as a sum of a deterministic ERA, a deterministically shaped, randomly occurring, artifact and a random noise. The simulator has been customized in order to generate (i) an ERA that emulates an EEG-TMS Event Related Potential (ERP), matching a four waves model (N44, P60, N100, P300), (ii) an artifact which is localized in time and that adds to each trial with probability q, and (iii) an additive white, zero mean, random noise having Gaussian distribution.

The ERA estimation component of the simulator processes the trials in order to extract the ERP activity. The EA processing is carried out by the simple averaging of all the generated trials. The CAD processing performs first the simulation of the classification process based on the following rules:

Then, CAD performs the averaging of all the trials classified as artifact-free, i.e. the averaging includes the trial xp if the condition $C_p = 1$ is met. The CAW method is driven by an external provided W_p value. CAW, hence, uses the results of the same classification process of CAD to compute the value of W_H and to sum up all the trials, weighting the trial x_P with the value $W_p = C_p w_H + (1 - C_p) w_L$. The simulator results provide a validation benchmark for predictions of previously presented models.

Considering the simulation parameters set as in the following table the models presented above have been validated as shown in figure 1, 2, 3.

Parameter Name	Symbol	Parameter Value
Signal Power	P_s	1
Noise and Artifact Power	$P_t = qP_a + P_\eta$	100
Runs for each configuration	R	500
Sampling Rate	f_s	500 Hz
Number of trials	M	100
True Positive Rate	p_{TP}	0.90
True Negative Rate	p_{TN}	0.90
Trial Duration	T	1 s
Minimum Weight	w_L	Optimal Value

In each examined scenario the average signal to noise interference ratio (SNIR) that every trial in the dataset exhibits is hold fixed. The SNIR is defined as $\frac{P_s}{P_t} = \frac{Ps}{P_\eta + q\,P_a}$ where Ps is the ERA power and Pt is the sum of the average interference and noise powers. Every analysed scenario differ in the fraction of the total power caused by artifacts qP_a/P_t, this fraction is varied in the range [0,q]. The W_L value of CAW is always chosen as the optimal value. The results report both modelling (lines) and simulation results (error bars).The simulation results are reported as average values and 99% confidence interval over R=500 runs for every configuration of parameters. In each plot the results are grouped in curves of fixed q value, with $q \in \{0, 0.1, 0.2, \ldots 1\}$.

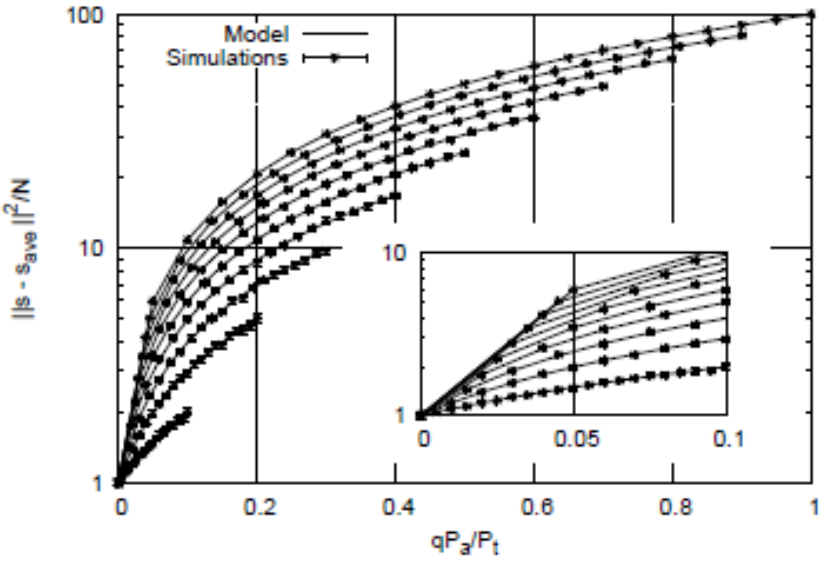

Figure 1: Error power for the Enseble Averging Method

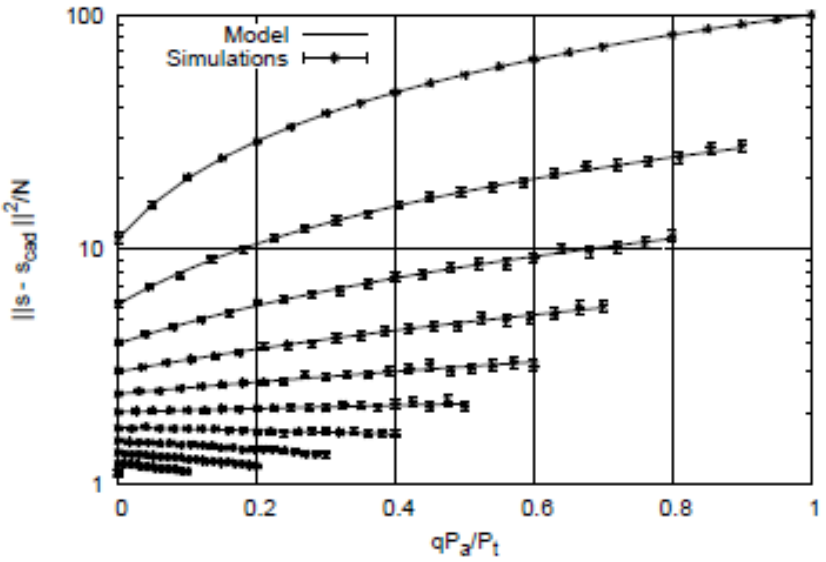

Figure 2: Error Power for the Classification and dropping method

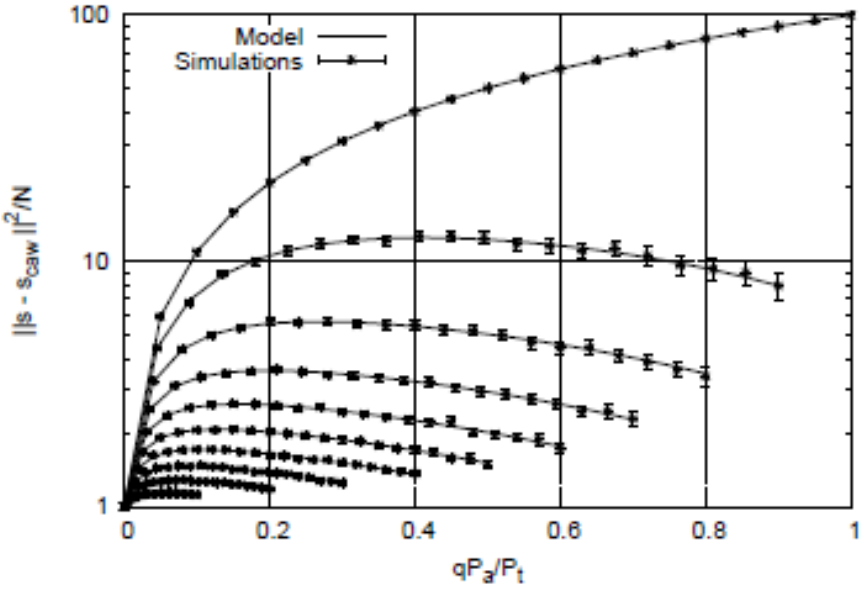

Figure 3 : Error Power for the Classification and Weight Method

The validation results prove that the models describe exactly the performance that the three ERA extraction mechanisms exhibit.

2.2.3 Performance Evaluation

For assessing the performance gain of the Classification and Dropping Method and the Classification and Weight Method over the Ensamble Averaging, we considered another set of simulation based on the parameters in the following table and evaluating the following metrics:

$$G_{cad} = \frac{SNIR_{cad}}{SNIR_{ave}}$$

$$G_{caw} = \frac{SNIR_{caw}}{SNIR_{ave}}.$$

The two gains express the interference reduction that the CAW and CAD methods introduce with respect to the EA method in processing the same datasets of trials. In each condition the optimal value w_L was used.

Fixing the simulation parameters as in the following table:

Parameter Name	Symbol	Parameter Value
Signal Power	P_s	1
Noise and Artifact Power	$qP_a + P_\eta$	100
Number of runs for each configuration	R	500
Sampling Rate	f_s	500 Hz
Artifact Maximum Power	P_a	50
Trial Duration	T	1 s

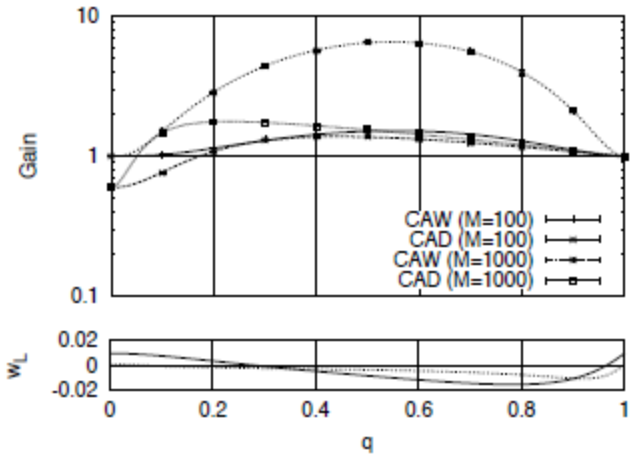

Figure 4: Gain and w_L considering q as variable with $p_{TP} = 0.6$ and $p_{TN} = 0.6$. It is showed the model (lines) and simulation results (errorbars) reported as average values and 99% confidence intervals. The results are shown in the top panel, while in the bottom one the value of the corresponding optimal w_L is shown.

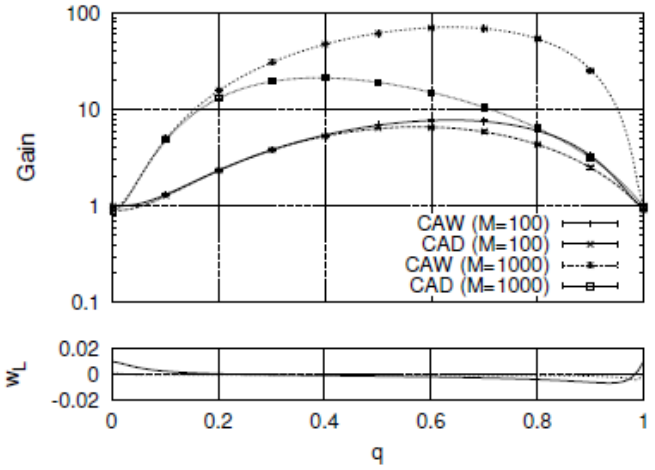

Figure 5: Gain and w_L considering q as variable with $p_{TP} = 0.9$ and $p_{TN} = 0.9$

In this set of experiments we evaluate the gain of CAD and CAW for different values of the artifact occurrence rate q. We consider two conditions for the number of trials: M = 100, the former, and M = 1000, the latter, in order to asses also the impact of such a parameter on attainable results. All the other parameters are configured with the values summarized in the Table.

As shown in figure 5, when q = 0, both CAW and EA outperforms CAD. Indeed, in this configuration the artifact occurrence rate is zero and trials discarding due to the false-positive rate limits the noise reduction of CAD. When q is increased, both CAD and CAW performance improves but, while CAW is always better than EA, CAD becomes better than EA only when the artifact component present across trials becomes sufficiently higher than the noise component. When q = 1, there is no difference between CAW, CAD and EA, since in this configuration the total interference is due to the artifact and there is not gain from one of the methods instead of another.

2.2.4 Estimation and performance in the practical scenario

The aim of this section is to show the performance of the proposed method in the practical scenario where all the parameters needed in the configuration of w_L have to be estimated from the dataset of trials. In this test we simulate the estimation of the ERP activity elicited by a TMS stimulus following the same model previously used.

The values of the simulation parameters for dataset generation and the nominal classifier performance parameters that we assume known are summerized in the following table:

Parameter	Real Value	Estimated Value
M	1000	–
p_{TN}	0.85	–
p_{TP}	0.85	–
q	0.4	0.398
$\mathrm{P_s}$	1	0.99
P_η	6	6.02
$\mathrm{P_a}$	10	9.96
Artifact Window	$30 - 70$ ms	–

In order to apply CAW, we need to determine the optimal w_L that attains the minimum reconstruction error. Hence, we have to fill the model previously used with the classifier performance parameters, p_{TP} and p_{TN}, the power level of noise, P_η, the power level of artifact, P_a, and the artifact occurrence probability, q. Except the classifier performance parameters, all the other parameters have to be estimated from the dataset. This can be realized performing typical steps of real applications. Hence, the noise power P_η is estimated on a signal segment free of artifacts and, in particular, we used a time window preceding the stimulation artifact. The artifact power can be estimated from the distribution of the trials powers. In our dataset, the power levels have a bimodal distribution with peaks at about $P_s + P_\eta$ and $P_s + P_\eta + P_a$. Knowing P_η , P_s and P_a can be estimated. Eventually, the artifact occurrence rate is estimated from the histogram of power levels too. In this test we computed the artifact rate as the cumulative sum of the histogram values corresponding to power levels higher enough $P > P_s + P_\eta + \frac{1}{2}P_a$) to identify trials affected by the artifact. The estimated parameters are reported in previous table. $w_L{}^{\sim}$, the value obtained by using empirical estimated parameters, coincides almost with that w_L^* obtained by using the exact simulation parameters.

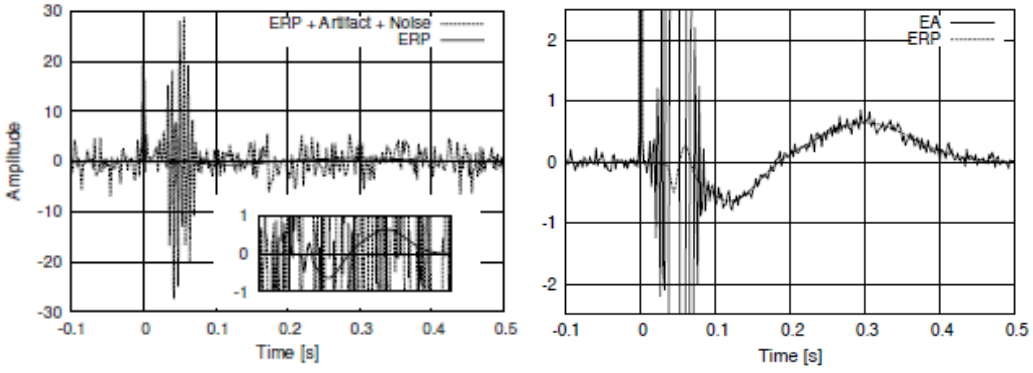

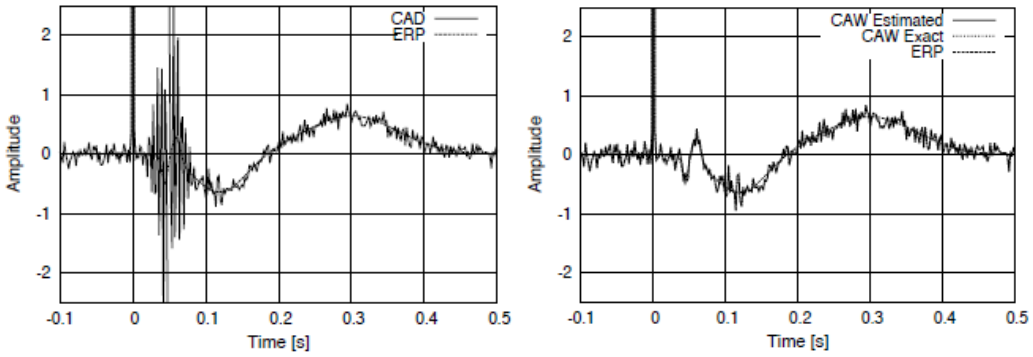

Figure 6: top ERP, artifact and noise (Trial Example) and ERP estimation with the EA Method, bottom:. ERP estimation in CAD and CAW method.

The results obtained in the Event Related Activities (ERA) estimation are shown in Figure 6, where it is possible to see that CAW introduces a reduction in the artifact that is better than that shown by EA and CAD. The cost that CAW pays with respect to EA is a slightly lower noise reduction in the region that is not artifact affected, but this is a cost it is worth to be paid in change of a clean highlight of the small dynamics that the N44 and P60 waves show in our ERP template.

2.2.5 Conclusions

We presented a new method for the extraction of ERAs from multiple trials in the presence of random artifacts and noise. The method relies on general hypothesis on trials generation and it does not make any restrictive hypothesis on ERA, noise and artifacts. The CAW method has been designed to be used in conjunction with practical procedures, as EA and CAD, in the extraction of ERA activities from EEG and electrocardiography (ECG) datasets. The method is analytically modeled, validated and, based on the model, it is optimally configured showing remarkable performance improvement with respect to standard methods. A practical test ends the paper showing the applicability in the data processing when the parameters driving the configuration have to be established from the data itself. The same section shows the robustness of CAW when the real values on which the method relies deviates from the nominal ones, providing the effectviness of CAW in the practical scenario.

2.3 TMS EEG trigger reconstruction

The study of evoked potentials strongly relies on the correct alignment of different segments of the EEG activity. The onsets, i.e. the time latencies of stimuli that allow such an alignment, are usually logged by the acquisition system used in the recording of the EEG activity. Unfortunately, the wrong configuration of the acquisition system or human errors during the acquisition or the storage of data may make this information unavailable. Usually, these errors are discovered during the datasets analysis stage, and this stage can take place even several months after the acquisition of datasets. Unluckily, changes on patients' status and the expensiveness of EEG registrations make unfeasible to repeat the acquisitions.

In this section, we presented and evaluate two mechanisms that we included in an EEGLAB plugin for the automatic reconstruction of onsets in EEG-TMS recordings which is a innovative contribution of this thesis. The methods of the TMS Triggers Reconstruction Software (TRS-TMS) plugin are discussed and evaluated obtaining guidelines for their correct configuration in the routine usage. The first method is based on the detention of the maximum (MAX METHOD) and the second is based on the Shannon Energy and Hilbert Transform (SAH Method).

The signal model behind both methods is the follow:

$$s[n] = \sum_{k=1}^{N_o} t[n - n_k] + \sum_{k=1}^{N_o} e_k[n - n_k] + \eta\,[k]$$

Where $t[n]$ is the stimulus artifact, $e_k[n]$ is the ERP activity by the k^{th} stimulus, $\eta[n]$ is sum of the noise of background EEG and acquisition noise. N_o is the number of stimulation onsets and n_k with k $\in \{1,2,\dots N_o\}$ is the onset of the k^{th} stimulus. Based on real signal characteristics, the following hypotheses can be made on signal components:

- $t[n]$ is a fast varying signal having either or both polarity, high amplitude and small time support. The signal's time support spans in the range of 0.5 -1 ms based on the quality of the stimulation/acquisition system. The spike of the $t[n]$ signal satures or it is close to saturate the acquisition sensor. This signal can be characterized by its shape and its maximum instantaneous power $P_t = E\{t^2[0]\}$;
- $e_k[n]$ is a non-stationary causal process having a power quicky decaying to zero. The vanishing time of the ERP process is a function of subject sensibility to stimulation. Common ERP vanishing times span the range 0.3-0.8 s. The average ERP power of the signal in a

vanishing window, assuming that the distribution of $e_k[n]$ does not depend on k, can be computed as:

$$P_{ERP} = \frac{1}{M} \sum_{n=0}^{M} E\{e_k^2\,[n]\};$$

- $\eta[n]$ is a white Gaussian noise having zero mean and constant power: $P_{NOISE} = \sigma_\eta^2$. The background EEG signal is independent of both the ERP and the ERP and the TMS stimulus signal

The maxima detection method relies on the behaviour of the $t[n]$ signal whose shape is confined in a small time window around the corresponding onset and with a power level that makes it distinguishable along the signal. The algorithm is based on the following steps:

1. the $s[n]$ signal is first filtered by a proper configured band-pass filter. The goal is to remove the baseline and to reduce the noise activity.
2. The filtered signal is thresholded in order to generate a set of candidates onset values. For each window composed of succeeding candidate values, the first sample of the window is marked as an effective onset candidate. Onset candidates are filtered out by a proximity algorithm: starting from the last onset, every candidate onset too close in time to the candidate onset preceding it is suppressed.

The SAH method is composed by the following steps:

1. The $s[n]$ signal is first filtered by a proper configured band-pass filter. The goal is to remove the baseline and to reduce the noise activity.
2. The filtered signal is differentiated in order to emphasize fast waves in the signal: $d[n] = s[n] - s[n-1]$;
3. The differentiated signal is rectified and normalized: $\frac{|d[n]|}{max_n\{|d[n]|\}}$;
4. The Shannon energy envelope is computed as:

$$s_s[n] = -2(d[n])^2 log(d[n])$$

5. The Hilbert Transform of the Shannon Energy is computed in order to detect the stimuli by mean of a zero crossing algorithm.

The methods have been evaluated by means of the positive predictivity, the sensitivity, the jitter. The sensitivity and positive predictivity are:

$$S = \frac{N_{TP}}{N_{TP} + N_{FN}}$$

$$P^{+} = \frac{N_{TP}}{N_{TP} + N_{FP}}$$

Where N_{TP} is the number of true positive, $N_{FN}$the number if false positive, $N_{FP}$is the number of false positive.

The jitter is computed as the root value of the sum of the square errors between the true onset latencies and the estimated ones, computed over all the true positive detected onsets:

$$\Delta = \sqrt{\frac{1}{N_{TP}} \sum_{q=1}^{N_{TP}} \left(n_{kq} - n_{kq}\right)^2}$$

All the powers in the following are expressed in decibels and are referred to the power of the maximum measurable TMS activity, that we fixed equal to $s_{max} = -s_{min}$= 10 V.

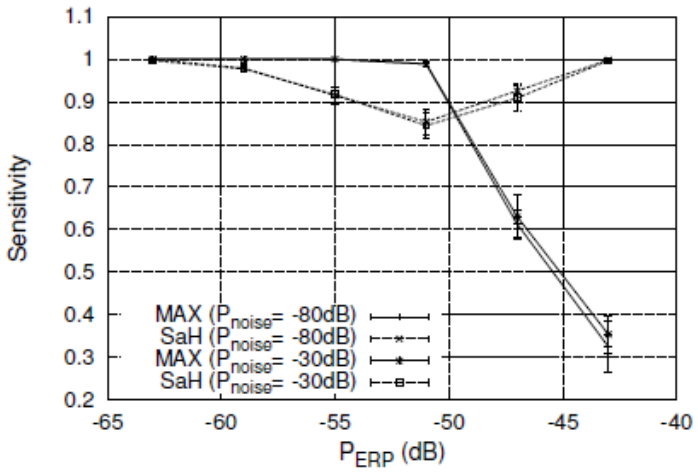

Figure 7: Sensitivity for fixed P_{NOISE}

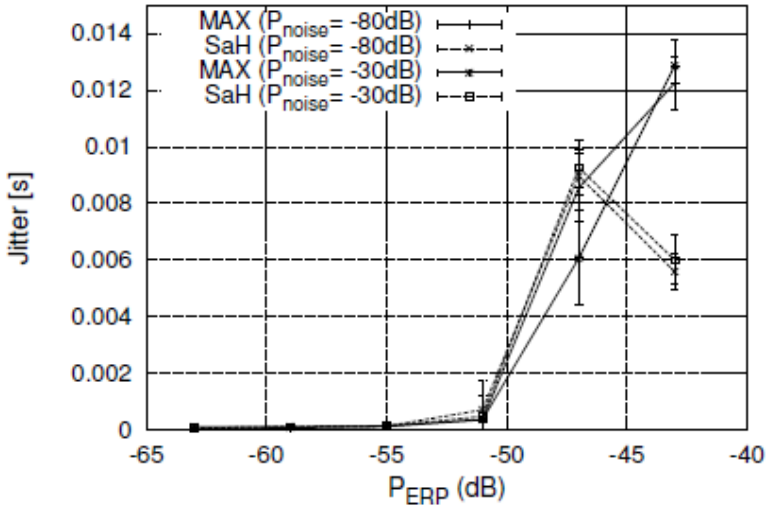

Figure 8: Positive Predictivity for fixed P_{NOISE}

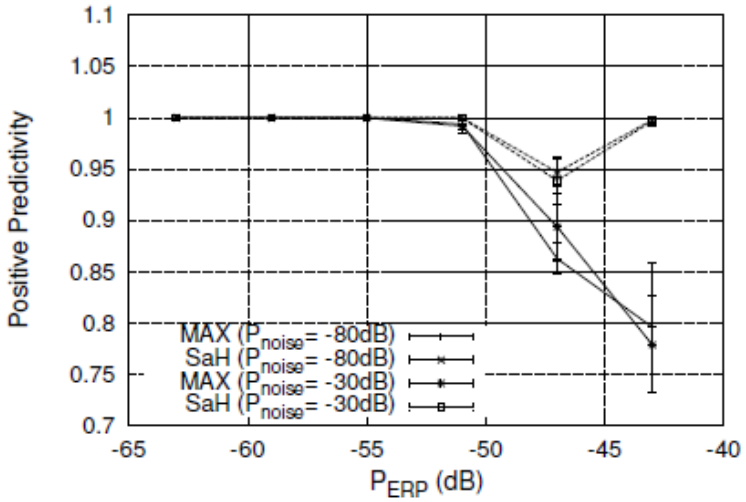

Figure 9: Jitter for fixed P_{NOISE}

Figure 7 shows the sensitivity performance that the two mechanisms provide fixing the background activity either at the smallest or the greater power value and for an increasing level of excitability of the subject, i.e. for an increasing power of ERP activity. Every condition has been repeated 50 times and the results show the average values and the 95% confidence intervals of the estimated figure of merit. We can observe that the performance of both mechanisms do not depend on the level of background EEG activity, while they show a marked dependency on the power of elicited ERP activity. When the ERP has a low power level both mechanisms perform pretty well, while the SaH method is better under low ERP powers while the MAX method is preferable when the ERP power increases.

Figure 8 shows the Positive Predictivity performance that the two mechanisms exhibit (average values and 95% confidence intervals of the figure of merit over 50 simulations).

In all the conditions the SaH method performance are better than those of the MAX method. Hence, the SaH method is better than the MAX method when the false positives may impact in the reconstruction of evoked potentials, as in the case of repeated acquisition close in time and with high power in noise activity.

Eventually, figure 9 shows the performance of the jitter between the true offsets and the estimated ones (average values and 95% confidence intervals of the figure of merit over 50 simulations). When the power of elicited ERP is low, both methods show a low jitter. However, when the power of elicited ERP activity is high, the SaH is preferable if the waves to extract have a time support higher than 10 ms.

In this paper we present and evaluate two mechanisms for the onset reconstruction in EEG-TMS signals available in the TRS-TMS EEGLAB plugin that we developed. Based on a simulated model of continuous EEG-TMS recordings, we evaluated the ability of the two mechanism to correctly identifying the onset of stimuli and the jitter that the reconstruction process introduces. This evaluation constitutes a benchmark in the choice of the mechanism to adopt in a real scenario when the plugin need to be used.

2.4 Channel Interpolation in EEG-TMS: a quantitative study

Channel drops are one of the main problems that can be encountered in TMS EEG studies and that can have an important impact on attainable results. In this section we present an evaluation of interpolation methods in the reconstruction of channels in the context of TMS EEG ERPs which is a innovative contribution of this thesis.

In this section we analyse the inverse distance method (i.e.) and spherical spline method (s.s.). The formulation for the first method (Fletcher et al 1996) is the following.

Let $v_k$be the data value at point p_k, for k = 1,. . . ,N. Let x be the point to be interpolated, and dk be the distance of x to p_k. Let M be the number of nearest neighbors specified. The interpolated signals has the following formulation:

$$H_m(x) = \frac{\sum_{k=1}^{M} \frac{v_k}{m d_k^m}}{\sum_{k=1}^{M} \frac{1}{d_k^m}}$$

The distance exponent m was set to 2 in our study. The number of neighbours M was set to 4.

The spherical spline method has the following formulation. Let s,t be two points on a sphere and $(\cos(s,t))$ be the cosine of the angle between s and t. P_k is the kth degree Legendre.

The interpolated signals has the following formulation:

$$q_m(s,t) = \frac{1}{4\pi}\sum_{k=1}^{\infty}\frac{2K+1}{k^m(k+1)^m}P_k\left(\cos(s,t)\right)$$

m=4, kth degree Legendre polynomial between 1 and 7.

The first database is related to eight healthy young female volunteers (age range, 18–30 years) TMS Single of the left M1. Each session contains 60 TMS trials. Two supra-threshold single pulse (120% resting motor threshold, baseline condition) blocks were registered (n 120 trials in total). The EEG activity was continuously acquired from19 scalp sites using electrodes positioned according to the 10–20 International System. The ground electrode was positioned in Oz in order to have maximal distance from the stimulating coil. The linked mastoid served as the reference for all electrodes. The signal was bandpass filtered at 0.1–500 Hz and digitized at a sampling rate of 2.5 kHz. In order to minimize overheating of the electrodes by the stimulating coil, TMS-compatible Ag/AgCl-coated electrodes were used. Skin/electrode impedance was maintained below 5 kOhm. The second database is related to nine healthy young subjects. The intensity of the TMS was 120% of the rMT. The EEG was recorded with a 60-channel TMS-compatible amplifier (Nextim) continuously throughout the experiments. A total of 120 trials were collected.

Data analysis of the two database was conducted using MATLAB 2009b version 7.9 (MathWorks, Natick, Mass.) and the public license toolbox EEGLAB. TMS evoked EEG-activity, i.e. TMS-evoked potentials (TEPs), were visually inspected in each channel and trials contaminated by environmental artefacts, muscle activity, or eye movement were rejected. Following this procedure, EEG signals of the first database were divided in segments of 3000 ms including a 1000 ms pre-stimulus baseline, baseline corrected (100 ms prestimulus), average referenced and averaged for ach subject; for the second database EEG signals were bandpass filtered between 2 and 80 Hz, divided in segments of 1100 ms including a 200 ms pre-stimulus baseline, baseline corrected (100 ms prestimulus), average referenced, averaged for each subject.

We test the efficiency of the reconstruction methods related to interpolation through the evaluation method for the two database in a time range between 10 ms and 2 s and at fixed latency (100 ms and 300 ms). The performance metric for the evaluation is the norm of the global error, defined as:

error=$\sqrt{\frac{\sum_{i=1}^{n}(s-\hat{s})^2}{n}}$, s is the measured signal from EEG electrodes and $\hat{s}$ is the estimated signal from the two interpolation methods.

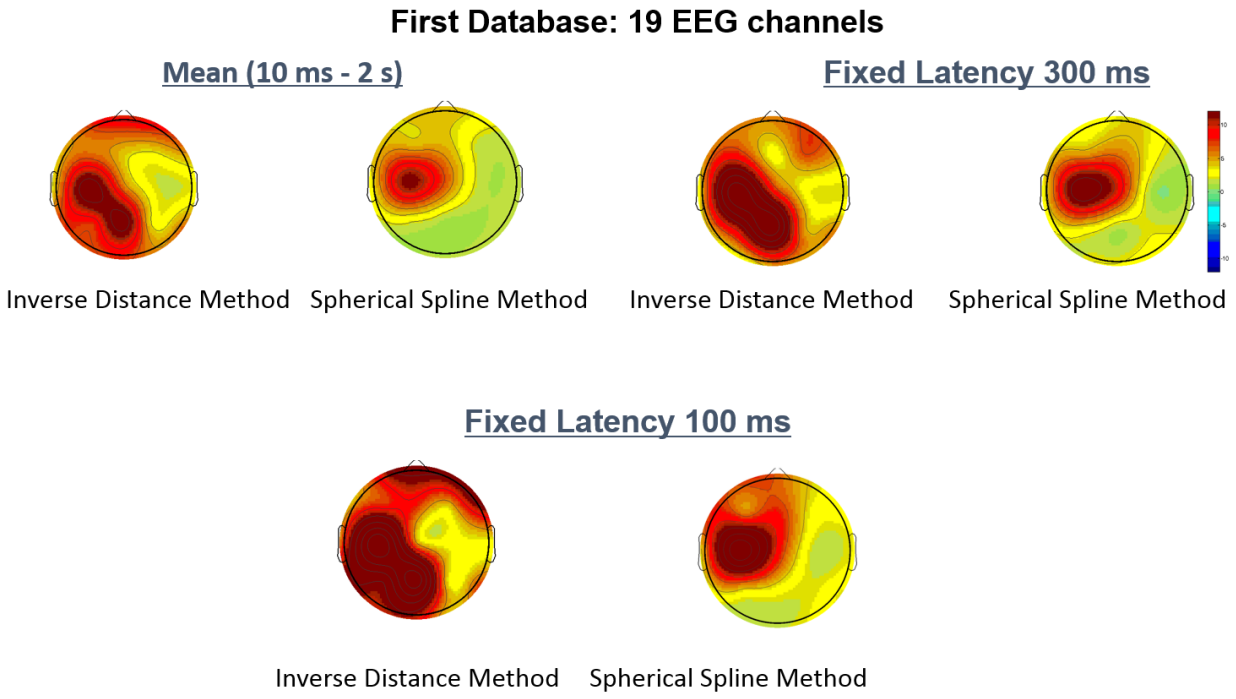

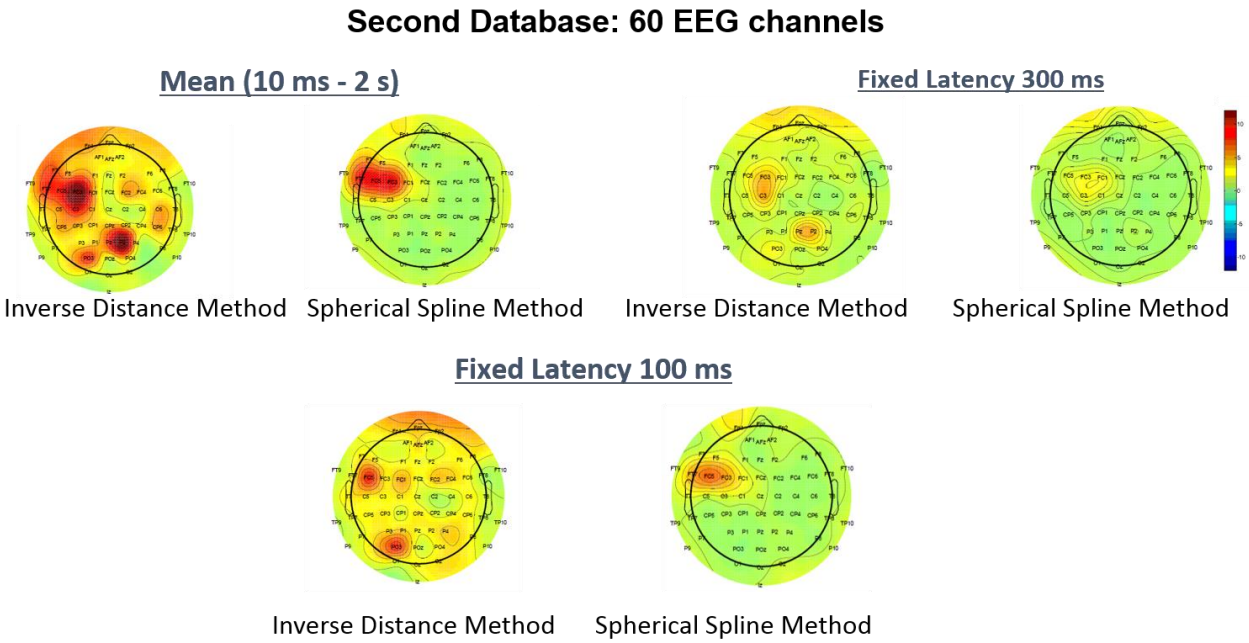

Figure 10: Global error in topographical maps to compare the two interpolation method in the two experimental conditions: top, the 19 EEG electrodes montage, bottom, the 64 EEG electrodes montage.

In figure 10, for the first database the results shows that spherical spline method outperforms the inverse distance method in a time interval between 10 ms – 2s also at fixed latency 300 ms and 100 ms. In the second database the results are the same but there is a better interpolation since the global error is in a smaller brain region.

In conclusion from our study the Spherical Spline Method performs better than the Inverse Distance Method, above all in the case of the second dataset and at fixed latency rather than considering a time interval.

2.5 Source Localization: Inverse Problem Formulation

The study of cortical activity through the analysis of potential EEG presents, therefore, a limit in dependence of the data recorded by the reference employed. Possible variations of the electric potential adopted as a reference for the recording of the potential on the scalp, in fact, can mitigate or obscure some cortical generators, by acting, therefore, as a disturbing factor in space-time. In addition, source imaging has a physiological relevance: it resembles the potential distribution that would be invasively be measured from the cortical surface.

Since EEG signals are an attenuated and distorted measure (caused by the current flow through tissue with different conductivity) of the cortical activity, the inverse problem solution is implement to obtain an accurate localization of the cortical generators of the scalp potential.

In this problem (Astolfi et al. 2005a), the cortical sources to be estimated are related to the noninvasive measurements by means of a transfer matrix (leadfiled matrix) that mimics the effects of the volume conductor. In mathematical terms, the relationship between the modeled source $\boldsymbol{x}$, the lead field matrix $\boldsymbol{A}$, the EEG measurements $\boldsymbol{b}$ and the noise $\boldsymbol{n}$ can be written as:

$$\boldsymbol{Ax} = \boldsymbol{b} + \boldsymbol{n}$$

The solution of this linear system provides an estimation of the dipole source configuration $\boldsymbol{x}$ that generates the measured EEG potential distribution $\boldsymbol{b}$. The system includes the measurement noise $\boldsymbol{n}$, which is assumed to be normally distributed. $\boldsymbol{A}$ is the lead field matrix or the forward transmission matrix, whose jth column describes the potential distribution generated on the scalp electrodes by the jth unitary dipole. The current density solution vector $\boldsymbol{\xi}$ is obtained as:

$$\boldsymbol{\xi} = argmin_x \left(\|\boldsymbol{Ax} - \boldsymbol{b}\|_{\boldsymbol{M}}^2\right) + \lambda^2 \|\boldsymbol{x}\|_{\boldsymbol{N}}^2$$

Where $\boldsymbol{M}$ and $\boldsymbol{N}$ are the matrices associated with the metrics with the data and of the source space, respectevely, λ is the regularization parameter and $\|\boldsymbol{x}\|_{\boldsymbol{N}}$ represents the $\boldsymbol{M}$ norm of the vector $\boldsymbol{x}$. The solution of precedent equation is given in the inverse operator $\boldsymbol{G}$:

$$\boldsymbol{\xi} = \boldsymbol{Gb} \quad \boldsymbol{G} = \boldsymbol{N}^{-1}\boldsymbol{A}'(\boldsymbol{A}\boldsymbol{N}^{-1}\boldsymbol{A}' + \boldsymbol{\lambda}\boldsymbol{M}^{-1})^{-1}$$

An optimal regularization of this linear system is obtained by the L-curve approach. As a metric in the data space was used the identity matrix, whereas as a norm in the source space is used the following metric:

$$(\boldsymbol{N}^{-1})_{ii} = \|\boldsymbol{A_i}\|^{-2}$$

Where $(\boldsymbol{N}^{-1})_{ii}$ is the ith element of the inverse of the diagonal matrix $\boldsymbol{N}$ and all the other matrix elements $\boldsymbol{N}_{ij}$ are set to 0. The L_2 norm of the ith column of the lead field matrix $\boldsymbol{A}$ is denoted by $\|\boldsymbol{A}_i\|$.

Noise estimation (automatically calculated) is subsequently used to determine the sensor weighting and the regularization parameter (λ) of the current density reconstruction. The inverse problem solution is usually implemented using a Boundary Element Model (He et al., 1987; Hämäläinen & Sarvas, 1989) of the head having 3 compartments of fixed conductivities (scalp: 0.33 S/m; skull: 0.0042 S/m; brain: 0.33 S/m).

2.6 Dynamical Connectivity evaluation technique: Network analysis and Non Invasive Brain Stimulation (NIBS)

NIBSs are tools daily used to improve human performance on a wide variety of tasks. The underlying mechanisms of such enhancement are still poorly understood. To advance the understanding on these mechanisms it is necessary to focus on intrinsic *network dynamics* of the brain.

TMS changes neural activity directly in a spatially and temporally manner. By studying how the changes induced by TMS are then propagated through the rest of the brain, the connectivity of the stimulated brain region can be causally accessed and the results compared with the findings of the traditional analysis. Because neuroimaging data are amenable to functional connectivity and network analysis techniques, the combination with brain stimulation techniques permits the study of the effects of these techniques on widespread networks composed of a number of different cortical regions.

By virtue of recent developments in technical instrumentation and analysis, as can be seen in the TMS-EEG field, concurrent recordings have become not only possible but also very appealing. This research topic shows how we can now measure and analyze brain activity with these combined methods to probe the neural dynamics, brain state, excitability, plasticity, networking, and information flow in the intact brain (Kitajo et al 2015).

A promising technique to evaluate the connectivity is the following: the analysis can be performed using adaptive Directed Transfer Function (aDTF, see Wilke et al 2008 as reference) through the use of a multivariate adaptive autoregressive model to study the time-variant propagation of TEPs in terms of activated cortical areas connections. The application of this time-varying connectivity estimator to TMS EEG signals is an original contribution of this thesis. It is a method to extract the directional information flow between EEG electrodes or Region of Interest (ROIs) using time-varying coefficient to obtain the connectivity information instantaneously in a time period of interest.

A Multivariate Adaptive Autoregressive (MVAAR) model can be constructed and used to describe the dataset composed by data vector over time.

$$X(t) = \sum_{i=1}^{p} \Lambda(i,t)X(t-i) + E(t) \quad \text{Eq.(1)}$$

Where $X(t)$ is the data vector over time (EEG electrodes or ROIs), $\Lambda(i,t)$ are the matrices of time-varying model coefficients, $E(t)$ is multivariate independent white noise and p is the model order. The time-varying coefficient matrices by the Kalman filter algorithm which describes the behavior of the

multivariate signals by the observations equation i.e. Eq.(1) are described the following state equation:

$$\Lambda(i,t) = \Lambda(i,t-1) + V(i,t-1) \quad \text{Eq.(2)}$$

The time-varying modeling makes it possible to calculate these parameters instantaneously (Arnold et al 1998). The observation and state equations of this algorithm can be solve by the recursive Least Squares (RLS) algorithm with forgetting factor. The optimum order for the model can be determined by the Schwarz Bayesian Criterion (SBC).

The Direct Transfer Function (DTF) function, *H*(*f*), can be obtained from the MVAR model and is described by transforming Eq.(1), where Λ is a function of *t*, into the frequency domain. The DTF is computed by:

$$\Lambda(f)X(f) = E(f) \; where \; \Lambda(f) = \sum_{k=0}^{p} \Lambda_k \, e^{-j2\pi f \Delta t k} \quad \text{Eq.(3)}$$

$$X(f) = \Lambda^{-1}(f)E(f) = H(f)E(f) \quad \text{Eq.(4)}$$

where $\Lambda_{k=0}$=I. Since it is possible to characterize the time-varying model coefficients, Λ(*i*,*t*), the function *H*(*f*,*t*) can thus be obtained from the time-varying transfer matrix. Its elements, *Hij*, represent the connection between the jth and ith elements of the system for each time point *t*. Similarly to the DTF function in Eq. (4), the normalized ADTF is defined by the elements of the transfer matrix in the spectral domain, which describes the directional causal interaction from the jth to the ith element as:

$$\gamma_{ij}^2(f,t) = \frac{\left|H_{ij}(f,t)\right|^2}{\sum_{m=1}^{n}|H_{im}(f,t)|^2}$$

In order to evaluate the total information flow from a single node, it is possible define the so-called integrated ADTF by summing the ADTF values over the frequency bands of interest. The integrated ADTF over the frequency bands is normalized to be between (0,1).

$$\Theta_{ij}^2(t) = \frac{\sum_{k=f_1}^{f_2} \gamma_{ij}^2(k,t)}{f_2 - f_1}$$

The total information outflow from each node is further given by summing across subscript i for each jth node and is normalized by dividing by the number of outflow nodes:

$$\Theta_j^2(t) = \frac{\sum_{k=1}^{n} \Theta_{kj}^2\,(t)}{n-1}$$

The aDTF that measures both direct and indirect paths of connections in form of matrix ADTF (t,i,j,f) indicates the dynamic information flow from region of interest (ROI) or to ROI i at frequency f at time instant t. aDTF (t,i,j,f) is expressed as the percentage of power of the current density from region of interest (ROI) or to ROI i due to the current density in the ROI j (normalized aDTF).

The outflow of each ROI is the summation of information flow from this ROI to all the other ROIs calculated as the outflow from ROI j to i divided by the outflow from the ROI i to all the other ROIs (normalized aDTF).

Similarly, the inflow of each ROI counts the total inflow from all the other ROIs calculated as the inflow from ROI j to i divided by the inflow in the ROI i from the other ROIs (normalized aDTF).

In Babiloni et al 2005b is proved from a simulation study a substantial equivalence of the estimate connectivity patterns computed with the different model orders p.

There is a statistical influence of a variable Signal to noise Ratio (SNR) level imposed on the high resolution EEG data on the accuracy of the connectivity pattern estimation obtained by DTF. However, a SNR equals to 3 seems to be sufficient to obtain a good accuracy, since higher values do not show a significant improvement in the performances. Usually the average noise level is blow 1 μV (Supplementary Material Massimini et al 2005).

Furthermore, errors in amplitude estimation of the cortical current density are systematic along the time course of the estimated data, due to the time independence of the linear inverse operator G that maps recorded data b onto the cortical activity. This means that the connectivity errors will be systematic along all the scalp data provided. Therefore, these connectivity patterns induced by erroneous cortical estimates will be present also during the procedure of the shuffling, that is used to generate the probability distribution of the null hypothesis. This will raise the statistical threshold computed for such patterns, increasing the protection against the appearance of connectivity patterns related to the inaccuracies of the cortical waveforms estimation. (Astolfi et al 2005a).

In Chapter 4 an original contribution will be presented on TMS EEG analysis applied on both the right and left M1 area in the evaluation of cortico-cortical connectivity in a population of healthy subjects after the inverse problem solution. In particular, the aDTF is used as estimator to evaluate the connectivity between the areas activated during the TEPs.

2.7 Time domain indices of TEPs

Main indices in the analysis of TMS EEG ERP signals in the time domain follow:

Global Mean Field Power (GMFP): In TMS EEG total EEG activity can be calculated as:

$$GMFP(t) = \sqrt{\frac{[\sum_i^k V_i(t) - V_{mean}(t)^2]}{K}}$$

where *t* is time, *K* the number of channels, *V*i the voltage in channel *i* averaged across subjects and *V*mean is the mean of the voltages in all channels. Peaks were identified as local maxima that exceeded three times the standard deviation of the prestimulation activity. Corresponding peaks in individual subjects can be chosen as the maximum or minimum value occurring within 10 ms of the grand average peak (Esser et al 2006).

Significant current density (SCD): is expressed in units of microampere per square millimiter and represents the sum of the absolute amplitude of all significant TMS-evoked currents observed over a given time interval σ and/or cortical region s which where identifed with a non parametric statistical procedure. Starting from the spatio-temporal distribution of statistically significant source $SS(x_j, t)$ the SCD is defined as:

$$SCD_s(t) = \sum_{x \in S} SS(x_j, t) \left| j_0 \ (x_j, t) \right|$$

$$SCD_\sigma(tx_j) = \sum_{t \in \sigma} SS(x_j, t) \left| j_0 \ (x_j, t) \right|$$

$$SCD_{s\sigma} = \sum_{x \in S} \sum_{t \in \sigma} SS(x_j, t) \left| j_0 \ (x_j, t) \right|$$

Therefore, SCDsσ is a single number representing the absolute total current of the sources significantly activated by TMS pulses in a cortical volume s and time interval σ. $\left| j_0 \ (x_j, t) \right|$ is the average cortical response after source modelling

Significant current scattering (SCS): is calculated as the sum of the geodesic distance ($d(x_j)$in mm) between the stimulated region and any significant current source over a given time interval σ and cortical volume s. This index captures the spatial spread of TMS-induced currents to distal brain

regions, growing proportionally larger as significant TMS activations spread away from the target area (Casali et al 2010). It is defined as:

$$SCS_s(t) = \sum_{x \in S} SS(x_j, t) d(x_j)$$

$$SCS_\sigma(x_j) = \sum_{t \in \sigma} SS(x_j, t) d(x_j)$$

$$SCS_{s\sigma} = \sum_{x \in S} \sum_{t \in \sigma} SS(x_j, t) d(x_j)$$

Perturbational Complexity Index (PCI) gauges the amount of information contained in the integrated response of the thalamocortical system to a direct perturbation. The idea is that the level of consciousness could be estimated empirically by perturbing the cortexto engage distributed interactions and measuring the information content of the ensuing responses by algorithmic compressibility ("zipping") (Sarasso et al 2014).

2.8 Frequency domain indices of TEPs

Main indices in the analysis of TMS EEG ERP signals in the frequency domain follow:

Event related spectral perturbation (ERSP): measures the modulation of amplitude induced by a specific event (e.g., TMS pulse), relative to a baseline (e.g., prestimulus condition). In particular, the baseline amplitude spectra values of the EEG preceding the event (TMS pulse) can be measured for each trial. Next, the amplitude spectra (event-related spectral perturbation) values of the evoked responses (EEG recorded after TMS) can be calculated, and the average baseline spectra value can be subtracted from all amplitude values. This procedure can be repeated for each trial included and single-trial event-related spectral perturbation values can be averaged across all trials in order to compute the mean event-related spectral perturbation (Ferrarelli et al 2008).

Inter-trial coherence (ITC): or more precisely, inter-trial phase coherence, introduced as 'phase-locking factor' by Tallon-Baudry et al. (Tallon-Baudry et al, 1996), measures the degree of consistency, across trials, of the phase of the best-fitting time/frequency basis element at each latency/frequency point (Johnson et al 2012).

3 TMS and TMS EEG Clinical applications

Introduction

This chapter collects results of studies on single subjects and groups. These results represent examples of personal and original results in the fields of TMS EEG data analysis. Moreover, these studies are also examples of the great power of TMS EEG in the characterization of brain disorders.

3.1 Unilateral cortical hyperexcitability in congenital hydrocephalus: A TMS study

The goal of this study is the characterization of excitability in a caucasian ambidextrous, 40 years old woman admitted to our department of neurology for a congenital occult spina bifida and a congenital symmetrical hydrocephalus (her skull's diameter at birth was above normal limit). During first years of life, the psychological and somatic development of the subject had been normal, except for delayed walking at the age of 2 years. At that time, radiography of vertebral spine had evidenced the presence of spina bifida. During childhood, she presented further walking and balance disturbance and was submitted to intense rehabilitation, gaining a good functional outcome and becoming able to walk autonomously. At the age of 20 years old the patient underwent breast surgery for a mastopathy. During hospitalization, she took a cerebral computed tomography (CT) scan that showed "*moderate hydrocephalus. Absence of signs of trans ependymal absorbance. These characteristics suggest a congenital hydrocephalus. The presence of cranium bifidum has to be noted*". Being asymptomatic, the patient did not take other cerebral scans until an episode of sinusitis and was advised by an otorhinolaryngologist to undergo a spiral CT scan of facial bones. It showed as collateral finding a "*very severe triventricular hydrocephalus with prevalent dilatation of left lateral ventricle*", suggesting a progression of the evidenced hydrocephalus in spite of a steady clinical condition. She then underwent a control magnetic resonance imaging (MRI) that showed "*triventricular hydrocephalus with colpocephalic appearance of lateral ventricles.*

There is neither evidence of trans-ependymal absorbance of cerebrospinal fluid nor evidence of atresia of Sylvian fissure. The presence of cingulated gyrus allows to interpret the partial representation of posterior parts of corpus callosum as a consequence of a destructive event with consensual dilatation of lateral ventricles" .

When admitted to our department the patient complained often headaches with migraine features and a slight laming. She had a high scholar level (university) and had a responsibility position at work. Moreover, she currently speaks seven languages, at least two of them acquired before 6 years of age.

Her neurological exam evidenced: no mental status impairment, normal cranial nerves with monocular vision for a previous retinal hemorrhage, slight strength deficit of muscles of left lower limb against resistance (4+/5), symmetrical tendon reflexes of upper and lower limbs, presence of Babinski sign bilaterally, no sensory deficit, good performance in coordination and balance tests, no nystagmus.

During hospitalization she also underwent complete neuropsychological evaluation that evidenced normal performances in all cognitive areas tested.

The protocol of the study was approved by the appropriate institutional ethics committee and the proband gave her written informed consent, according to the declaration of Helsinki. The handedness of the subject was determined by means of the Italian version of the Edinburgh Handedness Inventory.

3.1.1 Transcranial magnetic stimulation

The patient underwent to TMS examination in three different sessions, each with 1 week interval. In order to examine deeply some parameters of motor cortex physiology, we employed the intracortical-paired pulse (PP) paradigm, the interhemispheric PP paradigm and the mapping technique.

The stimulator used was a Magstim 200 mono pulse connected to a bistim module (Magstim Company Limited, Dyfed, UK) and to figure-of-eight coil with internal wing diameters of 7 cm. The peak magnetic field produced by such coils was 2.0 T.

The motor evoked potentials (MEPs) of the hand muscle were recorded from the abductor digiti minimi (ADM) muscle. Two Ag-AgCl surface cup electrodes of 9 mm diameter were used: the active electrode was firmly taped over the muscle belly, while the reference electrode over the metacarpophalangeal joint of the little finger after gentle skin cleaning and conductive jelly application in order to lower skin-electrode conductance to less than 10 kΩ. Signal recording was carried out using PHASIS equipment (Esaote Biomedica channels) via 1–2000 Hz filter setting, and a poststimulus analysis time of 50ms with a 5kHz sampling rate. The most effective point (hot spot) on the subject's scalp for eliciting a ADM stimulation was localized by positioning the coil so that the junction region of the figure-of-eight coil was approximately over the central sulcus, and moving

the coil in 1 cm steps. The hot spot was defined as the point from which stimuli at the minimal excitability threshold of TMS triggered MEPs of maximal amplitude and minimal latency in the target muscle. The hot spot position was marked (on a transparent and adherent elastic cap) to facilitate an exact coil re-positioning during the entire experiment. Immediately after the definition of the effective hot spot, motor threshold at rest was determined.

The proband was ever tested while lying supine in a bed, fully relaxed, with very dim light and minimal verbal interactions, in order to facilitate complete muscular relaxation and reduce possible influences on cortical excitability. Motor thresholds (MTs) were measured according to international guidelines as the stimulator's output able to elicit reproducible MEPs (>50 μV in amplitude) in about 50% of 14 consecutive stimuli. Amplitudes of MEPs were measured between the two major and stable peaks of opposite polarity. MTs were assessed before each of the sessions (intracortical PP paradigm, interhemispheric PP paradigm and mapping technique).

3.1.2 Intracortical PP technique

According to the intracortical PP, two magnetic stimuli were delivered in close sequence to the motor cortex through a single stimulating coil. Thus, the effect of a conditioning stimulus (CS), delivered on the motor cortex on the MEP amplitude evoked in the contralateral ADM muscles by a magnetic test stimulus (TS) applied to the same cortex, was assessed. The stimulus intensity for the first, conditioning pulse was set at 80% of the rest motor threshold. The second pulse (TS) was given suprathreshold with an intensity of 120% of the rest motor threshold. We selected interstimulus intervals (ISIs) of 1, 2, 3, and 5 ms to test ICI (intracortical inhibition), while ISIs of 7, 9, 11, 13, 15 and 17ms were studied to test ICF (intra-cortical facilitation). The same procedure was repeated twice for each of the hemispheres.

Six responses per condition, both test and conditioning pulses, were collected and their peak-to-peak amplitude was measured off-line and, subsequently, averaged. Paired stimuli with different ISI were randomly mixed with single suprathreshold stimuli. Changes in MEP amplitudes, as a consequence of conditioning pulse administration, were expressed in terms of the ratio between conditioned (preceded by conditioning pulse) and unconditioned responses. The position of the coil was kept constant throughout each stimulation block, and the level of EMG was monitored in order to check that the muscles were maintained relaxed. The whole session lasted about 1.5 hours.

3.1.3 Interhemispheric PP technique

One week later, the proband underwent to the interhemispheric PP technique by means of two magnetic stimulators (coils) to investigate the effect of a CS over the motor cortex of one hemisphere on the size of MEP evoked in the ADMmuscle by a TS given over the opposite homologous hemisphere. The intensity of both the CS and TS was set at 120% of the individual resting MT. Also in this case, several ISIs were assessed (2, 4, 6, 8, 10, 12, 14, 16, 18, 20 ms) centred around ISI 12 where the greatest inhibition can be observed. The same procedure was repeated twice for each of the hemispheres. Six responses per condition, both CS and TS, were collected and their peak-to-peak amplitude was measured off-line and, subsequently, averaged. Paired stimuli with different ISI were randomly mixed with single suprathreshold stimuli. Changes in MEP amplitude, as a consequence of conditioning pulse administration, were expressed in terms of the ratio between conditioned (preceded by conditioning pulse) and unconditioned responses. The position of the coil was kept constant throughout each block of stimulations, and the level of EMG was monitored in order to check that the muscles were maintained relaxed. The whole session lasted about 2 hours.

3.1.4 Mapping technique

Mapping session was carried out 1 week after interhemispheric PP session. The muscles ADM and extensor digitorum communis (ECD) which are known to share the same "hot-spot" and excitability threshold were examined in order to map motor cortex. Stimulus repetition rate was 0.1–0.2 c/s with a stable intensity 10% above the resting MT.

In order to map out the motor cortex representation on the scalp, subjects wore a tight elastic cap depicting a grid of 49 numbered squares. The cap was taped in a stable position with respect to scalp anatomical landmarks (nasion, inion, vertex, metal foramina). Square n.1 of the grid corresponded to the designated hot-spot and the remaining squares were subsequently numbered in a spiral fashion and were tested in a random sequence.

Twelve consecutive MEPs were gathered from each grid position, four at rest, four during contraction and four during motor imagery (imagination of the movement of dorsiflexion of the wrist and abduction of the little finger). In order to maintain alertness, subject was often verbally encouraged

to stay awake. A complete procedure was carried out for each hemisphere with a total of 1176 stimuli (12 stimuli for 49 position for two hemi-scalps), the whole session lasting around 1.5 hours.

3.1.5 Statistical analysis

Descriptive statistics were calculated for each parameter of cortical excitability of the proband. Moreover, for both intracortical and interhemispheric PP techniques, a statistical comparison was carried out between the two hemispheres. More specifically, in the intracortical PP session a t-test was calculated for each ISIs on the MEP ratios between conditioned and unconditioned responses for left (LH) versus right (RH) hemisphere (1, 2, 3, 5, 7, 9, 11, 13, 15, 17 ms), while in the interhemispheric PP session the same analysis was done on the studied ISIs (2, 4, 6, 8, 10, 12, 14, 16, 18, 20 ms).

3.1.6 Results

The mean motor thresholds (percentage of maximum stimulator output) of corticospinally mediated responses evaluated across the three experimental sessions were 34.33% ($\pm$ 1.15) of stimulator output for the RH and 35.67% ($\pm$ 0.67) for the LH. The values of motor thresholds were within normal limits for absolute values and interhemispheric differences.

Regarding the **intracortical PP technique**: the comparison between the two hemispheres (Figure 2), showed significant differences at several ISIs. More specifically, an absence of inhibition was observed in the classical inhibitory ISIs; the ISI 1 was statistically different between the hemispheres ($t = -43.593$; $p = .00003$), indicating a loss of inhibition for the RH with respect to the LH (that showed a limited but effective inhibition), and a similar effect with the same trend was observed also for ISI 2 ($t = -7.538$; $p = .005$) and 3 ($t = -6.424$; $p = .008$).

An increase of facilitation in the RH was also observed in some excitatory ISIs. At ISI 9 the response of RH was significantly higher than that of the LH ($t = -3.743$; $p = .03$), and a similar effect was seen at ISI 11 ($t = -3.702$; $p = .03$) and 13 ($t = -3.898$; $p = .03$).

Concerning the **interhemispheric PP technique**:

the comparison between the two hemispheres (Figure 3), showed significant differences at several ISIs. More specifically a general hyper-excitability was observed on RH (when conditioned by LH) and a general hypo-excitability in the LH (when conditioned by RH). The ISI 2 ms showed a statistically significant difference between the facilitation of RH and the inhibition of the LH ($t = -3.037$; $p = .04$); a similar effect was seen at ISI 4 ms ($t = -3.821$; $p = .02$), 6 ms ($t = -2.825$; $p = .04$), 8 ms ($t = -7.481$; $p = .002$) and 12 ms ($t = -3.103$; $p = .03$).

Concerning the **mapping technique**:

results of mapping procedure showed that the number of scalp sites from which it was possible to evoke a MEP was very different between the two hemispheres.

On RH, MEPs were evoked from 13 grid positions at rest, 26 positions during contraction and 16 positions during motor imagery; conversely, on LH MEPs were evoked, respectively, from 5, 16 and 6 grid positions. These results support the evidence of an asymmetric RH change of excitability.

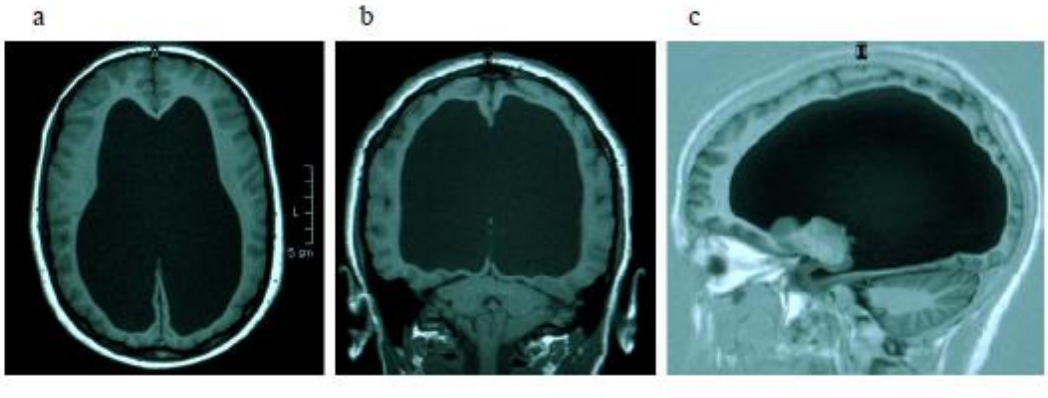

FIGURE 1 Patient's Magnetic Resonance Images, respectively in axial (panel a), coronal (panel b) and sagittal (panel c) section. A severe symmetric hydrocephalus is evident

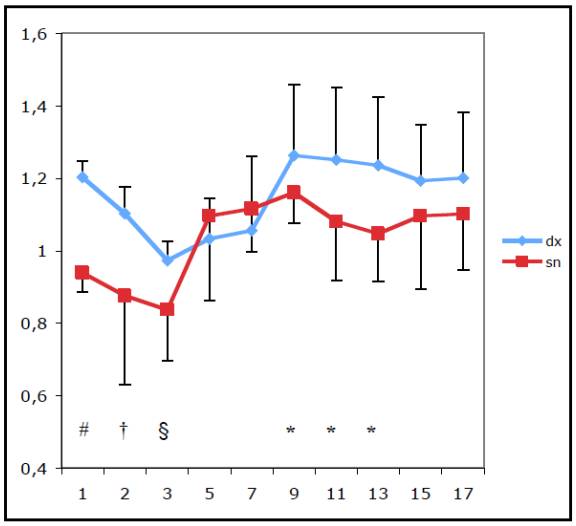

FIGURE 2 Intracortical PP curves for each hemisphere. On axis x are shown the different inter-stimulus intervals (ISI) tested; on axis y there are changes in MEP amplitude (ratio to resting motor threshold). [#: p= 0.00003; †: p= 0.005; §: p= 0.008; *: p= 0.03]

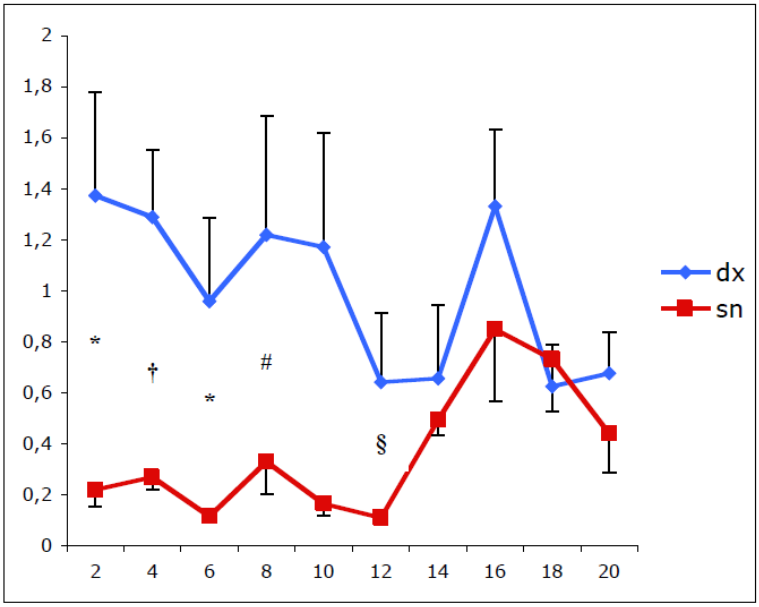

FIGURE 3 Interhemispheric inhibition-facilitation PP curves for each hemisphere. On axis x are shown the different inter-stimulus intervals (ISI) tested; on axis y there are changes in MEP amplitude (ratio to resting motor threshold). [#: p= 0.002; †: p= 0.02; §: p= 0.03; *: p= 0.04]

3.1.7 Discussion

In the described case of patient affected by symmetric arrested hydrocephalus and disruption of the posterior half of the corpus callosum, and almost no neurological sign, the analysis of the intracortical paired-pulse curves showed a significant inter-hemispheric asymmetry.

In the same vein, interhemispheric curves showed a clear decrease of transcallosal inhibition from left-to-right motor cortex, as compared to that from right-to-left one. These findings highlight the selective hyper-excitability of the right hemisphere, which is further confirmed by the mapping technique evidences: primary motor cortex showed a remarkable interhemispheric change in map size with an increased amount of excitability in RH with respect to LH.

It is noteworthy that an asymmetric right hemisphere (RH) change of excitability was observed by means of mapping technique. We hypothesize that in this ambidextrous subject, the observed RH hyper-excitability could represent a mechanism of plasticity to preserve functionality of specific brain areas possibly devoted to some special skills, such as multilingualism.

3.2 Neurophysiological features of motor cortex excitability and plasticity in Subcortical Ischemic Vascular Dementia (SIVD): a TMS mapping study

In this study, data from representative groups of 9 AD patients (9 women; aged 74.3 years; MMSE 21.1), 9 healthy subjects (3 men and 6 women; aged 75 years; MMSE 28.2) and 7 SIVD patients (2 men and 5 women; aged 78.1 years; MMSE 20) are evaluated for comparative analysis.

AD patients were recruited according to the National Institute of Neurological and Communicative Disorders and Stroke−Alzheimer's Disease and Related Dementias Association criteria for a diagnosis of possible or probable AD. No clinical evidence of motor disturbances was found in any of the patients after detailed neurological evaluation. SIVD patients satisfied modified clinical and brain imaging criteria for probable diagnosis of VaD of the NINDS-AIREN criteria and fitted with the more recent proposed clinical criteria for the diagnosis of SIVD. In some SIVD patients, the clinical examination showed some mild neurological signs such as dysarthria, mild apraxic gait and inconstant dysphagia; however, patients with reduced hand or upper limb motor strength were not

included to the study. Hand motor strength was evaluated by means of a rating scale derived from the Medical Research Council (MRC) scale.

To characterize the symptoms of Alzheimer's and vascular dementia patients underwent neuropsychological testing, including (I) The mental deterioration battery (MDB) consisting of 7 parts: the Rey's 15 words immediate and delayed recall, word fluency, sentence construction, Raven's progressive matrices '47, immediate visual memory, freehand copying of drawings and copying drawings with landmarks; (II) The Prose memory test; (III) The Corsi block-tapping task; (IV) The mini mental state examination (MMSE) scores; and (V) The trail-making test part A and B. They also underwent a functional evaluation (Instrumental Activity of Daily Living scale), evaluation of affective symptoms, magnetic resonance imaging (MRI) and laboratory screening to rule out other causes of dementia than AD or SIVD.

Neither the patients nor the controls had ever suffered from epilepsy or were taking drugs, which are known to influence corticospinal excitability. None of the demented patients was medicated with acetylcholinesterase inhibitors. The international safety standards for TMS were taken into account, patients with metallic prosthesis or fragments in the cranial and thoracic districts, tinnitus, previous retinal detachment, brain hemorrhage, clinical evidence of motor deficits were not accepted to the study. The study was approved by the local ethical committee and subjects and caregivers provided informed written consent.

The TMS procedure was performed with the subject lying supine on a bed to facilitate complete muscular relaxation. Two muscles, namely the extensor digitorum communis (ECD) and abductor digiti minimi (ADM), which are known to share the same motor representation area and motor threshold during scalp were examined (from each arm) bilaterally via Ag/AgCl disks filled with conductive jelly in a belly/tendon montage were examined (from each arm) bilaterally via Ag/AgCl disks filled with conductive jelly in a belly/tendon montage. Skin/electrode resistances were less than 10KΩ.

Recording of electromyography was conducted using PHASIS equipment (4 channels; Esaote-Biomedica) via 1 to 2,000Hz filter setting, and a post-stimulus analysis time of 50 ms with a 5 kHz sampling rate.

TMS was conducted using MAGSTIM 200 equipment (Magstim Company Limited, Whitland, South West Wales) and an eight-shaped coil with an inner diameter of 70 mm for each wing. To locate the stimulation spots on the scalp the subjects wore a tight elastic cap, that was fixed according to scalp

anatomical landmarks (nasion, inion, meatal foramina and vertex, where Cz was located using the international 10-20 system). A hypothetical motor area was mapped with TMS at supra-threshold intensity (approximately 80% of maximal stimulator output) by averaging approximately four stimuli each at various stimulation points.

The stimulation location with the highest muscle response was chosen as provisional hotspot and there the motor threshold intensity was determined, according to international guidelines, as the stimulator's output able to elicit reproducible MEPs (at least 50 μV in amplitude) in 50% of 10 to 20 consecutive stimuli. After that the sites adjacent to this provisional hot-spot were stimulated with an intensity 10% above the threshold in order to exclude the possibility that any more consistent or larger responses could be obtained. If any higher responses occurred the threshold was again determined at that point and the procedure was repeated. Once identified the definitive hotspot, defined as the point from which stimuli at the minimal intensity of TMS triggered MEPs of maximal amplitude and shortest latency, we placed on the cap a grid of 49 numbered squares of 1 cm each side, 7 by 7 matrix.

Square in the center of the grid corresponded to the designated hot-spot and the remaining squares were subsequently numbered in a (spiral) concentric fashion and tested in a random sequence for each hemiscalp (Figure 4). Stimulus repetition rate was 0.1 to 0.2 c/s with a stable intensity 10% above subjective excitability threshold. Four consecutive MEPs were gathered from each grid position at rest. To maintain alertness, we frequently encouraged the subjects verbally to stay awake. A complete procedure was performed for each hemisphere with a total of 392 stimuli (4 stimuli for 49 positions for two hemiscalps), the duration of the entire session being approximately 90 minutes. The motor cortex excitability was studied by the motor thresholds, the area of muscle representation and the volume of active cortical sites for each examined muscle with a stable intensity 10% above subjective excitability threshold. For the motor cortex plasticity the coordinates of the hot-spot and the center of gravity for each examined muscle were evaluated.

3.2.1 Data Analysis

The raw data file comprised 4900 rows: 25 subjects by 49 scalp positions by 4 repetitions. Amplitudes of MEPs were measured peak to peak between the two stable major peaks of opposite polarity. Variables consisted are the MEPs amplitude and latency values of each hemisphere for both muscles (ADM and ECD), resulting in four data columns. Amplitudes were log-transformed to better approximate the Gaussian distribution. When the MEP was not measurable, log-amplitude was

arbitrarily set to 0 (corresponding to an amplitude of 1 μV). An initial data aggregation was made taking the arithmetic mean of the four repetitions for each scalp position (corresponding to the geometric mean of the untransformed amplitude values). Successively, a new data file was created in which each subject was characterized each hemisphere by:

(1) the area of muscle representation, that is, the number of stimulation sites from which it was possible to obtain a response in target muscle;

(2) the volume of active cortical sites, that is, the sum of the averaged MEP log-amplitudes from each excitable cortical site for the target muscle;

(3) the excitability thresholds;

(4) the coordinates of the hot-spots expressed in centimeters from Cz (x for the mediolateral axis, y for the anteroposterior axis; see Table 1); and the coordinates of the center of gravity (CoG) expressed in centimeters from the hot-spots.

The *y* was considered positive for forward shifts, negative for backward shifts. The x was considered positive for lateral shifts, negative for medial shifts. The center of gravity for the subject j was expressed as:

$$x_j = \sum_i x_{ji} * \log_e(amp_{ji}) / \sum_i \log_e(amp_{ji});$$

$$y_j = \sum_i y_{ji} * \log_e(amp_{ji}) / \sum_i \log_e(amp_{ji})$$

Whenever the center of gravity of a subject's motor area was exactly coincident with the hot-spot, the coordinates were equal to (0;0).

ADM and ECD area, ADM and ECD volume and excitability thresholds were considered as five aspects to investigate of the cortical excitability. A multivariate analysis of variance (ANOVA) for repeated measures was chosen as the main statistical procedure, giving a global measure of cortical excitability. Hemisphere side (right, left) was entered as within-subjects factors, whereas group allocation (AD, SIVD or controls) was entered as between-subjects factor. The multivariate ANOVA helped to verify whether the three groups could be significantly discriminated in the five-dimensional space. To this end, Hotelling's T2, followed by univariate F-tests for the statistical evaluation of the single measures was used. No effect of hemisphere was found for the center of gravity, allowing to collapse the two maps. Because the center of gravity is defined by two coordinates, a multivariate

ANOVA was used. In this case, the Hotelling's T2 should be interpreted as the statistic for the bidimensional assessment of separation between different groups.

Since the motor excitability (Figure 5) and the distance between the COG and the hot-spot positions have large variability among subjects in the three groups, we proceeded with another type of statistical analysis: we explored the possible presence of some type of correlation between the degree of hyperexcitability and the plastic rearrangement of motor cortex in the whole sample of subjects. To do that we performed an analysis using Spearman's rank correlation coefficient between the excitability measures (area of muscle representation and the volume of active cortical sites) and the Euclidean distance (expressed in cm) between the COG and the hot-spot position calculated in each subjects of the three groups using an in-house written Matlab script (R2007b, The Mathworks Inc.). Throughout the statistical analysis, a <0.05 p- value was considered significant. The software SPSS 20.0.0 for Windows (IBM Corporation, Somers, NY, USA) was used for statistical analysis.

3.2.2 Results

As expected, at the visual examination of MR-images SIVD patients showed high degree of white matter hyperintensities compared to AD patients who showed clear cortical atrophy, including medial temporal atrophy. Moreover, according with the well-known literature, the neuropsychological profile of SIVD patients was characterized from a greater impairment of frontal executive functions when compared to AD patients.

No significant statistical differences between the AD and Controls groups were found for each of the considered excitability parameters (rMT, Area ADM, Area ECD, Volume ADM, Volume ECD) and also for the global measure of cortical excitability ($p > 0.05$ in each condition). No significant statistical differences between the groups were also found for the centers of gravity average spatial coordinates of the ADM and ECD muscles ($p > 0.05$).

3.2.3 Neurophysiological profile of SIVD patients

According to statistics, neither the effect of hemisphere [Hotelling's trace = 0.01; F= 0.086; p =0.994] nor the interaction group x hemisphere [Hotelling's trace = 0.423; F= 1.65; p = 0.108] were significant, indicating the absence of a global significant asymmetry of the motor cortex parameters in the whole sample.

Since we aimed at investigating a measure of global excitability a multivariate analysis including all the motor cortex functionality measures available was carried out. We found differentiation in cortical excitability between the AD and the Control group [Hotelling's trace = 3.853; F= 9.248; p = 0.001]. On the other hand we were also able to demonstrate a clear differentiation between the SIVD and the Control group [Hotelling's trace = 1.684; F = 3.368; p = 0.048]. On the contrary, there were no differences between AD and SIVD patients [Hotelling's trace = 0.476; F= 0.952; p = 0.490]. These data suggest increased motor cortex global excitability in AD and SIVD patients versus controls; moreover, they indicate that AD and SIVD patients have a similarly enhanced cortical excitability.

The univariate analysis indicated that differences were less evident for threshold (p = 0.254 AD vs CO, p = 0.562 SIVD vs CO), more evident for ADM (p = 0.003 for area AD vs CO, p = 0.009 for area SIVD vs CO; p = 0.001 for volume AD vs CO, p = 0.002 for volume SIVD vs CO) and yet more extensive for ECD measures (p=0.001 for area AD vs CO, p = 0.003 for area SIVD vs CO; p < 0.0001 for volume AD vs CO, p = 0.004 for volume SIVD vs CO). No differences resulted in univariate analysis between AD and SIVD for threshold (p = 0.599), ADM area (p = 0.110), ADM volume (p = 0.074) and ECD area (p = 0.05). The only difference was found for ECD volume (p = 0.03). Excitability data from AD and SIVD patients and control subjects are summarized in Table 1 and Figure 5. Mapping grids obtained in one representative subject from each group is shown in Fig. 4.

When motor cortex functional plasticity was investigated in detail, it was evident that in controls the "hot-spot" was coincident with the center of gravity localized in the middle of the map whereas AD patients showed a clear combined medial and frontal shift (Figure 6). A multivariate test revealed a significant bi-dimensional separation between AD and controls groups [Hotelling's trace = 0.608; F =4.562; p = 0.028], that was evident neither comparing AD and SIVD patients [Hotelling's trace =0.042; F =0.272; p =0.766] nor comparing SIVD and controls groups [Hotelling's trace =0.373; F =2.425; p =0.127]; however, a clear trend of medial and anterior shifting was observed also in SIVD patients, with only a slightly lesser center of gravity's frontal shift with respect to AD group. In effect, when the results were examined in the two dimensions with a univariate type of analysis, differences for x axis were significant neither in AD vs Controls (p = 0.153) nor in SIVD vs Controls (p = 0.112); differences for y axis resulted significant in AD vs Controls (p = 0.028) but not significant in SIVD vs Controls (p = 0.184). However, no differences were found between AD and SIVD patients (p = 0.999 for x axis, p = 0.460 for y axis).

Finally, when motor cortex functional plasticity in relation to excitability was taken into comparative analysis, a direct correlation between excitability measures (both in terms of mean volume and in terms of mean area of the two investigated muscles) and the center of gravity's Euclidean distance from hot-spot calculated for each subject was found in the entire sample ($p < 0.0092$, $r = 0.51$ for volume and distance; $p < 0.028$, $r = 0.44$ for area and distance) as shown in Figure 4.

	AD		SIVD		Controls	
	mean	*SD*	*mean*	*SD*	*mean*	*SD*
Excitability threshold (%)	39,72	5,1	41,21	5,9	43,22	7,2
Area ADM (N)	6,28	3,0	4,14	1,4	2,61	0,7
Area ECD (N)	7,39	3,3	4,57	1,2	2,78	0,8
Volume ADM (ln µV)	35,51	13,0	24,40	8,9	11,77	3,1
Volume ECD (ln µV)	46,37	18,1	27,56	10,8	14,31	3,3

Table 1. Hot-spot localization and cortical excitability measures in the three different groups. Hot-spot localization: Cartesian coordinates on the scalp were used; SD = standard deviation. Cortical excitability measures: ADM = abductor digiti minimi; ECD = extensor communis digitorum; N = number of excitable sites; because no interhemispheric asymmetry was found, measures refer to the "average" hemisphere.

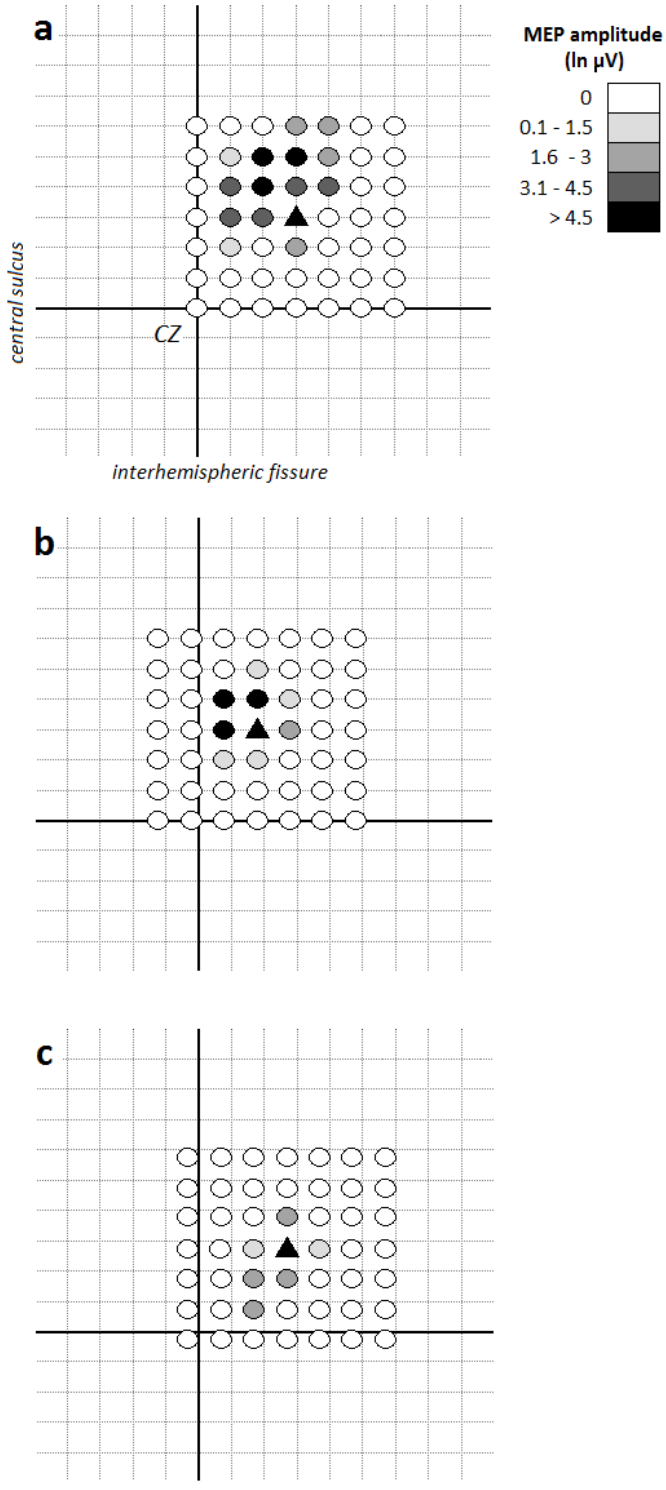

Figure 4. Two-dimensional diagram of the mapping grid obtained in a representative subject from each group (a= AD patient; b= SIVD patient; c= control subject). Stimulation points were spaced at 1 cm intervals with the grid origin centered at the motor hotspot (triangle). Each site was stimulated four times and the color code indicates the size of the mean ECD and ADM MEP amplitude at that site. The black reference vertical line corresponds to the interhemispheric fissure; the black reference horizontal line corresponds to the central sulcus. Measures refer to the "average" hemisphere, although the right hemisphere has been chosen for the Cartesian representation

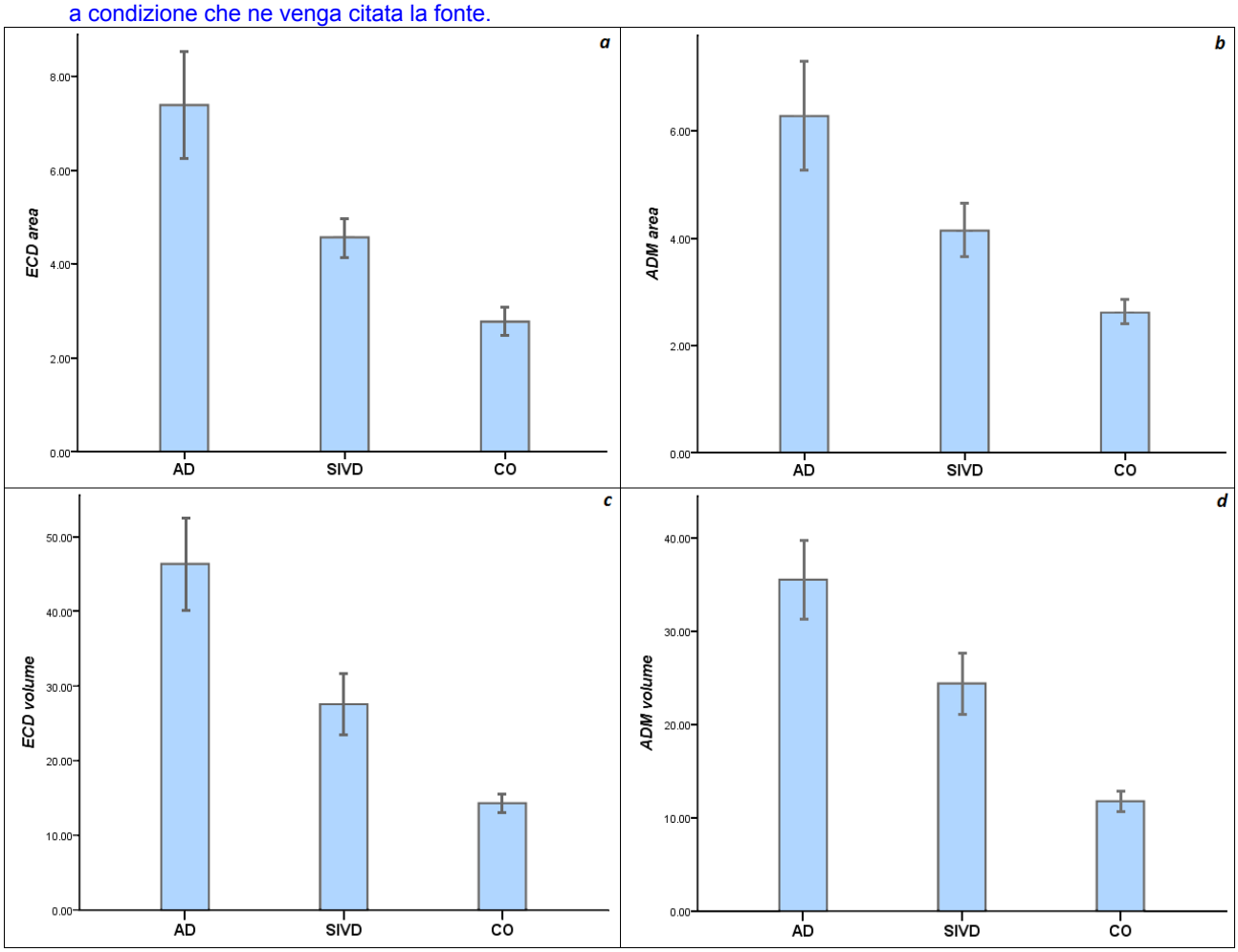

Figure 5. Main results of mapping technique in the three different groups.

A) Extensor Communis Digitorum area (axis y is number of excitable sites) B) Abductor Digiti Minimi area (axis y is number of excitable sites). C) Extensor Communis Digitorum volume (axis y is the log μV) D) Abductor Digiti Minimi volume (axis y is the log μV).

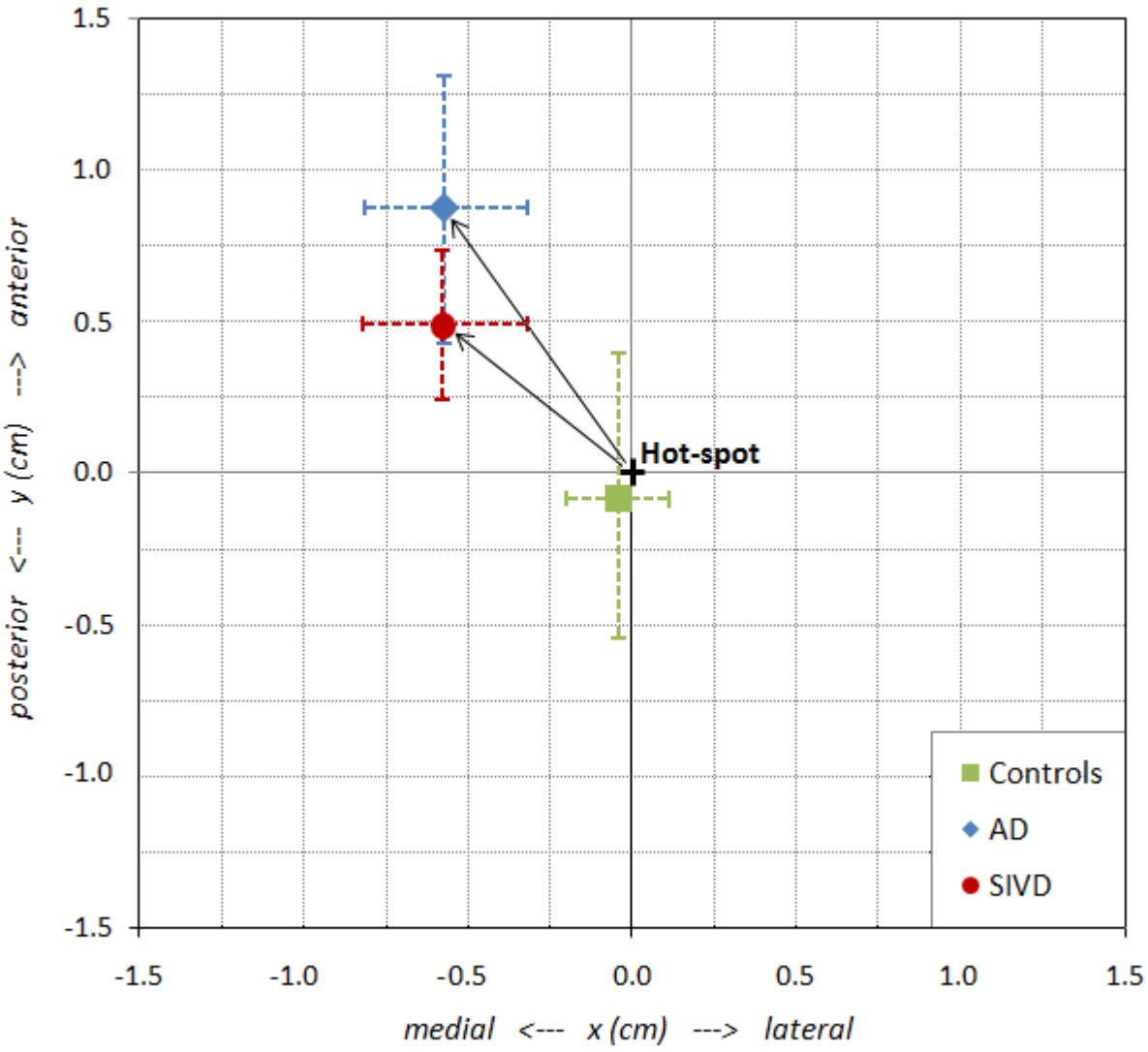

Figure 6. Centers of gravity average coordinates of a mean of ADM and ECD in the three groups.

Dotted lines represent the error bars for each group. Because no interhemispheric asymmetry was found, measures refer to the"average"hemisphere, although the right hemisphere has been chosen for the Cartesian representation.

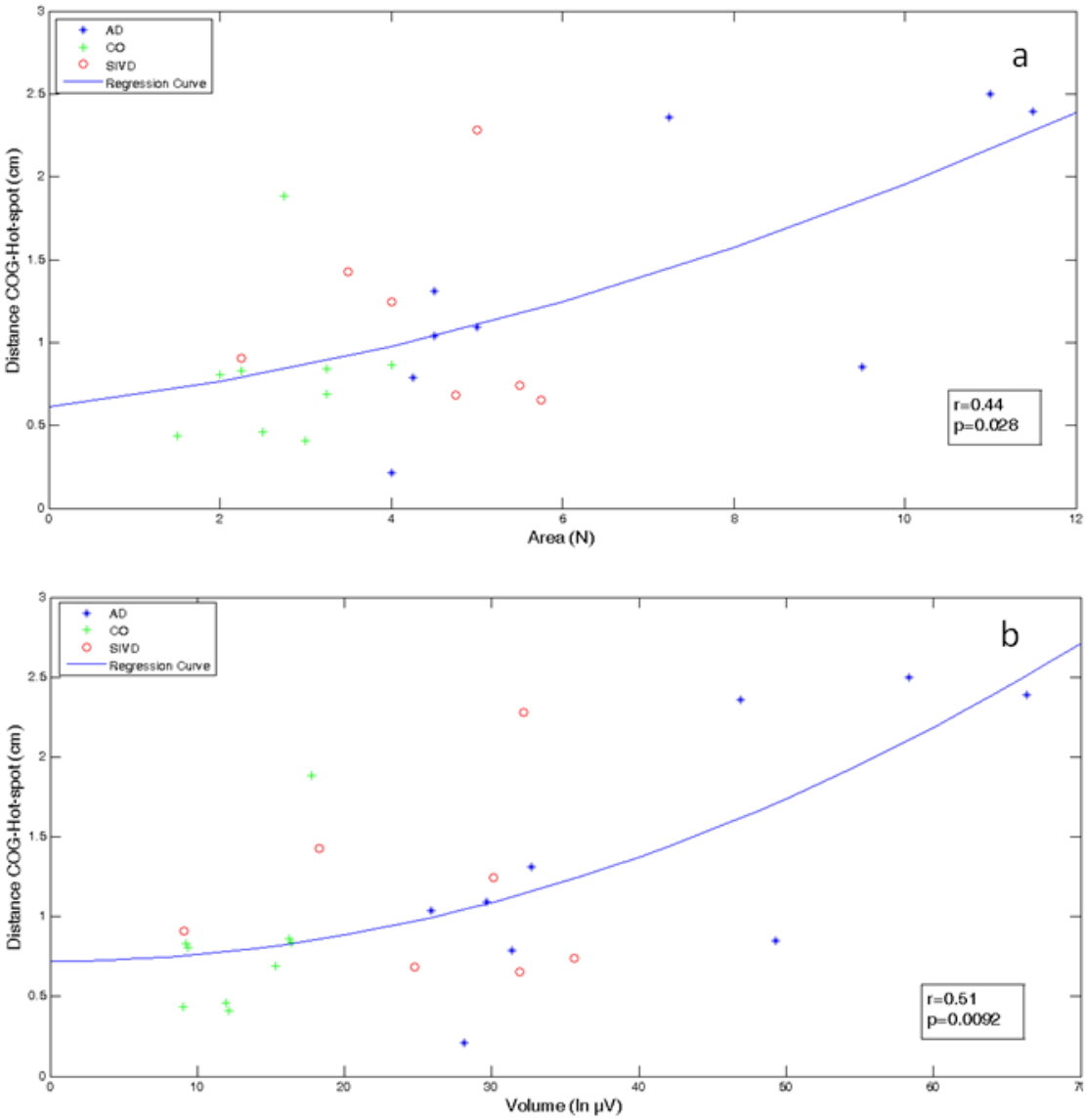

Figure 7.

a) Spearman's rank correlation between mean ADM and ECD area values (number of excitable sites - axis x) and the Euclidean distance between CoG and hot-spot (expressed in cm - axis y) calculated for each subject of the entire sample. b) Spearman's rank correlation between mean ADM and ECD volume values (expressed in log µV – axis x) and the Euclidean distance between CoG and hot-spot (expressed in cm - axis y) calculated for each subject of the entire sample.

3.2.4 Discussion

The present study suggests that in SIVD the primary motor cortex is hyperexcitable. Moreover, for the first time we have also shown in these patients a clear trend towards a motor cortex functional

reorganization. Finally, in the current sample of subjects a direct correlation between parameters related to cortical excitability and parameters related to cortical plasticity was demonstrated.

According to our results that show a direct correlation between motor cortex excitability and plasticity, it has recently been hypothesized that cortical networks hyperexcitability could favor the strengthening of existing synapses in a Hebbian and drive axonal outgrowth.

3.3 Sensorimotor cortex excitability and connectivity in Alzheimer's disease: an EEG-TMS co-registration study

In this study twelve patients (5 male, 7 females; age range, 72.4 ± 5.9 years, education: 8 ± 3.5 years; MMSE 20.8 ± 2.7) at their first diagnosis of dementia were recruited meeting current diagnostic criteria. Patients had to score at least 18 on MMSE, and symptoms manifested less than 2 years previously they were enrolled. All of them were free of relevant behavioral disturbances. Patients underwent neuropsychological testing, including the Mental Deterioration Battery, the Mini- Mental State Examination, a functional evaluation (Instrumental Activity of Daily Living scale), and evaluation of affective symptoms. They also underwent brain magnetic resonance imaging (MRI) and laboratory screening to rule out other causes of dementia. No clinical evidence of motor disturbances was found in any of the patients after detailed neurological evaluation. No recruited patient was yet taking acetylcholinesterase inhibitors or other drugs which are known to influence corticospinal excitability during TMS. None had ever suffered from epilepsy. Further exclusion criteria, in line with international safety standards for TMS, were metallic prosthesis or fragments in the cranial and thoracic districts, tinnitus, previous retinal detachment, brain hemorrhage.

An age matched control group were also recruited and consisted of 12 healthy volunteers (6 male, 6 female; age range 68.6 ± 7.1 years; education: 9.1 ± 4.5 years; MMSE 28.8 ± 1.2). Both patients and subjects were right-handed (handedness score 0.70), as evaluated by the Handedness Questionnaire and were instructed to abstain from caffeine and alcohol the day before the experimental session.

Patients and caregivers provided informed consent, and the study was approved by the local ethical committee.

3.3.1 Transcranial Magnetic Stimulation

Single pulse TMS (monophasic pulse configuration; Magstim Company Limited, Whitland, UK) of the left M1 was performed during a multi-channel EEG recording by means of a standard figure-of-eight double 70 mm coil oriented to elicit a posterolateral-anteromedial current flow in the brain. The

virtual cathode of the coil was placed over the 'hot spot' of hand area of left M1, defined as the point from which stimuli at the minimal excitability threshold of TMS triggered MEPs of maximal amplitude and minimal latency in the target hand muscle. Then, the resting motor threshold (RMT) was identified according to international guidelines as the stimulator's output able to elicit reproducible MEPs (at least 50 μV in amplitude) in about 50% of 10-20 consecutive stimuli. Being this a stereotactic TMS–EEG experiment, the coordinates of the head, the EEG electrodes, and the coil were determined and transformed to the same coordinate system with magnetic resonance (MR) images. In this way TMS was continuously targeted to the hot spot. Each subject underwent a 1-h session consisting of about 120 TMS trials; the intertrial interval was 6-8 s that avoids habituation with repeated stimulation. The TMS was given supra-threshold with an intensity of 120% of the RMT. Amplitudes of MEPs were measured between the two major and stable peaks of opposite polarity, latencies of the MEPs were measured at the maximum positive peak. The elicited compound EMG responses were recorded bilaterally from the first dorsal interosseus muscle (FDI), Ag/AgCl-coated electrodes filled with conductive jelly in a belly/tendon montage. Skin/electrode resistances were below 10 KΩ.

3.3.2 EEG recordings

TMS-compatible EEG equipment (BrainAmp 32MRplus, BrainProducts GmbH, Munich, Germany) was used allowing continuous data recording without saturation of the EEG signals and not requiring pinning the preamplifier output to a constant level during TMS. The EEG activity was continuously acquired from 32 scalp sites using electrodes positioned according to the 10–20 International System. Additional electrodes were used as ground and reference. The ground electrode was positioned in Oz in order to have maximal distance from the stimulating coil. The linked mastoid served as the reference for all electrodes). The click associated with the coil's discharge propagates through air and bone and can elicit an auditory N1–P2 complex at latencies of 100–200 ms. To mask coil-generated clicks a white noise, obtained from the waveform of the TMS click digitized and processed to produce a continuous audio signal with its specific time-varying frequencies, was continuously delivered through earphones. We adjusted the masking volume until the subjects reported that the TMS click was not audible (always below 90 dB). To ensure wakefulness throughout the recording sessions, subjects were required to keep their eyes open and to fixate on a target over the opposite wall. The signals recorded were bandpass filtered at 0.1–500 Hz and digitised at a sampling rate of 2.5 kHz. In order to minimize overheating of the electrodes by the stimulating coil, TMS-compatible Ag/AgCl-coated electrodes were used. Skin/electrode impedance was maintained below 5 kΩ. Horizontal and

vertical eye movements were detected by recording the electro-oculogram (EOG). The voltage between two electrodes located to the left and right of the external canthi recorded horizontal eye movements. The voltage between reference electrodes and electrodes located beneath the right eye recorded vertical eye movements and blinks.

3.3.3 Data Analysis

Data analysis was conducted using MATLAB 2008b version 7.7 (MathWorks, Natick, Mass.) and the public license toolbox EEGLAB (Delorme and Makeig, 2004). All the EEG and EMG signals were split into segments (epochs) lasting 3s and including 1s pre-stimulus baseline and baseline corrected (100ms pre-stimulus). All epochs showing an EEG-TMS evoked activity contaminated by extreme values were automatically rejected. In particular, epochs exceeding 120μV in the 20ms-1s time window after stimulus or ±100μV in the 100ms-1s time window after stimulus were marked for rejection. Similarly, epochs showing EMG evoked activities contaminated by extreme values were rejected too. In particular, epochs exceeding ±200μV in the 100ms-1s time window after stimulus were marked for rejection. Rejection results were visually inspected and manually confirmed by an expert. After epochs selection, EEG signals were bandpass (2-80Hz) and notch (50Hz) filtered, down sampled from 2500Hz to 500Hz and average referenced. Eventually ERP activities for each subject have been extracted by means of ensemble averaging.

Time domain was the main aspect investigated. First, the GMFP (See Chapter 2 for the definition) was calculated and a t-test was performed to evaluate significant differences between the examined groups (Alzheimer's and Controls). Next for a first topographical assessment we integrated in maps the EEG activity of each channel using three time-frames chosen upon the visual inspection of the GMFP activity, 6-22 ms, 24-90 ms and 92-190ms, and we performed an ANOVA analysis with two factors (groups and channels) in order to assess difference in global excitability.

Then, a semi-automatic amplitude/latency measurement of each TMS-evoked EEG-potential (TEP) -identified at the vertex by a visual inspection of the TMS-evoked responses- and MEP was carried out. Considering the data collected from both groups, two ANOVA analyses (hierarchical model II type) with two factors (groups and channels) have been performed for each peak. The first ANOVA has been performed on raw potential values with the aim of detecting global general differences among groups. When this difference was present, we then performed a second ANOVA analysis with two factors (groups and channels) on average-corrected potentials in order to see if the global

difference was coupled with a spatial modulation in the excitability and, in this case, Bonferroni corrected marginal means were extracted and discussed. An unpaired t-test (Bonferroni corrected) was used for the study of the latencies. These procedures allowed evaluating whether the peaks were being modulated by groups' behavior. Only results indicating statistically significant between-groups main effect have been reported.

Finally, upon visual inspection, we found that an additional component was present around 80 ms in the GMFP of the AD patients. Therefore, we conducted an additional analysis on this peak that was statistically contrasted, after a semi-automatic amplitude/latency measurement, against the 60 peak and the 100 peak by means of two ANOVA analyses with two factors: the peaks (two levels: 60 and 80 or 80 and 100) and the channels (32 levels), with dependent variable TMS–EEG amplitudes each. The 80 peak of AD patients has been then contrasted with the nominal values of the Control group at the same latency in order to fully characterize the wave.

3.3.4 Cortical sources analysis of the ERPs

Current densities for the TEPs components that revealed more significant differences between AD and Control groups were estimated using sLORETA (standardized low resolution brain electromagnetic tomography) in Curry software (v 6.0.2, Compumedics Neuroscan Ltd., Charlotte, NC, USA), for illustrative purposes. Basically, sLORETA gives a single linear solution to the inverse problem of localization of brain function based on scalp recordings and produces images of standardized current density with no localization bias. The same individual 3D T1-weighted image (Philips Achieva 3T, Philips Medical System, The Netherlands) was used for realistic head model as volume conductor for both groups. A three-compartment boundary element model (BEM 7/9/10mm) and standard conductivity values were used (0.33 S/m for the brain fluid, 0.0042 S/m for skull, and 0.33 S/m for skin). The regularization parameter was automatically determined by the $\chi 2$ criterion method implemented in Curry. The analysis was performed with the ERP data obtained at the time points that showed local maxims in the GMFP (i.e. AD: 34, 42, 64, 82, 110 and 188ms post-stimulus, and Control: 28, 44, 60, 92 and 200ms post-stimulus).

The sLORETA method is a properly standardized discrete, linear, minimum norm, inverse solution method that solves the problem to compute the three-dimensional cortical distribution of the electric neuronal source activity from the EEG measurements, which are recorded on the head surface. Several independent research groups have repeatedly demonstrated that LORETA solutions are able to faithfully model cortical responses to sensorimotor events. However, it should be stressed that

sLORETA has a spatial resolution (centimeters) lower than that of positron emission tomography and fMRI imaging (millimeters). The so-called sLORETA solutions consisted of voxel current density values that were able to predict ERP voltage at scalp electrodes. The sLORETA solutions predicting scalp ERPs were regularized to estimate distributed rather than punctual EEG source activity. It should be remarked that the head template of the originals sLORETA package cannot account for differences in individual cortical envelope as typically done in the analysis of functional magnetic resonance imaging (i.e., normalization, coregistering, smoothing).

3.3.5 Results

- **Motor Threshold and MEP**

  The RMT was 57.9 ± 7.4% for Controls and 53.6 ± 2.8% for AD. The average MEP amplitude and 95% confidence interval were 417 ± 197 μV for Controls and 992 ± 673 μV for AD. No statistical difference between the groups was seen in the RMT and MEPs amplitude using an unpaired t-test.

- **TMS-evoked EEG responses**

  As already well described, supra-threshold single pulse TMS of the left M1 evoked in both the experimental groups EEG activity lasting up to 200ms and peaking on the GMFP at approximately 30, 44, 60, 100 and 180ms post-TMS, as illustrated in figures 8 and 9. Moreover, in most of AD patients (9 out of 12) an additional component was observed around 80 ms post stimulus (figure 9).

  The GMFP analysis revealed an increase in amplitude between 20 and 150ms poststimulus in AD patients, which was maximal between 24 and 90ms as highlighted in the figure 10 ($p<0.01$). When the integrated cortical activity in the chosen timeframes (that is 6-22 ms, 24-90 ms and 92-190 ms, figure 10) was calculated, the resulting maps confirmed a clear increase in the cortical excitability of AD patients only in the timeframe 24-90 ms ($p<0.05$). Particularly, significant differences were evident in the stimulated sensorimotor cortices (that is in the electrodes C3 P3 and CP1, figure 10). Moreover when looking at the individual latencies (the polarity according to what observed at the vertex: N7, P30, N44, P60, N100 and P180), the maps analysis showed a significant group difference in some waves, with AD showing a clear increase in the cortical excitability. Particularly, the analysis showed a significant group difference ($p<0.05$) at the P30 wave, which peaked in FC1 in both groups. The analysis of average-corrected potential showed a significant channel-group interaction

with significant marginal means in C3, P3 and CP1 ($p<0.05$ Bonferroni corrected, figure 11). The analysis did not show any significance at the N44 wave. Finally, the analysis showed a significant group difference ($p<0.05$) at the P60 wave, which peaked in C3 in both groups, while analysis of average-corrected potential showed a significant channel-group interaction with significant marginal means in CP5 ($p<0.05$ Bonferroni corrected, figure 4). The latency analysis showed a significant difference only in the N100 ($p < 0.001$) with the CO showing a shorter latency then AD (figure 10).

Finally in order to better describe the additional component seen in AD patients around 80 ms (figure 12) this was contrasted against the 60 and the 100 peaks. The first analysis showed a significant global difference between the 60 and the 80 peaks (being the 60 globally stronger than the 80, $p < 0.05$) with a not significant channel-peak interaction, suggesting the same spatial topography for both waves. Conversely, the second analysis between P80 and N100 showed a significant channel-peak interaction ($p<0.05$), suggesting a different spatial topography. This topological difference was corroborated by the result of marginal means that highlighted a significant difference in the CP1 and in the C3 channels ($p<0.05$ Bonferroni corrected). The analysis of the 80 peak across groups (AD and CO, figure 12) showed a significant global difference among groups for the raw potentials, peaking the EEG activity in C3 in both groups, while the analysis of the average-corrected potentials showed only a trend in the group-channel interaction. A coarse view of the topology through four ROIs[2] and the application of an ANOVA analysis with two factors (groups and ROIs), showed a significant group-ROI interaction, with a significant hyperexitability of AD groups in the center-left-posterior area. Then, we evaluated the specificity and sensitivity of this component in AD patients computing the amount of activations in CP1 and P3 with respect to C3. Considering as positive a patient showing an activation greater or equal than the 65% of that measured in C3, we found a value of sensitivity equal to 75% and a value of specificity equal to 75%.

- **Sources computed by sLORETA**

The figures 8.C and 9.C show grand average (N= 12 AD and 12 Control) of the sLORETA source solutions of the activity occurring during each peak of the GMFP, presented for

[2] We used the left-anterior (FC1-FC5-F3), right-anterior (FC2-FC5-F4), left-center-posterior (C3-P3-CP1-CP5), right-center-posterior (C4-P4-CP2-CP6) ROI, whose values have been obtained through the averaging of electrodes.

illustrative purpose. The visual inspection of activation showed clear differences between AD and Control groups in response to magnetic stimulation.

Particularly it could be observed that after TMS, healthy subjects showed current maxima (reflecting the center of neural activity) shifting from the premotor cortex (around 30 ms), to the motor cortex (around 44 ms), to the somatosensory cortices (around 60 ms). Thus, in healthy brains the direct perturbation of the motor cortex is followed by spatially and temporally differentiated patterns of activation that appear to propagate along the anatomical connections of M1 with related cortical areas

In contrast, the cortical activation in AD patients was spatially wider and for longer broadly localized in the stimulated sensorimotor cortex (since 30 to at least 60 ms). Thus, in AD although the direct perturbation of the motor cortex elicits responses that are even stronger than in healthy brains, these responses remain stereotypically segregated to the stimulated area and not transmitted outside it, possibly reverberating and reinforcing, suggesting a disruption of intracortical information transmission in line with the view of brain's networks disconnection.

3.3.6 Discussion

Motor cortex hyperexcitability is a well-defined neurophysiological feature of AD patients namely in the early disease stages. This parameter is related to disease severity and progression even though it has been so far evaluated only via traditional TMS techniques which provide indirect measures of M1 excitability alone. Here, by using the EEG-TMS coregistration approach, we have directly observed this phenomenon on the scalp (brain convexity) for the first time, extending it to the whole sensorimotor system. We have also demonstrated that a clear rearrangement of motor cortex effective connectivity is present in mild AD possibly reflecting its plastic reorganization via alternative and/or reverberating circuits.

There is a growing body of neuro-pathological evidence that -in contrast with traditional views the motor cortex is actually already involved in the early AD stages, despite the lack of clinically evident motor deficits which only appear in the later stages. The reasons of this discrepancy is still matter of debate and it has been preliminary ascribed to motor cortex ability to plastic reorganize itself via alternative circuits, even recruiting additional cortices in the sensorimotor system. By using EEG-TMS co-registration, the present study has clearly demonstrated that the sensorimotor system is deeply rearranged in mild AD patients without motor symptoms with the recruitment of additional

neural sources, the activation of reverberant circuits and their integration in the distributed excitatory network subtending sensorimotor functions.

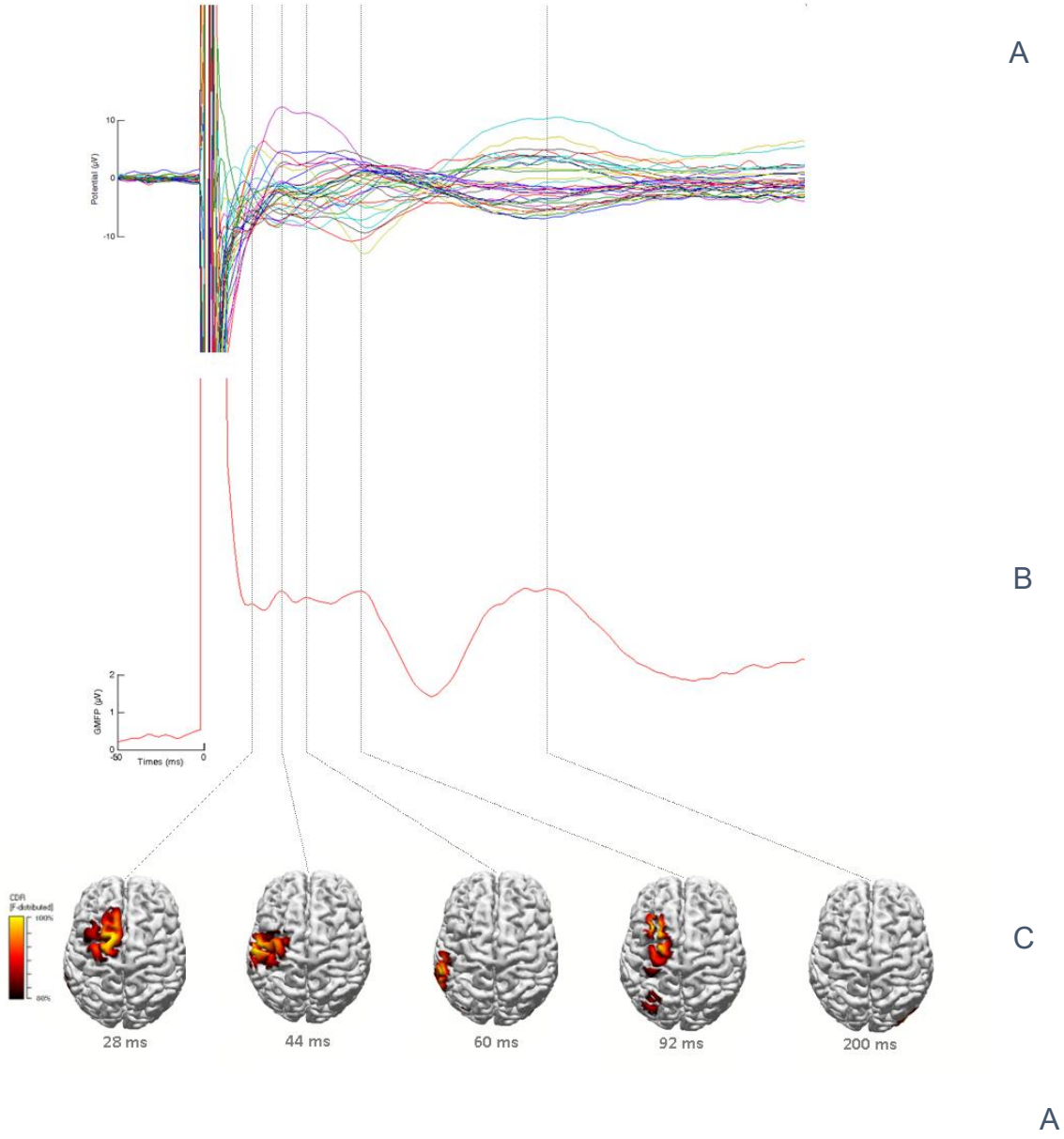

Figure 8. Control subjects

A. Averaged TMS evoked potentials recorded at all electrodes, superimposed in a butterfly diagram
B. Global activation produced by TMS as measured by the GMFP
C. Source localization of the activity occurring during each peak in the GMFP calculated using standardized low-resolution brain electromagnetic tomography (sLORETA) and plotted on the cortical surface. At eachtime point, the results were auto-scaled and thresholded at 80% to highlight maximum current density sources.

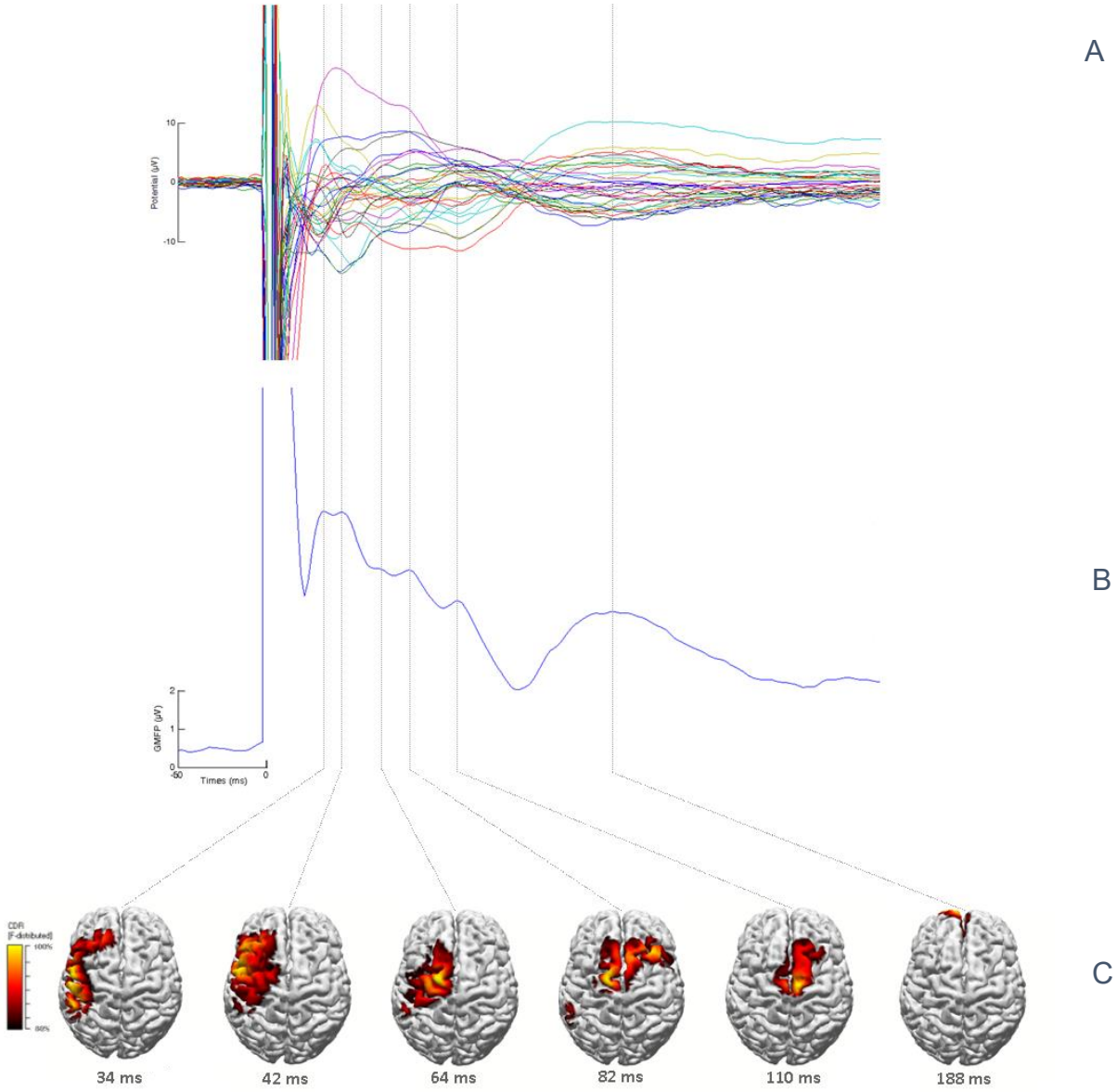

Figure 9. Alzheimer's subjects

A. Averaged TMS evoked potentials recorded at all electrodes, superimposed in a butterfly diagram
B. Global activation produced by TMS as measured by the GMFP
C. Source localization of the activity occurring during each peak in the GMFP calculated using standardized low-resolution brain electromagnetic tomography (sLORETA) and plotted on the cortical surface. At eachtime point, the results were auto-scaled and thresholded at 80% to highlight maximum current density sources.

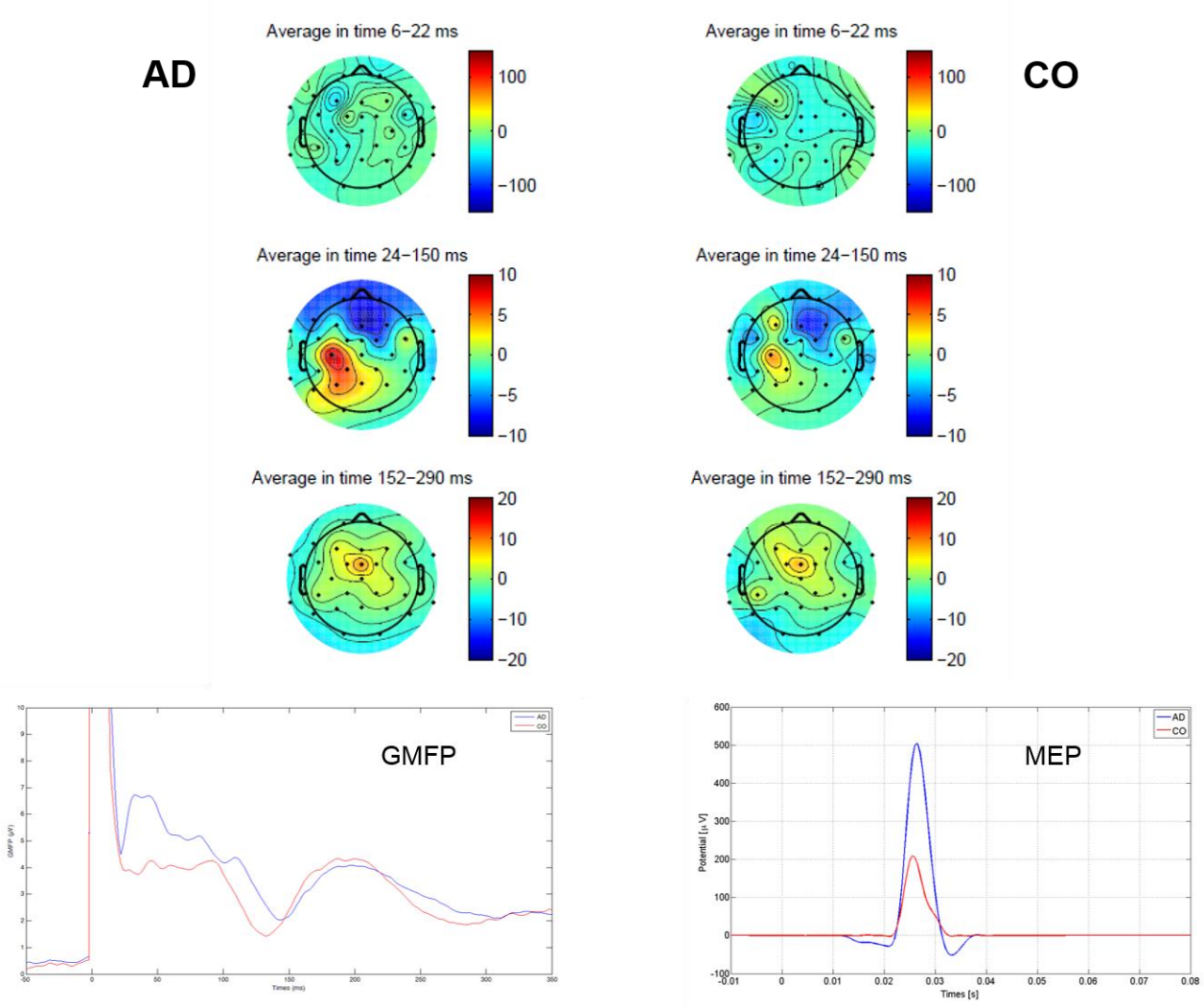

Figure 10. Topographic distribution of the average integrated TMS evoked activity

Average integrated evoked responses in CO subjects and AD patients for the time-frames 6-22, 24-90 and 92-190 ms after the TMS over the left M1; the white crosses indicate significant differences. Bottom , average GMFP and MEP for each group superimposed for visual purpose.

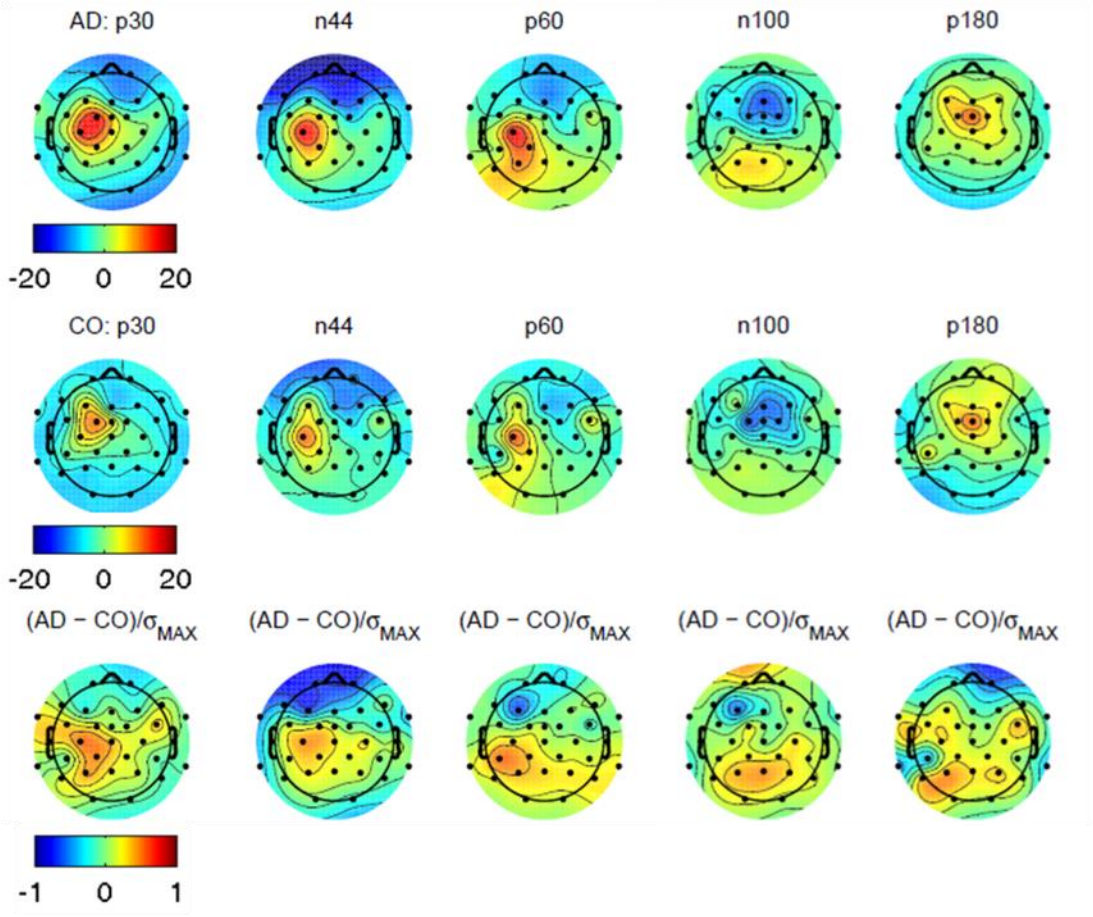

Figure 11. Topographic distribution of the TMS evoked activity

Scalp distribution maps at 30, 44, 60, 100, 180 ms after the TMS over the left M1 in CO subjects and AD patients and maps difference. The map at 30 and 60 ms are outlined and the white crosses indicate significance difference.

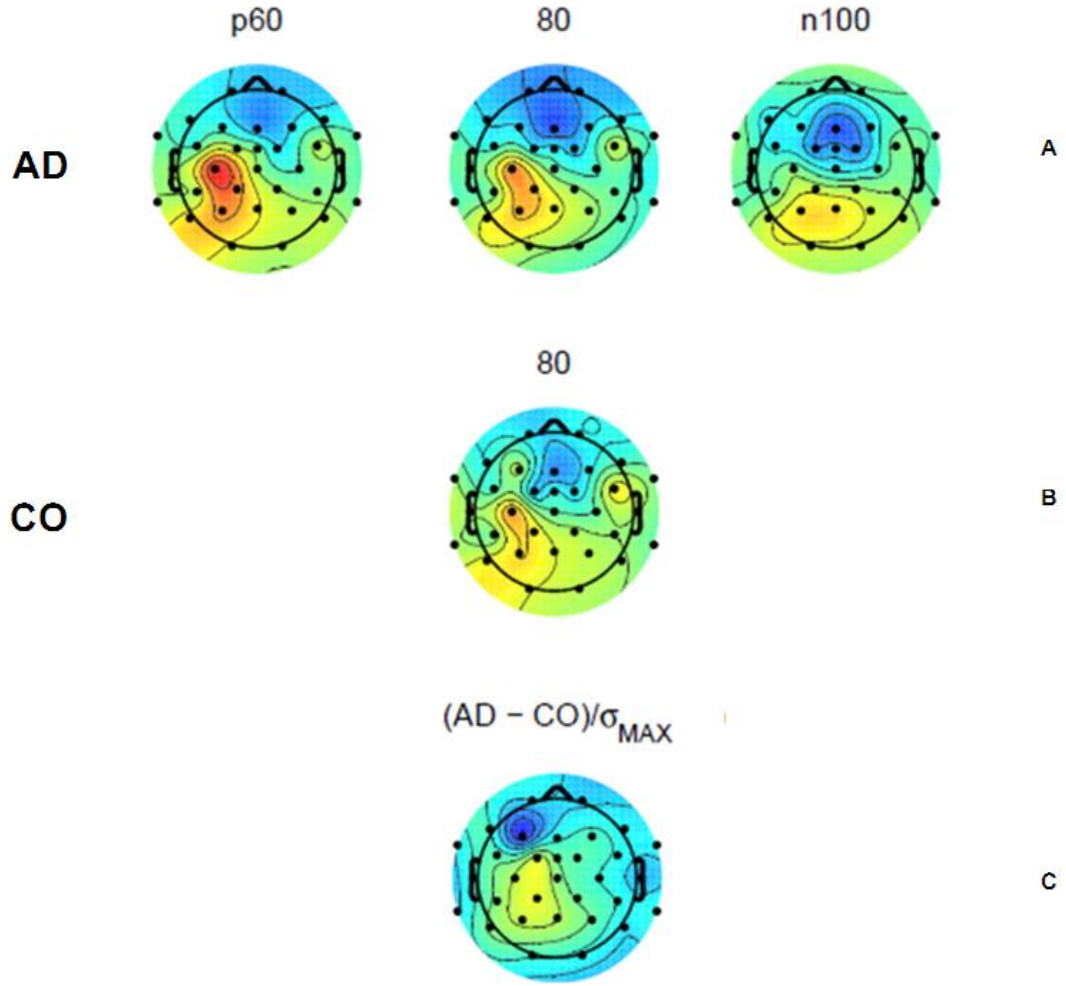

Figure 12. Topographic distribution of the TMS evoked activity between 60 and 100 ms after the TMS in AD and statistical comparison at 80 ms with CO.

A. Scalp distribution maps at 60, 80, 100 ms after the TMS over the left M1 in AD group. The overlapped topographical distribution between the P60 and the wave at 80 ms is evident.

B. Scalp distribution map at 80 ms after the TMS over the left M1in CO group.

C. AD and CO groups map difference at 80 ms.

3.4 Does an intraneural interface short-term implant for robotic hand control modulate sensorimotor cortical integration? An EEG-TMS co-registration study.

A short description of the methods is given in the following section, while a complete report of the clinical, surgical and technical aspects of this case can be found elsewhere (Rossini et al., 2010). Briefly, within an experimental protocol that aims at achieving the control of a robotic hand prosthesis via peripheral nerves interface, a 26 years-old, right-handed male (P.P.) was selected 2 years after the traumatic transradial amputation of his left upper limb, due to a car accident. Previous medical history

was negative for neurological and systemic diseases and for surgeries. The study was approved by the local Ethics Committee and by the assigned office of Italian Ministry of Health, and an informed consent was signed by the participant.

By means of surgical procedure two multichannel electrodes were inserted in the left ulnar and two in the median nerves for 1 month. The neural electrodes belong to the family of tf-LIFE4 (thin-film Longitudinal Intra Fascicular Electrodes, 4th generation), which is a perspective, highly selective, neural interface that can be used as a chronically implanted interface to work with advanced functional electrical stimulation and recording systems. Thanks to thin-film fabrication technology each wire electrode was equipped with 8 active sites, plus 4 additional sites for references and grounds. The participant did not report any side effect during the 12-month follow-up. As previously detailed (Rossini et al., 2010), phantom awareness and presence of phantom limb pain (PLP) were evaluated presurgically, post-training and after 3 months using an abbreviated version of the McGill Pain Questionnaire (sfMcGill), the Present Pain Intensity Scale (PPI), the PainVisual Analogue Scale (VAS), and an open section for description of phantom awareness.

During the two weeks that preceded the implant, P.P. was trained in dispatching motor commands to produce various hand and finger movements without activating stump muscles. Once the electrodes were placed in the nerves, the participant was trained to perform a palmar grasp, pinch grasp, and little-finger flexion with the robotic hand as showed in videos representing those tasks that were randomly presented to him on a computer screen. The video presentation has also been exploited as the theoretical onset for each motor command. After 4 weeks of training, a clear clinical improvement of PLP with a progressive return to normal perception of the upper limb and of the hand motion was reported (pre-implant scores: sfMcGill = 18, PPI = 3, VAS = 38; 1 week post-LIFE removal scores: sfMcGill = 11, PPI = 2, VAS = 23). This improvement disappeared 3 months later (sfMcGill = 17; PPI = 3; VAS = 36).

3.4.1. EEG-TMS co-registration procedure

Before tf-LIFEs implant (T0) and after the training period and the removal of tf-LIFEs (T1), P.P corticocortical excitability, connectivity and plasticity were directly tested via a neuronavigated EEG-TMS setup. During the experiments, the patient sat in an adjustable chair with a headrest that ensured a stable head position, and was instructed to keep his eyes open and to look at a fixation point on a screen in front of him. TMS-compatible EEG equipment (BrainAmp 32MRplus, BrainProducts GmbH, Munich, Germany) was used allowing continuous data recording without saturation of the

EEG signals and not requiring pinning the preamplifier output to a constant level during TMS. The EEG activity was continuously acquired from 32 scalp sites and electrodes were used as ground and reference. The ground electrode was positioned in Oz in order to have maximal distance from the stimulating coil. The linked mastoid served as the reference for all electrodesThe signal was bandpass filtered at 0.1–500 Hz and digitized at a sampling rate of 2.5 kHz. In order to minimize overheating of the electrodes by the stimulating coil, TMS-compatible /AgCl-coated electrodes were used. Skin/electrode impedance was maintained below 5 kΩ. Horizontal and vertical eye movements were detected by recording the electro-oculogram. The voltage between two electrodes located to the left and right of the external canthi recorded horizontal eye movements. The voltage between reference electrodes and electrodes located beneath the right eye recorded vertical eye movements and blinks. To mask coil-generated clicks a white noise, obtained from the waveform of the TMS click digitized and processed to produce a continuous audio signal with its specific time-varying frequencies was continuously delivered through earphones. We adjusted the masking volume until the subject reported that the TMS click was not audible (below 90 dB).

Single pulse TMS (monophasic pulse configuration, 120 stimuli) of the right and left M1was performed during the multi-channel EEG recording, starting always from the left hemisphere. TMS was carried out using MAGSTIM 200 equipment (Magstim Company Limited) and a standard figure-of-eight double 70 mm coil, oriented to elicit a posterolateral-anteromedial current flow in the brain. Being this a neuronavigated EEG-TMS experiment, the coordinates of the head, the EEG electrodes, and the coil were determined and transformed to the same coordinate system with magnetic resonance images by means of the SofTaxic Optic Navigator system; in this way TMS was continuously targeted to the optimal cortical representation area of the target right first dorsal interosseus (FDI) muscle determined as follows. In the first step, using magnetic resonance images, the hand area on the anterior bank of the left central sulcus was identified. As a second step, the subject's left primary motor cortex was mapped around the anatomic "hand knob", to find the area evoking the largest response in the right FDI muscle. Finally, resting motor threshold (RMT) was defined according to international guidelines as the stimulator's output able to elicit reproducible motor evoked potentials (MEPs) (at least 50 μV in amplitude) in 5 of 10 consecutive stimuli. Stimulus repetition rate was 0.1–0.2 c/s with a stable intensity 10% above subjective excitability threshold. To test the contralateral M1 we used the anatomically homologous area in the contralateral hemisphere and the same intensity of stimulation.

3.4.2. Data analysis

Data analysis was conducted using MATLAB2008b version 7.7 (MathWorks, Natick, Mass.) and the public license toolbox EEGLAB. TMS evoked EEG-activity, i.e. TMS-evoked potentials (TEPs), were visually inspected in each channel and trials contaminated by environmental artefacts, muscle activity, or eye movements were rejected. Following this procedure, EEG signals were low pass filtered (80 Hz cut-off frequency), notch filtered (50 Hz), down sampled to 500 Hz, divided into segments lasting 3000 ms and including a 1000 ms prestimulus baseline. Then, the segments were baseline corrected (100 ms prestimulus), and averaged. Averaged TMS-EEG responses over all the included trials (about 70 trials for each condition) for each electrode were computed. Then, the potential maps were produced using EEGLAB and visually inspected.

Statistical analyses were conduced with the statistical toolbox of MATLAB and the GEEQBOX library. The significance threshold of the results was fixed at $p = 0.05$. Time domain was investigated as the main aspect of the TMS-evoked potentials and the following assessments were performed:

- the global EEG-TMS amplitude response at T0 was contrasted with the same response at T1 for the stimulation of the right hemisphere and,
- the global EEG-TMS amplitude response at T0 was contrasted with the same response at T1 for the stimulation of the left hemisphere.

To this aim, first, we calculated the total brain activation evoked by TMS in each hemisphere (right and left) and in each condition (T0 and T1) by means of the GMFP (See Chapter 2 for the definition).

Then, the amplitude of TMS-evoked responses was analysed by means of the generalized estimating equations (GEE) model to detect significant global effects of condition for physiological significant evoked peaks (7, 30, 44, 60, 100 and 180 ms), identified by means of semi-automatic amplitude/ latency measurements. The GEE method was used as a generalization of the General Linear Model, allowing us to model correlated data (due to repeated measures within the same subject for each condition/position/latency). In particular, the GEE approach uses weighted combinations of observations to extract the appropriate amount of information from correlated data. Finally, two ANOVA analyses with a Sidak's *post hoc* test were applied, the former on the average activity in the 30–100 ms time window and, the latter for each peak previously analysed with the GEE approach. The two ANOVA analyses were applied, first, with one factor (condition T0 and T1) and, then, with two factors: the EEG electrodes (32 levels) and the conditions (two levels: T0 and T1). This procedure

allowed us to evaluate whether the peaks were being modulated by conditions. Only results indicating statistically significance between-condition main effects have been reported.

3.4.3 Results

RMT was 43% of the maximal stimulator's output for the stimulation of the left hemisphere at T0 while 45% at T1. Supra-threshold single pulse TMS of both left and right M1, both at T0 and at T1, evoked an EEG activity lasting up to 300 ms (Figs. 13 and 14). This activity, as previously described in healthy subjects, is composed at vertex (channel Cz, Fig. 15, right column) by a sequence of deflections of negative polarity peaking at approximately 7, 46, and 100 ms alternated with positive polarity peaks at approximately 30, 60 and 190 ms post-TMS. Figures 13 and 14 show the average of TMS-evoked potentials recorded at all electrodes superimposed in a butterfly diagram, and the well know potential maps for each TEPs at T0 condition and at T1 for the left and the right hemisphere stimulation, respectively. In order to directly probe the excitability of the motor cortices, we further analyzed the cortical responses to TMS targeted to the hot spot of the FDI muscle of both the hemispheres, calculating the GMFP in each condition (Fig. 15, left column). The GMFP revealed no differences between T0 and T1 conditions for the stimulation of the left hemisphere, while a significant modulation (with *t*-test $p < 0.0001$) in amplitude between 30 and 100 ms post-stimulus was evident for the stimulation of the right hemisphere that controls the affected limb (Fig. 15, left column). When the average activity in the time range (30–100 ms) at which significant differences between the two conditions (T0 e T1) ocurred was calculated, the resulting maps revealed a clear reduction of the **global** cortical excitability for TMS of the right hemisphere, evident in the stimulated hemisphere but also in the contralateral one (Fig. 16).

Particularly, the ANOVA analysis on average activity showed significant differences ($p < 0.01$) in F3, F4, C3, C4, Fz, Cz, FC1, FCz (with Sidaks' *post hoc* test).

No significant effect was instead seen for TMS of the left hemisphere (Fig. 16). Moreover, when looking at the individual latencies in that time range, a **global** amplitude modulation was present in most of the TMS-evoked potentials elicited by the stimulation of the right hemisphere. Particularly, the GEE analysis showed a significant difference between T0 and T1 condition at 30 ms ($p < 0.0404$), 46 ms ($p < 0.0001$) and 60 ms ($p < 0.007$) latencies for the stimulation of the right hemisphere. The ANOVA with one factor (condition: T0 and T1) confirmed the above results.

Finally, from the result of theAVOVAanalysis performed with two factors (electrodes and conditions) emerged a clear **local** decrement in N46 amplitude over C4 (Electrodes* Conditions – $p < 0.0034$

with Sidak's test *post hoc*) after the stimulation of the right hemisphere (contralateral to the stump). It was also evident a partial disruption of the dipole at 46 ms that after the stimulation of the right hemisphere is centred over the pre-motor area while after the stimulation of the lefth emisphere is, as expected, steadily centred over the stimulation site -that is the primary motor cortex – (Fig. 17).

3.4.4 Discussion

The N46 wave reflects the selective activity of M1 (Paus et al., 2001; Ferreri et al., 2011), so we can speculate that the findings observed at T0 could represents the direct sign of the well described M1 cortical hyperexcitability and post-amputation aberrant plasticity and that its modulation observed at T1 in the right hemisphere could be due to the regaining of a para-physiological condition as the result of a 30-days use of the neurally interfaced robotic artifact.

The increase of intracortical inhibition in our experimental subject may be attributed to increased GABAergic inhibition with an involvement of the corpus callosum, as suggested by the topographical distribution of such a modulation. GABA is the most important inhibitory neurotransmitter in the brain and the well known hyperexcitability and reorganization of the motor cortex after amputation are considered to be mediated by unmasking of "silent" excitatory synapses attributed to reduction of GABAergic inhibition. The function of this pathway has been extensively investigated and the transcallosal inhibitory mechanism is considered to play a fundamental role at an integrative level of analysis for the effective control of bilateral (i.e. bimanual) movements.

EEG-TMS coregistration showed that this reorganization involves bi-hemispheric networks and that intracortical and transcortical modulation of the GABAergic inhibition could be strongly involved in plastic changes observed both in response to the amputation and after the attempt of their modulation.

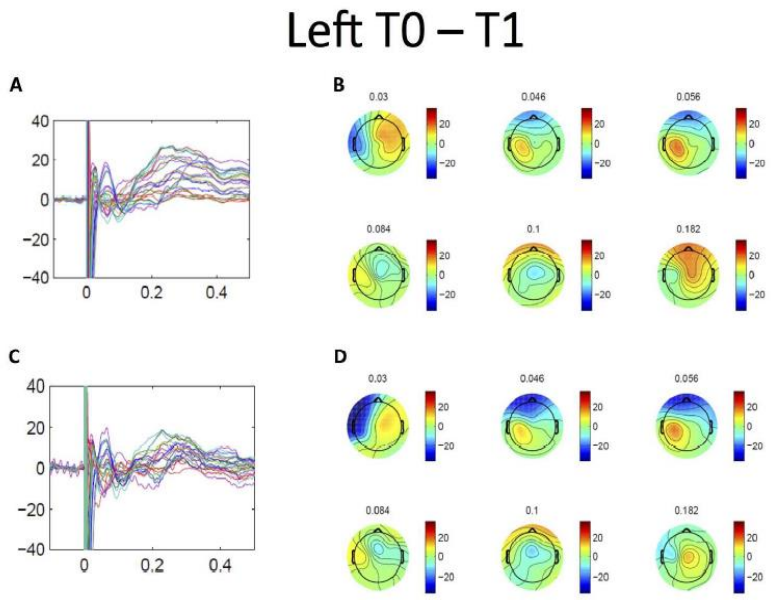

Fig. 13. Average of TEPs recorded at all electrodes superimposed in a butterfly diagram (A and C) and scalp distribution maps (B and D) at 30, 46, 56, 84, 100, 182 ms after sugnle pulse stimulation over the left M1 at T0 and T1

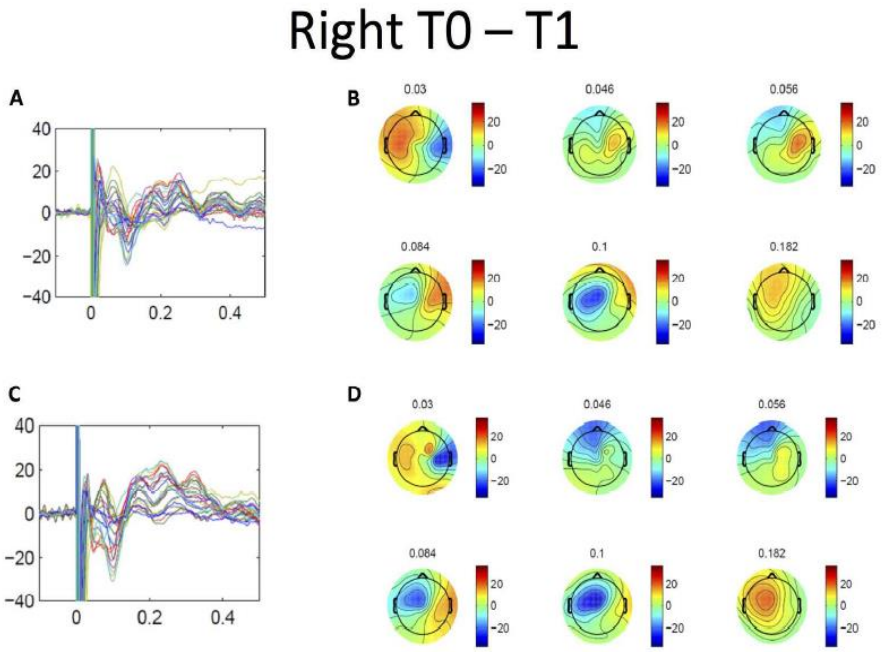

Fig. 14. Average of TEPs recorded at all electrodes superimposed in a butterfly diagram (A and C) and scalp distribution maps (B and D) at 30, 46, 56, 84, 100, 182 ms after sugnle pulse stimulation over the right M1 at T0 and T1

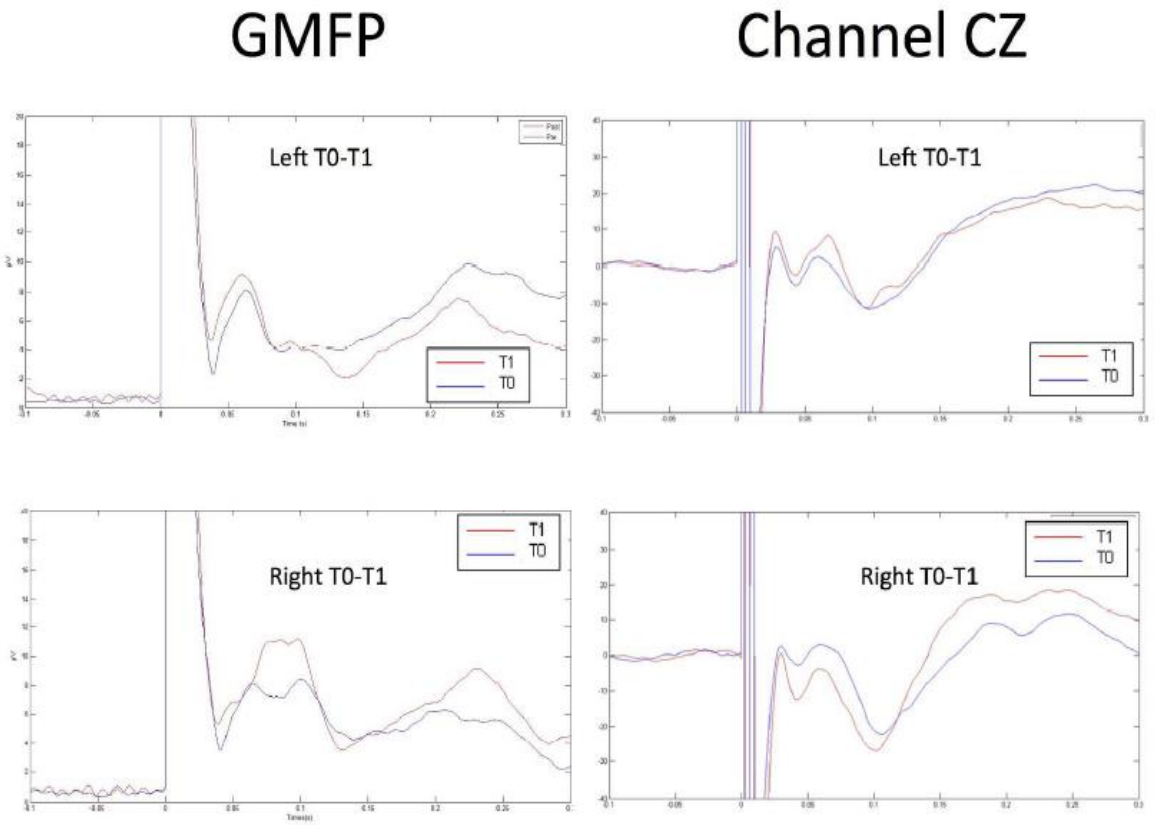

Fig. 15. A: Total activation produced by TMS over the right and left M1 as measured by the GMF at T0 and T1. B: average of the EEG responses recorded at vertex (Cz) by TMS over the right and left M1at T0 and T1.

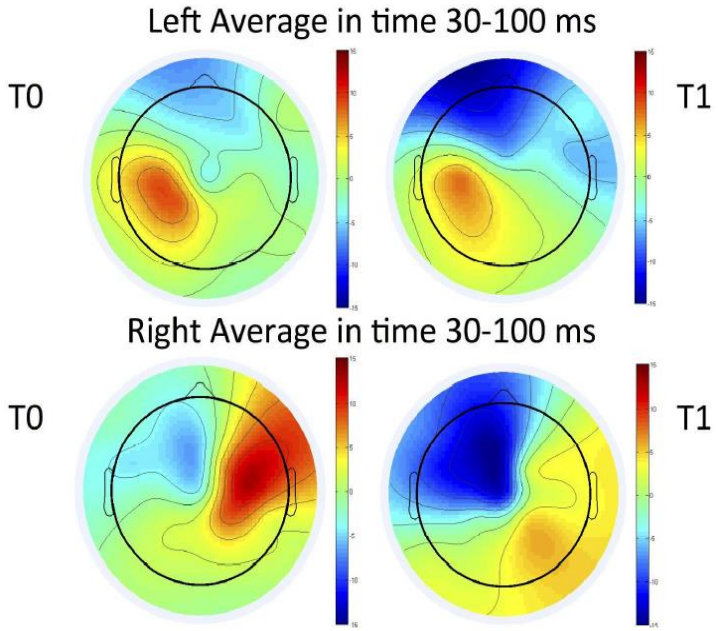

Fig. 16. Left and Right Scalp distribution maps at the average in time 30–100 ms after the TMS.

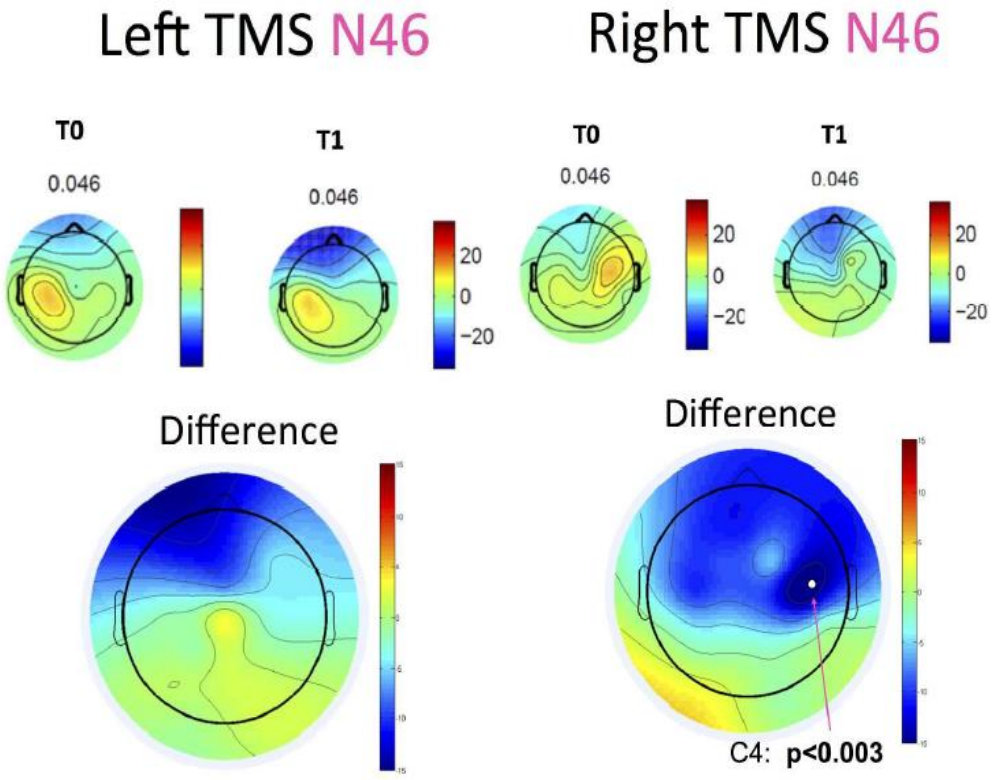

Fig. 17: Scalp distribution maps at 46 ms after the TMS over the left and right M1 at T0 and T1 and maps difference.

3.5 Relationship among diffusion tensor imaging, TMS EEG activity, and cognitive status in mild cognitive impairment and Alzheimer's disease patients

MRI studies with tractography (DTI) show that in people with AD white matter changes in the level of the limbic system, the associative cortices, interhemisferic traits and corticospinal tracts are present (Bozzali et al., 2012; Scola et al., 2010).

Subjects

In the study presented in Section 3.3 we enrolled 24 test subjects divided into 12 AD patients (diagnosis made according to the NINCDS-ADRDA, McKhann et al., 2011) and 12 control subjects homogeneous for demographic characteristics (age, sex, education).

Transcranial Mgnetic Stimulation

The details are in paragraph 3.3.1.

EEG

The details are in paragraph 3.3.2.

3.5.1 Data Analysis and Methods

A subgroup of 12 subjects (6 AD and 6 controls) was also subjected to MRI exam, using equipment operating at 1.5 T; the Protocol provided a morphological study performed by scanning planes axial and coronal sequences MPRAGE T1-weighted, T2-weighted TSE sequences and a sequence EPI diffusion-weighted. All MR images were examined for artifacts by our radiologists. DICOM Images were first converted to Nifti using MRIcron (Chris Rorden's MRIcron, 300 copyright 2007). The T1 3D MPRAGE images were first converted from DICOM to NIFTI format using the MRIcron software (http://www.mccauslandcenter.sc.edu/mricro/mricron/). The images were then manually reoriented according to the line passing through the anterior and posterior brain commissures (AC-PC line) by means of MRIcro software (http://www cabiatl.com/mricro/mricro/index.html). Hippocampal segmentation was performed by two independent tracers, neuroradiologists experienced in hippocampal segmentation, using Multitracer software (http://air.bmap.ucla.edu/MultiTracer/); the inter-rater agreement coefficientwas also calculated. The segmentation was performed by manual delineation of hippocampal boundaries on coronal slices from rostral to caudal direction and using also sagittal plane as a reference. Diffusion-weighted images were processed with the FMRIB Software Library (FSL) program. Image deformation in the DTI data induced by eddy currents and head movements, were corrected applying a full affine line-up of each image to the mean no-diffusion weighted image. A diffusion tensor model was fit at each voxel, generating FA maps.

There were later tracked the VOI (volume of interest) typically ellipsoidal shape and positioned at the level of the white matter bilaterally in the periventricular prefrontal region, in the temporal region, in the periventricular occipital region, in the corpus callosum, at splenium.

The TMS EEG analysis was performed as in paragraph 3.3.3.

These subjects are studied in terms of Pearson correlation between DTI data and TMS EEG responses with $p<0.05$.

3.5.2 Results

As expected the two groups (AD and controls) differ in the features of cortical responses as assessed by GMFP scalp, with patients having a response significantly stronger than control subjects. In particular the analysis of TEPs through ANOVA showed the following results: the P30 wave appears to be stronger channels C3, Cp1, Cp2 and CP6 compared with controls ($p < 0.01$); N44 wave appears to be stronger in channels C3, FC5 and CP6 in the AD group compared than those of controls ($p < 0.005$); P60 wave appears to be stronger in channels C3, CP5 of AD group compared than those of controls ($p < 0.05$). Moreover, the two groups, also differ when the values of fractional anisotropy (FA) statistically significant differences between the two groups at the level of the white matter of the right frontal regions ($p<0.0001$), front left ($p<0.01$), body (middle third) ($p<0.001$) and genu of the corpus callosum ($p<0.005$) and a trend for bilateral temporal regions ($p<0.01$), with patients presenting values statistically lower than in controls.

Correlation analysis of the DTI data and EEG-TMS allowed us to observe the presence of an inverse correlation between the amplitude of the P30 of CP2 and CP6 channels and the values of the right temporal region of the DTI, respectively ($p < 0.05$, $r = -0,603$) and the middle third of the corpus callosum ($p < 0.01$, $r = -0.756$). Similarly, an inverse correlation was observed between the amplitude of N44 of the FC5 and CP6 channels and the values of the left temporal region of the DTI, respectively ($p < 0.05$, $r = - 0.876$) and the middle third of the corpus callosum ($p < 0.01$, $r = 0766$).

3.5.3 Discussion

The presented study in this section is the first study that integrates EEG-TMS, MRI and DTI in the analysis and characterization of Alzheimer's disease estimating the relationship between brain responses at fixed latencies and DTI values. From our results emerges that patients with AD exhibit increased cortical excitability compared to controls, as proven by the evaluation of PEM as well as of TEPs. Moreover, in the subgroup studied with MRI, AD patients show DTI data with a significant reduction of the values of fractional anisotropy in certain defined areas of the brain. The progression of the disease proceeds with different dynamics in the structure and function of neuronal circuits from normal conditions to AD. This reduction in the fractional anisotropy values in those areas correlates significantly with the increase in cortical excitability at 30 ms and 44 ms after the stimulation. In Niskanen et al 2011 also the authors found that the motor cortex excitability correlates negatively with cortical thickness on the precuneus and cuneus. The correlation was significant both in AD and

MCI subjects. In neurodegenerative diseases they found that motor cortex excitability is not independent on the cortical thickness, indeed the cortical thinning is related to weaker cortical excitability. This not happens for the sensorimotor cortex thickness in AD, it seems to be related to a protective mechnisms of hyperexcitability in this area.

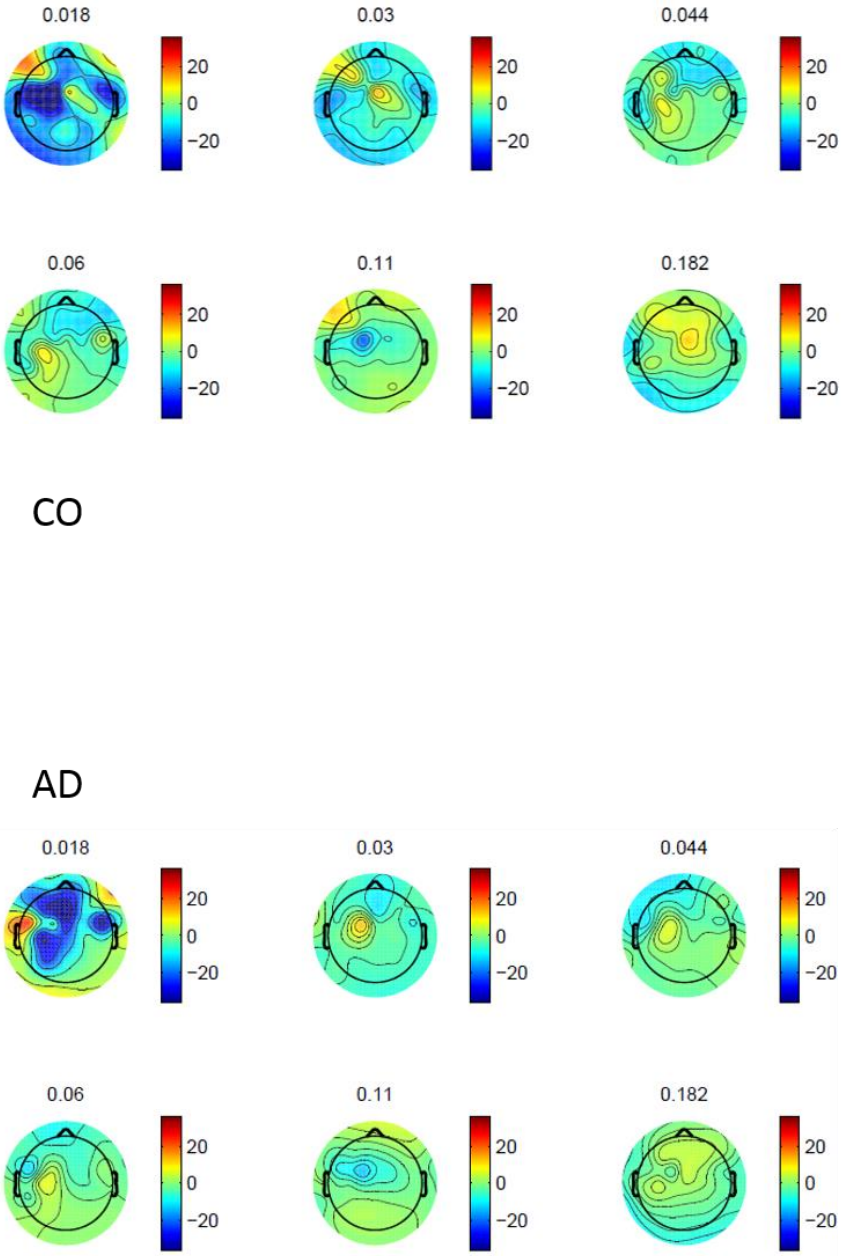

Fig. 18: Excitability results for 6 Control (top) and 6 Alzheimer's (bottom).

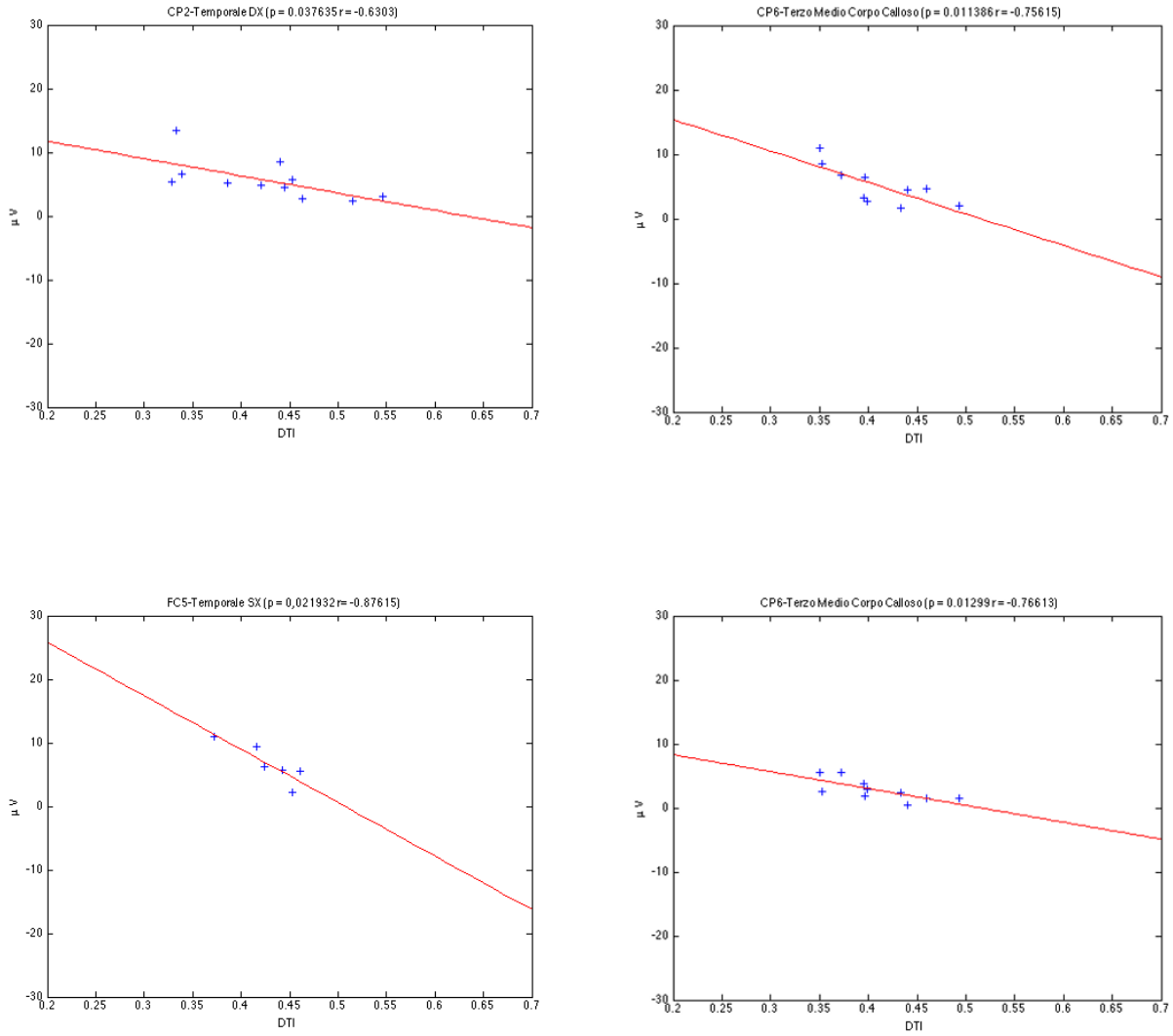

Figure 19: Average of TEPs recorded at all electrodes in the scalp distribution maps at 18, 30, 44, 60, 110, 182 ms after the single pulse stimulation over the left M1. Correlation between TMS EEG signals at 30 ms after the stimulation (first two graphics) at 44 ms (last two graphics) and DTI values in AD and CO.

4 The Influence of Corticospinal Tract Activation on Cortical Connectivity Evaluation in Healthy Subjects: A TMS-EEG Study

This chapter describes the research activity realized during a one-year visit spent at the University of Minnesota working in the Biomedical Functional Imaging and Neuroengineering Laboratory under the supervision of Prof. Bin He. The goal of the study was the deep characterization of the cortical areas activations and connections in healthy subjects caused by Single Pulse TMS EEG application on the motor area using the inverse problem solution and dynamical connectivity estimation following the spread of activations with special focus on the influence of corticospinal tract excitability.

4.1 TEPs and Motor evoked responses of TMS

It is well known that amplitudes and latencies of Motor Evoked Potentials (MEPs) during TMS are driven by a combination of excitatory and inhibitory events occurring at different neural levels in the sensory-motor and related networks and along the motor pathway (Barker et al., 1985; Amassian et al. 1989; Rossini et al., 1991, 1994, 2010; Kujirai et al., 1993; Hallett 2000; Ferreri et al., 2006), although the relative contribution of these events and networks is far from being fully elucidated (Ferreri et al., 2011, 2012). Moreover, it is also well known that MEPs elicited by a consecutive series of individual TMS stimuli show a clear time-fluctuation in amplitude, despite the stable spatial and physical stimulus characteristics, when recorded from a fully relaxed muscle (Amassian et al. 1989; Rossini et al., 1991, Kiers et al. 1993; van der Kamp et al. 1996; Ellaway et al. 1998). With respect to the motor threshold, most TMS-EEG studies to date have evaluated either subthreshold or suprathreshold stimulation, in which a motor evoked potential in peripheral muscles occurs in very few or nearly all trials, respectively. While studies have shown the TMS-EEG response to be stable across several stimulus intensities, with increasing TEP amplitudes with increased intensity, no study has directly evaluated the influence of peripheral muscle activity on TEPs and resultant connectivity. By applying TMS at the motor threshold, a peripheral motor response (MEP) results in approximately 50% of the trials, based on the definition of motor threshold, allowing for the direct comparison of TEPs between conditions without changing the stimulus intensity. TMS of the primary motor cortex (M1) evokes several volleys of corticospinal activity, causing a discharge in the spinal motor neurons directly inducing the elicitation of MEPs. As TMS-EEG has been thought

to measure primarily cortico-cortical interactions, the activation of the cortico-spinal tract - in the form of peripheral muscle activation or MEPs - has not been directly evaluated previously and has been assumed to have little effect on the resultant TMS-EEG response. . The principal aim of the current study is to evaluate the TMS evoked dynamics within the motor network, and to elucidate the effect of corticospinal excitability, measured by the peripheral motor evoked potentials, on the resultant cortical evoked activity and network connectivity.

4.2 Materials and methods

Subjects

Seventeen healthy subjects (mean age 23±11, 12 female, 5 male) participated in the present study according to a protocol approved by the Institutional Review Board of the University of Minnesota. All participants provided written informed consent prior to participation. The subjects received single pulse TMS to the left and right primary motor cortex while EEG was recorded. All participants were screened for any relevant medical history or contraindications to TMS (Rossi et al., 2009). Any medications or related medical history were reviewed and approved by a physician prior to participation.

Transcranial Magnetic Stimulation

TMS was carried out by a Magstim Rapid^2 stimulator (biphasic pulse configuration) and a 70 mm figure eight coil. The coil was placed tangentially on the scalp with the handle pointing backwards and laterally at a 45^o angle away from the midline, approximately perpendicular to the line of the central sulcus, suggesting that the flow of the induced electric current in the brain is optimal for stimulation of M1 (Brasil-Neto et al., 1992; Mills et al., 1992). The coil was moved from the M1 area localized on the MRI of the subject to find the motor hotspot with the lowest threshold for the first dorsal interosseous (FDI) muscle of the contralateral hand. After finding the motor hotspot, the coil was stabilized and immobilized by means of a mechanical support and the resting motor threshold (rMT) was determined as the lowest stimulus intensity which produced at least five MEPs of 50 μV out of ten consecutive stimuli (Rossini et al., 1994, 1999). A Brainsight neuronavigation system (Rogue Research, Montreal, Canada) was used to localize the stimulation targets on the individual

MRI of the subject. MNI (Montreal Neurological Institute) coordinates of cortical sites underlying coil locations were estimated for each subject by the Brainsight System, on the basis of digitized skull landmarks (nasion, inion and two preauricular points). Magnetic stimuli were delivered at 100% of resting motor threshold, and the same intensity of stimulation was maintained in the 100 trials. The EMG response was continuously monitored for all subjects bilaterally from the FDI using disposable EMG electrodes positioned in a belly-tendon montage and the Brainsight MEP Pod (Rogue Research, Montreal, Canada), and recorded for 11 subjects. Each subject underwent an experimental session consisting of 2 blocks of 100 trials of TMS delivered at a frequency of 0.2 Hz, 1 block on the left M1 hotspot and 1 block on the right M1 hotspot. The order of stimulation targets was balanced across subjects. TMS was applied while subjects were seated in a comfortable armchair with their hands pronated in a relaxed position and eyes open. To reduce auditory activation during stimulation, subjects wore earplugs for the duration of the experiment.

EEG

TMS-compatible 64 channel EEG caps (Fast N' Easy TMS Cap, Brain Products GmbH, Munich, Germany) were used along with TMS compatible EEG amplifiers (BrainAmp MR Plus, Brain Products GmbH, Munich, Germany) allowing continuous data recording without saturation of the EEG signals. Additional electrodes were used as ground and reference. The ground electrode was positioned in AFz and the FCz electrode served as the reference for all electrodes. The signals were bandpass filtered online at 0.1–500 Hz and digitized at a sampling rate of 5 kHz. Skin/electrode impedance was maintained below 10 kOhms for all subjects. Electrode positions were digitized and co-registered to each subject's magnetic resonance image (MRI) by means of the Brainsight System (Rogue Research, Montreal, Canada).

MRI

Anatomical MR images were obtained for each subject using a T1 weighted magnetization prepared rapid acquisition gradient echo (MP-RAGE) sequence on a Siemens Magnetom Trio 3T Scanner (Siemens, Munich, Germany). Anatomical images were imported into the Brainsight Neuronavigation system (Rogue Research, Montreal, Canada) and used to generate skin and curvilinear brain surfaces.

Data Analysis

Data analysis was conducted using MATLAB 2008b version 7.7 (MathWorks, Natick, Massachusetts, USA) and the public license toolbox EEGLAB (Delorme and Makeig 2004). TMS evoked EEG-activity, i.e. TMS-evoked potentials (TEPs), were visually inspected in each channel for each trial and trials contaminated by environmental artifacts, muscle activity, or eye movement were rejected. Following this procedure, EEG signals were divided in segments of 3 s including a pre-stimulus baseline, stimulus artifact, and post-stimulus period. The signals between -1 to 0 sec and 8ms to 2sec (i.e. not including the stimulus artifact) were then low pass filtered at 80 Hz and notch filtered at 60 Hz. All signals were then down sampled from 5000 Hz to 500 Hz, baseline corrected (100 ms prestimulus), and averaged. For each electrode, all epochs showing TEPs contaminated by values exceeding ± 200 μV in the time window from 20ms to 1s after the stimulus or ± 120 μV in the time window from 100ms to 1s after the stimulus were automatically rejected (Delorme and Makeig, 2004). Rejected trials for each electrode were visually inspected and manually confirmed. TMS-EEG responses over all the included trials for each electrode were averaged for each stimulation condition, and semi-automatic amplitude/latency measurements of each component of the EEG evoked potentials (using Cz as a reference to individualize the peak component latency) were performed to obtain the excitability results in all scalp electrodes. EEGLAB was used to produce potential maps at each latency corresponding to a peak in Cz. Additionally, for a subset of 11 subjects with recorded EMG data, the trials were divided into two sub-groups of *MEP* and *no-MEP*, based on the MEP values – corresponding to the presence of an MEP of at least 50 μV or lack thereof, respectively. Statistical analyses were performed using paired t-tests between the areas of the peak response. The significance threshold of the results was fixed at $p = 0.05$.

Cortical sources analysis of the ERPs

Source localization was conducted for the TEP components using the eConnectome MATLAB toolbox (He et al., 2011b) after the average of all trials and after the average of trials within the *MEP* and *no-MEP* sub-groups. The current density distribution of the averaged evoked response was then projected onto the template MNI brain. Noise estimation (automatically calculated) was subsequently used to determine the sensor weighting and the regularization parameter (λ) of the current density reconstruction. The head volume conduction model was implemented using the Boundary Element Method (He et al., 1987; Hämäläinen & Sarvas, 1989) of the head having 3 compartments of fixed conductivities (scalp: 0.33 S/m; skull: 0.0042 S/m; brain: 0.33 S/m). Cortical current density imaging (Dale & Sereno, 1993) was performed using the Minimum Norm Algorithm.

Connectivity analysis

Connectivity analysis was performed using the adaptive Directed Transfer Function (aDTF) (Wilke et al., 2008) within the eConnectome MATLAB toolbox (He et al., 2011b). Connectivity was calculated amongst regions of interest (ROIs) with centers located at the maximum of the activation corresponding to each peak in the evoked potential of channel Cz with a radius equal to 10 mm, in the window of the TMS-evoked response between 16 and 300 ms. A Multivariate Adaptive Autoregressive (MVAAR) model was constructed and used to describe the dataset composed by data vector over time, the matrices of time-varying model coefficients, and a multivariate independent white noise. The time-varying coefficient matrices were established using a Kalman filter algorithm, which describes the behavior of the multivariate signals by the MVAAR model. The time-varying modeling enables instantaneous calculation of the model parameters (Arnold et al., 1998). Phase shuffling of the original multivariate signal was performed 1000 times to disrupt any time-locked coupling between the estimated cortical activity in ROIs (Wilke et al., 2008; Astolfi et al., 2005a). Both direct and indirect paths of connections in form of matrix aDTF (t,i,j,f) indicate the dynamic information flow from ROI i to ROI j at frequency f at time instant t. aDTF (t,i,j,f) is expressed as the percentage of power of the current density of ROI i that is due to the current density in the ROI j (normalized aDTF). The outflow of each ROI is the summation of information flow from the ROI. Similarly, the inflow of each ROI counts the total inflow from all the other ROIs.

4.3 Results

For the population of 17 subjects, the average rMT for left M1 was 58±10% of the maximum stimulator output (MSO). The average rMT for right M1 in the population is 60±13% of the MSO. For the 11 subjects with recorded EMG activity, the peak-to-peak mean MEP value for left M1 TMS was 289 ± 152 μV, while the mean MEP value for right M1 TMS was 225 ± 143 μV. After dividing the trials into the *MEP* and *no-MEP* conditions, the peak-to-peak mean MEP value for left M1 was 402±243 μV for *MEP* trials and 16±3 μV for *no-MEP* trials. For right M1 TMS, the peak-to-peak mean MEP value after division was 429±196 μV for *MEP* trials and 16±3 μV for *no-MEP* trials. After subdivision, the proportions of *MEP* and *no-MEP* trials for left M1 TMS were 49±19% and 51%±17%, respectively. For right M1 TMS, the proportions of *MEP* and *no-MEP* trials were 56±25% and 43%±25%, respectively. Overall, the mean latency of MEP responses in the EMG was 31±4 ms for left M1 TMS and 31±3 ms for the right M1 TMS.

Excitability topographical maps

Single pulse TMS of both left and right M1 evoked EEG activity lasting up to 300 ms (Ilmoniemi et al., 1997; Komssi and Kahkonen, 2006; Ferreri et al., 2011, 2012) composed of a sequence of deflections of negative and positive polarity peaks, as reported previously in the literature. TMS-evoked potentials resulting from left M1 stimulation are shown in Figure 1. The stimulation resulted in positive peaks in channel Cz at 30ms, 60ms, and 170ms post-TMS, and a series of negative peaks at 46ms, 100ms, and 278ms post-TMS. The scalp topographies, along with the cortical current density estimates, shown in Figure 1, illustrate the spatio-temporal evolution of TMS-evoked activity. At 30 ms the evoked activity is positive central, followed by activity in left M1 at 44ms and 60ms. At 100 ms, the TMS evoked response is central negative in the site of the stimulation, followed by a central positive response at 170ms, and medial frontal activity at 278 ms. With respect to the cortical current density estimates for left M1 TMS, the maximum current density is in the left precentral gyrus corresponding to the hand area of primary motor cortex (Brodmann Area (BA) 4) at 30, 46, 60, and 170 ms after the stimulation, followed by the superior frontal gyrus corresponding to premotor cortex (BA 6) at 100 and 278 ms following the stimulation.

The TMS-evoked activity resulting from right M1 stimulation is shown in Figure 2, including a consistent pattern of positive and negative peaks in the evoked response. Similarly to left M1 stimulation, the evoked activity remained localized to the site of stimulation for early latencies (30, 44, and 54ms), then progressed to frontal (100 and 268ms) and central motor areas (178 ms). Cortical current density estimates indicate that the maximum current density progresses from the precentral gyrus hand area (BA 4) at 30, 44, and 176 ms, to the postcentral gyrus in somatosensory cortex (BA 3) at 54 ms, and the superior frontal gyrus in premotor cortex (BA 6) at 100 ms on the right side and at 268 ms on the left side.

For both stimulation conditions (left and right M1) the source localization from the site of stimulation (early latencies) spreads toward the premotor area and supplementary motor areas in a more central position in the later latencies.

TEPs in MEP verses no MEP condition: excitability and source localization results

The excitability results for left M1 TMS are shown in Figure 3 for the *MEP* condition (left) and the *no-MEP* condition (right) at latencies of 30, 44 ms, 60 ms, 100 ms, 164 ms and 270 ms, respectively; similarly the *MEP* and *no-MEP* condition results for right M1 TMS are shown in Figure 4 at latencies of 30, 44 ms, 54 ms, 100 ms, 164 ms and 270 ms, respectively. The topographical maps

show a significant difference between the two conditions (*MEP* and *no-MEP*) at 60 ms for left M1 TMS in CP3 (p=0.011), CP1 (p=0.035), and C1 (p=0.013). Similarly, for right M1 TMS a significant difference is shown at 54 ms in channels CP6 (p=0.037) and C6 (p= 0.0026). For both stimulation conditions (left and right M1), the difference in amplitude (μV) is not only present in the motor hand area but also in the centro-posterior areas, with increased amplitudes in the *MEP* condition compared to the *no-MEP* condition. Source localization results indicate similar patterns of activation in the two conditions *MEP* and *no-MEP* for both left and right M1 TMS, with no significant differences between conditions.

Dynamic Connectivity results

The functional connectivity results are shown as the average of all the frequency between 1-80 Hz. The results in each frequency band (δ, θ, α, β, γ, not shown) had similar patterns. The inflow and outflow connectivity patterns amongst the five ROIs are shown in Figure 5 for left M1 TMS and in Figure 7 for right M1 TMS. In Figure 5, the highest outflow for the *MEP* and *no-MEP* in terms of connectivity values is in the ROIs that correspond to the stimulated area after left M1 TMS in the time interval between 16 and 150 ms. From 160 ms after the stimulation the highest outflow is from the central motor areas in the left and right central BA 4.

The inflow patterns are similar to those of the outflow, with the highest inflow in M1 and in S1 between 16 and 150 ms. From 160 ms after stimulation, the highest inflow is from the left central M1 in the left and right central BA4 . For the *no-MEP* condition we observed the similar connectivity pattern with lower strength. Figure 6 shows the connectivity pattern constructed from the inflow and outflow time courses for latencies of 60, 100, 164, and 270 ms after left M1 TMS. At 60 ms, the connectivity flow is from the left M1 toward the somatosensory cortex (S1) for both the *MEP* and *no-MEP* conditions, but importantly with lower connectivity strength in the *no-MEP* condition. At 100ms, in the *MEP* condition, reciprocal connections are seen between the stimulated left M1 and S1, along with contributions from central left M1 to the stimulated left M1. In the *no-MEP* condition, the only connectivity seen is from the stimulated left M1 towards S1 with significantly reduced connection strength compared to the *MEP* condition. At 164 ms, connectivity is again shown between left M1 and the somatosensory cortex (S1) and from the contralateral right central M1 towards left M1. Importantly, a similar connectivity pattern is seen at 100 ms and at 164 ms between the *MEP* and *no-MEP* conditions, with a significant increase in the strength of the M1 to S1 connectivity in the

MEP condition. At 270 ms, the connectivity pattern is the similar for the two conditions with connections reciprocally between the contralateral central BA 4 and the stimulated left central BA 4.

For right M1 TMS (Figure 7), the highest outflow for the *MEP* condition in terms of connectivity values is in the ROI that corresponds to the right M1 for the entire time interval analyzed. The highest inflow is in the ROI that corresponds to the right M1 and to the somatosensory cortex from 16 and 250 ms. From 250 ms the highest outflow is from the right central M1. Importantly, for the *no-MEP* condition, the strength of the connectivity exhibits similar patterns with generally lower connectivity strengths for the time interval examined. The outflow is highest in the right M1 until 100 ms, while from 100 ms until 300 ms the outflow is highest in the left and right central M1. The highest inflow is from the stimulated right M1 until 100 ms then between 100 ms and 150 ms is from the supplementary motor area. From 150 ms until 300 ms, the highest inflow is from the left and right central M1.

Figure 8 shows the connectivity patterns constructed from the inflow and outflow information for the latencies 54, 100, 164, and 270 ms after right M1 TMS. At 54 ms and 100 ms for the *MEP* condition, the connectivity flow is reciprocally between right M1 and right S1. Importantly, for the *no-MEP* condition, the connectivity flow is from the right M1 to right S1, with significantly lower values in the strength of the connections. At 164 ms after the stimulation, the pattern for the *MEP* condition shows the same pattern seen at 60 and 100 ms, while in the *no-MEP* condition the connectivity flow is mainly from the contralateral central M1 to the right supplementary motor area, and reciprocally between the right central M1 and both contralateral central M1 and the stimulated right M1. At 270 ms, the connectivity flow pattern is the same for both the conditions between the contralateral central M1 and the right central M1 reciprocally, with higher connection strength in the *no-MEP* condition. The connectivity results reveal that, for both right and left M1 TMS at 60 ms, 100 ms and 164 ms, the connectivity values from the stimulated M1 to S1 corresponding with in the trials with an MEP are higher than the values calculated for the trials without an MEP. At 270 ms, the connectivity pattern between ipsilateral central M1 and contralateral central M1 is similar for the right and left M1 stimulation and between the conditions (MEP vs. no-MEP).

4.4 Discussion

Source localization: origins of TMS-evoked activity

The present results demonstrate that the spread of the activations for both left and right M1 TMS is from the stimulated motor area to central motor and parietal areas, along with areas in the middle, superior and inferior frontal lobe.

The source localization results for left M1stimulation reveal that the maximum current density at 30 ms and 44 ms after the stimulation is located in a stable site: the stimulated left BA 4 in the hand motor area. The 30ms latency is thought to involve subcortical pathways, perhaps the non-specific thalamic nuclei and/or basal ganglia which, in turn, project back diffusely to the cortex (Bonato et al., 2006). Regarding the origin of the 44 ms latency, it is possible that different neural structures separate from M1 (e.g. cingulate areas) or functionally connected (e.g. pre-motor and supplementary motor cortices) recruited by the suboptimal stimulation may be responsible for this negative component (Bonato et al., 2006). The activations in both latencies can be due to excitatory activity intrinsic to M1, while the response at 44 ms could also be represented by excitatory events at the precentral gyrus and subcortical events (Komssi et al., 2004). At 60 ms after the stimulation, the response in cortical current density map has its maximum in BA 4 and has an important spread toward the BA 3 corresponding to the hand area of primary somatosensory cortex. This area has thalamocortical projections (to the ventral postero-lateral nucleus) and its function includes stimuli localization and stimuli intensity proprioception. Parietal areas are also associated with the role this area has in the somatosensory-motor integration of the movement performed. Such an area could be regarded as a higher order somatosensory zone devoted to the analysis of proprioceptive information for joints appropriate motor control (Astolfi et al., 2004). In previous experiments, the N100-P190 complex has been associated with the sound emitted by the discharging coil (Nikouline et al., 1999; Tiitinen et al., 1999), although later studies that used white noise during stimulation to mask the coil click have partially excluded such possible contamination (Kähkönen et al., 2005; Komssi et al., 2004; Paus et al., 2001). The study by Bonato et al. (2006) adds further support to the possibility that these components might, at least in part, originate from cortically TMS-induced electric potentials as already proposed (Komssi et al., 2004). The present results indicate that for left M1TMS, the cortical current density maps at 100 ms and 278 ms have the maximum in the left superior frontal gyrus (BA 6) corresponding to the premotor area, and in the precentral gyrus (central BA 4) at 170 ms. Areas in the frontal lobe activated at later latencies not only demonstrate contralateral activation, but also are dedicated to high order associative functions. These associative areas of cortex serve to associate sensory inputs to a motor response and perform mental processes that intervene between sensory inputs and motor outputs.

For the right M1 TMS, the cortical current density distribution reveal that at 30 ms and 44 ms the maximum of the current density is in the right BA 4. At 54 ms, the maximum current density is located within somatosensory cortex (BA 3) in the parietal lobe (post-central gyrus), connected to ventral posterior nucleus of the thalamus. At 100 ms, the maximum of the current density is in the right superior frontal gyrus (BA 6), while at 176 ms the maximum is located in right central BA 4, followed by the left superior frontal gyrus (BA 6) at 268 ms.

Two studies have previously reported a defined pattern of activation following TMS to left primary motor cortex (Huber et al., 2008, Paus et al., 2001), in which TMS produced large deflections in scalp voltage primarily near the site of stimulation but also on the contralateral side. Huber et al. (2008) reported activation for left M1 stimulation in one subject at 30, 80, and 120 ms following TMS in the same region of the stimulation along with a contralateral activation at 40 ms after the stimulation. Paus et al. (2001) showed that, in a group of seven subjects, the mean evoked activity consisted in current density results for the left M1 TMS at 44 ms after the stimulation localized in the site of stimulation, as we reported. In summary, we found that for both stimulation conditions (left and right M1), the source localization from the site of stimulation (early latencies) spreads toward the somatosensory, premotor, and central motor areas in the later latencies.

TEPs in *MEP* and *no MEP* conditions

For both the left M1 and right M1 TMS conditions, a significant difference was seen in the amplitude of the response in the somatosensory area near 60 ms between the *MEP and no-MEP* conditions. This difference could be due to somatosensory feedback resulting from peripheral motor activation from the TMS pulse or to an unmasked silent period that provokes a reduction in the GABAergic inhibition (Jacobs and Donoghue, 1991). The conduction time between the brain and small hand muscles is approximately 30 ms in case of M1 hand area stimulation, as observed in the present experiment. The cortical deflections peaking approximately 50-60ms after the stimulus and later may be affected by the somatosensory feedback resulting from the target muscle activation (Maki et al., 2010, Bonato et al., 2006). Maki et al. (2010) suggested a relationship between TMS-induced peripheral and cortical activation measured around 15 ms and 30 ms after the TMS pulse, when the somatosensory feedback from the target muscle has not yet to reach the cortex. Ipsilateral and contralateral cortical areas are recruited by intra- and inter-hemispheric cortico-cortical and subcortico-cortical connections, with longer latency contributions of sensory feedback from the twitching muscles in the case of stimulation of the motor cortex (Giambattistelli et al., 2014). While the MEP amplitude is greatly affected by the excitability levels of the spinal motor neuron pools,

TMS-EEG signals are typically thought to measure primarily cortico-cortico interactions, without being affected by corticospinal activity. Indeed, it is well known that MEPs are extremely variable in amplitude when collected over time, despite very stable experimental conditions in relaxed subjects (Kiers et al., 1993). This variability is related, in part, to spontaneous changes in the excitability of the spinal motor neuron pools recruited by the cortical efferent volley induced by TMS (Bonato et al., 2006). Additionally, since area to area modulation is often inhibitory, corticospinal excitability does not necessarily increase with an increase in cortical activity (Rossini et al., 2015). Previous TMS-EEG studies have demonstrated that with increased stimulation intensity, the overall amplitude of TEP components tends to increase, while maintaining the original pattern of cortical origins and polarity of peaks. However, as stimulation intensity increases, the likelihood of generating peripheral MEPs from TMS also increases, with potential implications to the TEPs. Applying TMS at motor threshold presents a unique opportunity to study the differences between TEPs resulting from trials resulting in MEPs and those without MEPs, without changing the stimulation intensity. While other studies have investigated the relationship between pre-stimulus activity and MEP amplitudes (Schulz et al., 2014), no other studies, to our knowledge, have evaluated the influence of corticospinal tract activation, in the form of peripheral MEPs, on the cortico-cortico connectivity patterns seen in the TEPs.

Networks circuits evoked by TMS in healthy subjects in *MEP* and *no MEP* conditions

For both right and left M1 TMS in both conditions, the cortical connectivity is originated from the site of stimulation between 16 ms and 100 ms for frequencies from 1-80 Hz. The connectivity pattern for both the left and right M1 TMS and for both the conditions is ascendant in the time interval analyzed. This is confirmed by the spread of the activated regions during the studied time interval: for the early latencies (until 60 ms after the stimulation) the maximum of the outflow and inflow is in the stimulated area then for the later latencies it is contralateral and ipsilateral to the stimulation site in the central motor area (BA4) activated at 164 ms. The *no-MEP* condition shows overall lower values of outflow and inflow connectivity throughout the studied time interval, suggesting that the strength of connections between areas are correlated with MEP values.

In terms of the connectivity flow pattern for left and right M1 TMS and both conditions, the highest outflow and inflow is from the stimulated area and the somatosensory cortex between 16 ms and 100 ms, suggesting that the connectivity pattern clearly reflects the effect of the stimulation (although with lower strength for the *no-MEP* condition). The difference in the topographical maps at 60 ms suggests a difference in the somatosensory feedback pathway in the two conditions. The

highest differences in terms of connectivity strength between the two conditions are for the latency after the elicitation of the MEP (60 ms) that it is implicated in the sensory feedback. For the *MEP* condition, after both left and right TMS, the main connectivity flow pattern starts in the latency 164 ms from the stimulated M1 toward the sensorimotor area ipsilateral to the stimulation. For the *no-MEP* condition, the main connectivity flow pattern starts in the latency 164 ms from contralateral central M1 toward regions activated in the stimulated hemisphere. These findings suggest that this latency reflect the properties of the stimulated area not only in terms of activation (source localization) but also in terms of the connectivity flow pattern (functional connectivity). The latencies corresponding to TMS-evoked activity in the present studies have previously been shown to have properties that correspond to the network activated from the stimulated area. Casula et al. (2014) showed that the distribution of the N100 was not compatible with an auditory potential distribution, which agrees with the present results. Similarly, Liomis et al. (2009) demonstrated that the response amplitudes at 100 ms were smaller for prefrontal stimulation than for the primary motor cortex TMS, indicating different reactivity of the two regions (Kahkonen et al., 2003, 2004).

The thalamus is part of the cortico-thalamo-cortical circuits and transmits driving input from one cortical area to a higher order area (Guillery et al. 2002). It is the node to process sensory and motor output and sensory perception, and receives sensory input and cortical feedback. Unlike sensory stimulation, direct cortical stimulation does not activate the reticular formation and bypasses the thalamic gate (Massimini et al., 2005, Massimini et al., 2009). TMS-EEG therefore allows for recording from the cerebral cortex, by-passing sensory pathways, subcortical structures, and motor pathways (Ferreri et al., 2014). TMS-EEG presents a useful starting point for exploring the cumulative effects of fast and slow TMS trains, the induction of plastic changes in cortical circuits, and the long-range effects of TMS-induced volleys on connected cortical regions. Indeed in recent years, the use of plasticity inducing TMS protocols has become a powerful tool to investigate the neural activity within the hand representations in primary somatosensory and motor areas, along with touch perception and motor behavior. In particular understanding somatosensory physiology in humans and its influence on M1 and on motor control is crucial for further understanding of clinical neuroscience and potential treatments for stroke patients (Jacobs et al., 2012) and amputees (Ferreri et al., 2014). Indeed identifying methods to increase or decrease neural activity within hand representations may advance the development of therapies intended to improve hand function in clinical populations (Jacobs et al., 2012).

TMS-evoked EEG responses reflect the excitability of stimulated cortical neurons as well as the excitability of connected cortico- cortical and cortico-thalamocortical circuits. The activation of

these circuits results in the generation of EEG-recorded oscillatory activity, especially in the fast (gamma) frequency ranges (Ferrarelli et al., 2008). Movement-related changes emerge in the alpha and beta band (Schulz et al., 2014) and single pulse TMS induces a brief period of synchronized activity in the beta range in the vicinity of the stimulation site (Paus et al., 2001). The alpha rhythm is the prominent idling rhythm of the human brain prevailing in the primary motor cortex (Groppa et al., 2013) reflecting an inhibitory control process (Klimesch et al., 2007). Early TEPs responses are due to the GABA A neurotransmitter and later responses, from 100 ms are due to the GABA B neurotransmitter (Premoli et al., 2014). GABA A is associated with fast inhibition while GABA B is thought to induce changes in cortical excitability and plasticity and in dopaminergic activity in thalamic and cortical circuits through the primary spinal afferents. EEG does not discriminate between excitatory and inhibitory activity, so excitatory and inhibitory events may be summed in a complex manner to produce the recorded scalp potential. Komssi et al. (2004) suggested that early activity (up to approximately 100 ms) after motor cortex stimulation may be related to facilitation whereas late activity might reflect inhibition (Kähkönen et al., 2005). Later activation may have a different source than the earlier activity. For example, the earlier activity may be generated by evoked activity in various cortical areas, while the later components may be the result of partial phase resetting of ongoing cortical oscillations, similar to alpha ringing that is observed in visual evoked potentials (Esser et al., 2006, Komssi et al., 2004).

In addition to the cortical, cerebellar, and spinal structures, thalamic and basal ganglia nuclei may contribute to the EEG deflections recorded after TMS. As motor areas are part of the spinal-motor loop involving the putamen, globus pallidus, substantia nigra, and ventro-lateral nucleus, contribution of these structures in TMS-evoked activity at M1 is possible. In a recent study, an intensity-dependent increase of the cerebral blood flow was detected at these structures after motor-cortex TMS (Speer et al., 2003). From a connectivity perspective, TMS could be used to evaluate the connection between areas stimulating different parts of the network activated during the TEPs. Zanon et al. (2010) showed that TMS on the left parietal cortex activated a network of prefrontal regions in the contra-lateral hemisphere in a time range of 102– 167 ms after the stimulus. Moreover, activation in the ipsilateral middle temporal and fusiform gyri was observed at 171–177 ms after delivery of TMS. Findings suggest the existence of late driven connections between parietal and prefrontal regions that could partially represent the neural pathway related to attention, even if, in this experiment, no attentional processing was requested. TMS studies of premotor (Massimini et al., 2005) and sensorimotor areas (Massimini et al. 2007, Massimini et al., 2009) have demonstrated activations in bilateral SMA and frontal areas.

From the present study, along with previous literature, it is clear that EEG co-registered with TMS is a unique tool to evaluate not only the connectivity between areas as a result of stimulation, but also to measure the strength of connections existing between areas activated by TMS. Such quantification of cortical connectivity could be important for design of personalized network based neuromodulation approaches in clinical applications, such as stroke patients and amputees (Ferreri et al., 2014). When used in this manner, TMS-EEG motor mapping could not only measure the neuroplasticity induced by such a rehabilitation paradigm but also evaluating the change in the dynamic connectivity patterns and continuously adapt the intervention.

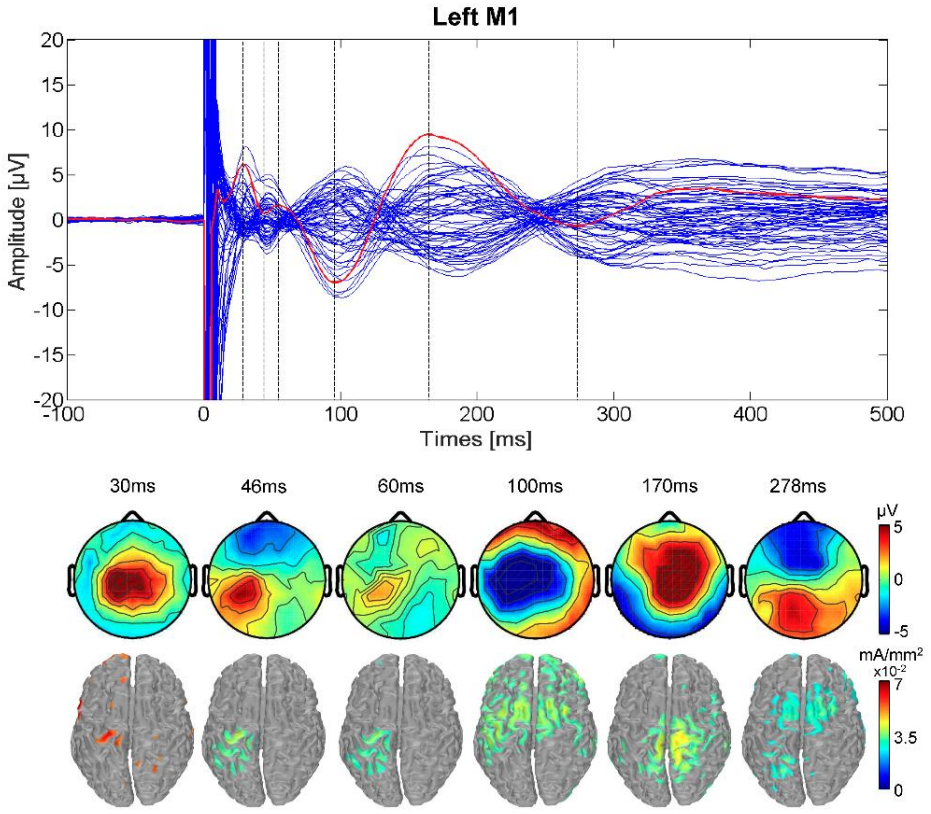

Figure 1: TMS-evoked potentials following stimulation over left primary motor cortex (average of all 17 participants). A) Butterfly plot of the average TMS-evoked activity from all electrodes. Red line indicates Cz electrode. Timing of the peaks are indicated by vertical dashed lines. B) Voltage distributions (top) and Minimum Norm estimates (bottom) of the TMS-evoked activity for each peak in the CzCz waveform. The Minimum Norm estimates have been thresholded to demonstrate the maximal activity at each peak.

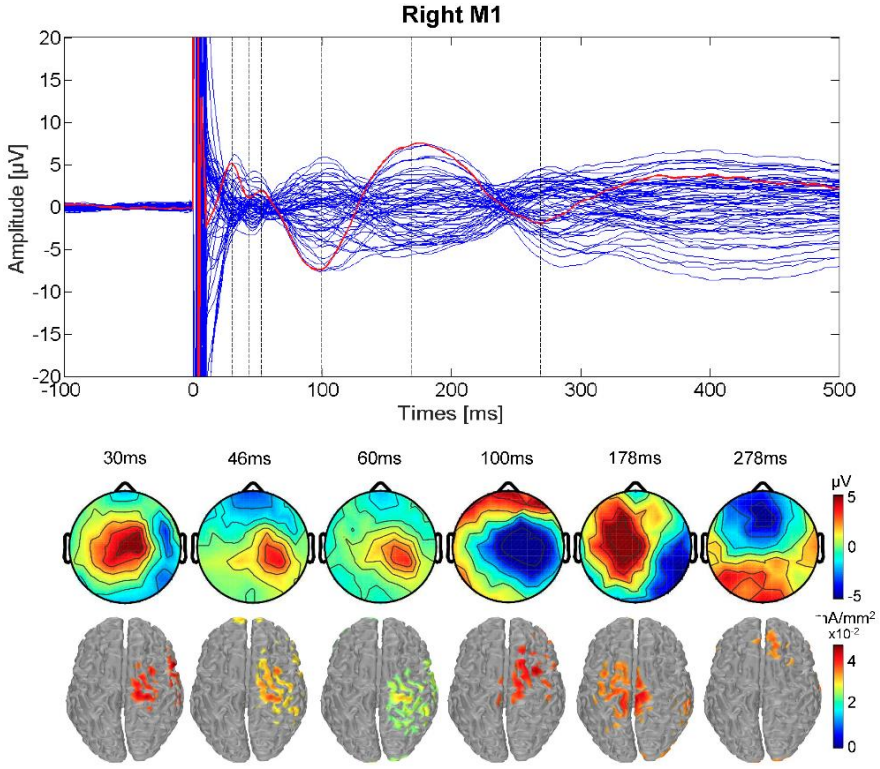

Figure 2: TMS-evoked potentials following stimulation over right primary motor cortex (average of all 17 participants). A) Butterfly plot of the average TMS-evoked activity from all electrodes. Red line indicates Cz electrode. Timing of the peaks are indicated by vertical dashed lines. B) Voltage distributions (top) and Minimum Norm estimates (bottom) of the TMS-evoked activity for each peak in the Cz waveform. The Minimum Norm estimates have been thresholded to demonstrate the maximal activity at each peak.

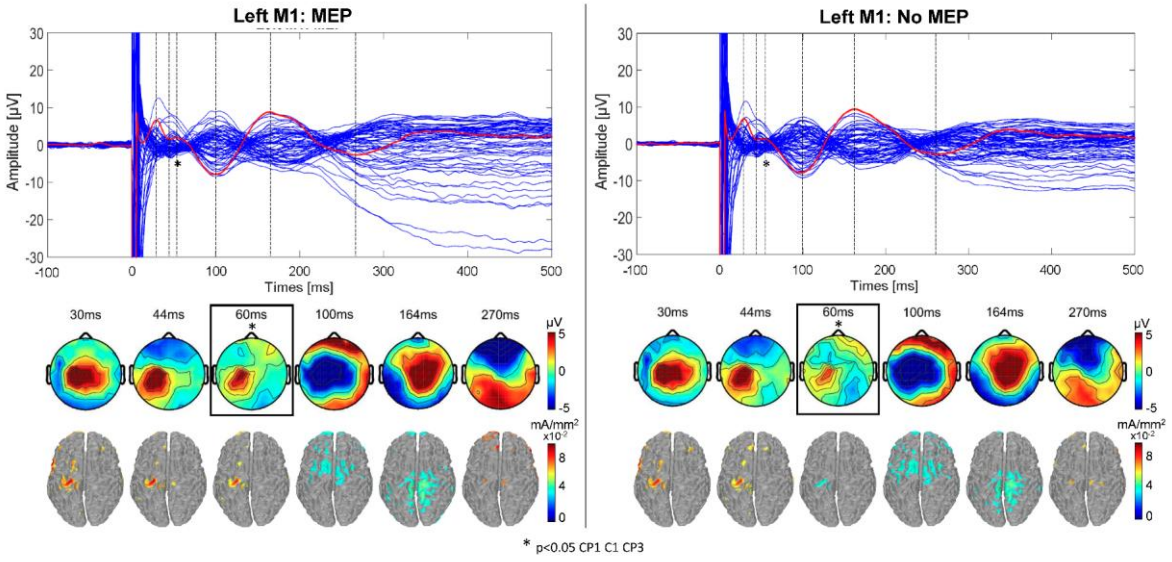

Figure 3: TMS-evoked potentials following stimulation over left primary motor cortex (average of 11 participants with simultaneous EMG recording) split between trials resulting in an hand muscle response (MEP) (left) and those without an MEP (right). A/C) Butterfly plot of the average TMS-evoked activity from all electrodes. Red line indicates Cz electrode. Timing of the peaks are indicated by vertical dashed lines. B/D) Voltage distributions (top) and Minimum Norm estimates (bottom) of the TMS-evoked activity for each peak in the Cz waveform. The blue box highlights the 60ms latency, for which the topography significantly differed between the MEP and no MEP conditions.

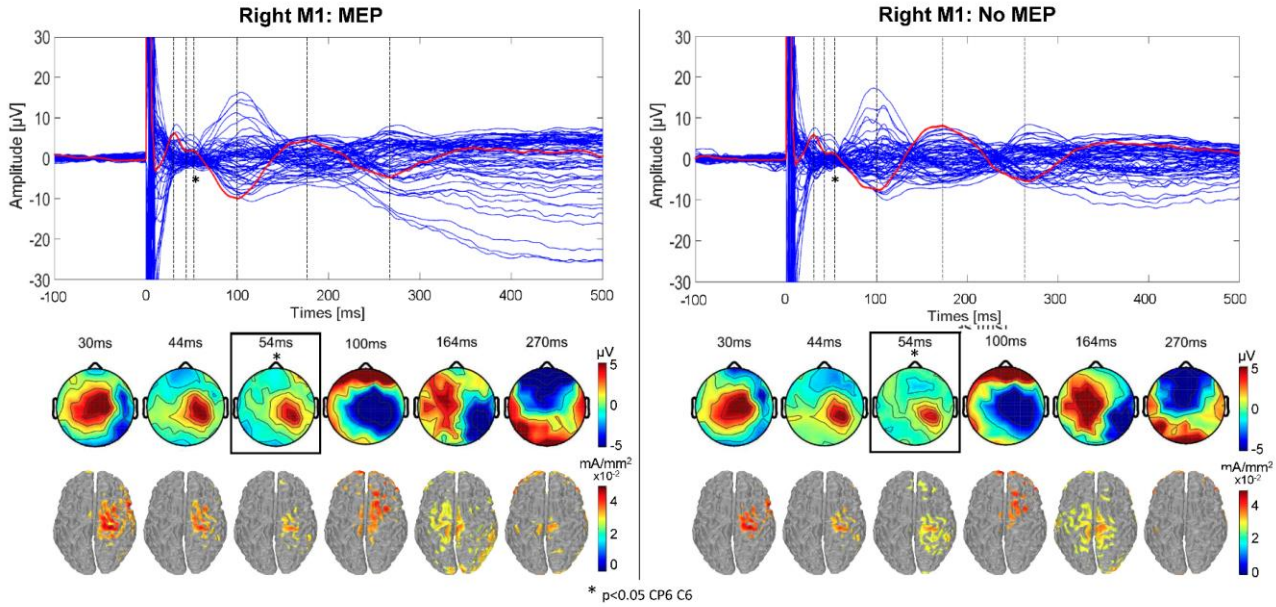

Figure 4: TMS-evoked potentials following stimulation over right primary motor cortex (average of 11 participants with simultaneous EMG recording) split between trials resulting in an hand muscle response (MEP) (left) and those without an MEP (right). A/C) Butterfly plot of the average TMS-evoked activity from all electrodes. Red line indicates Cz electrode. Timing of the peaks are indicated by vertical dashed lines. B/D) Voltage distributions (top) and Minimum Norm estimates (bottom) of the TMS-evoked activity for each peak in the Cz waveform. The blue box highlights the 54ms latency, for which the topography significantly differed between the MEP and no MEP conditions.

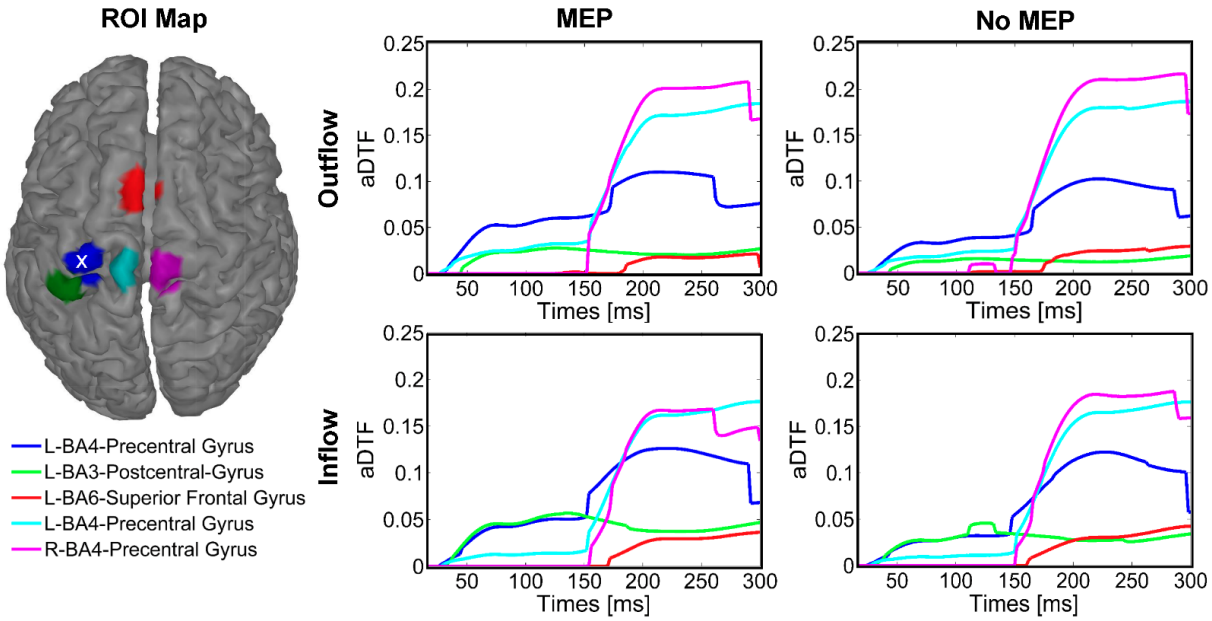

Figure 5: Information transfer amongst TMS-evoked regions of interest (ROIs) for left primary motor cortex stimulation. Five ROIs were selected (left) using the Minimum Norm estimates for each latency. Time varying connectivity as measured by the adaptive directed transfer function was calculated using the evoked activity from 1-80Hz for each of the five ROIs for trials containing MEPs (middle column) and trials without MEPs (right column), including both outflow (top row) and inflow (bottom row) patterns.

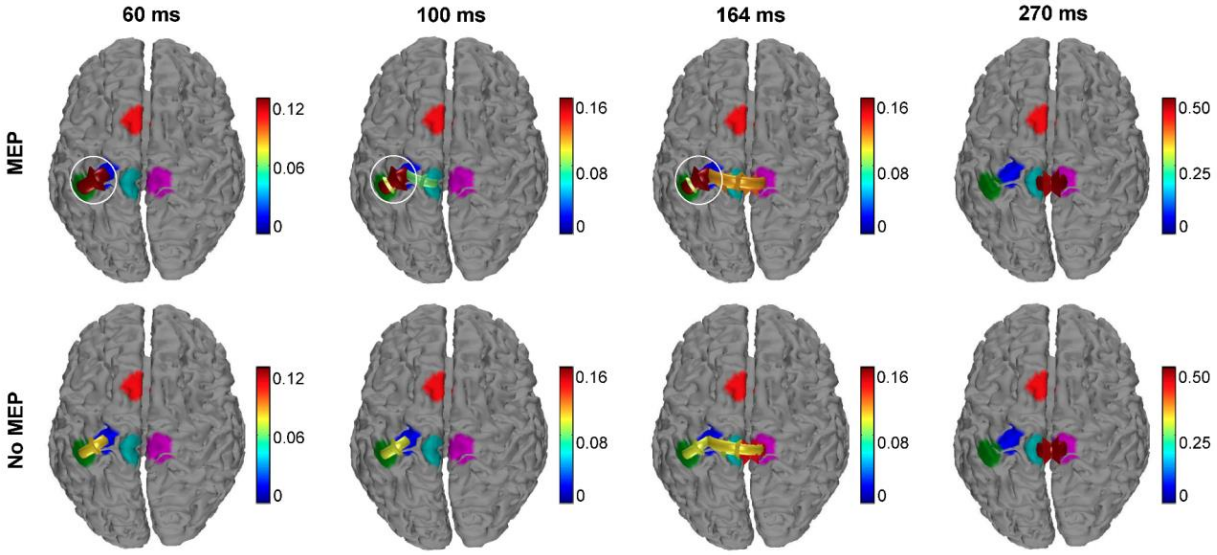

Figure 6: Connectivity patterns amongst TMS-evoked regions of interest (ROIs) for left primary motor cortex stimulation. Arrows indicate significant connectivity between ROIs at the 60ms, 100 ms, 164 ms, and 270 ms latencies. The color of the arrow indicates the strength of the connection. White circles emphasize differences in connectivity patterns amongst trials with MEPs (top) and without MEPs (bottom).

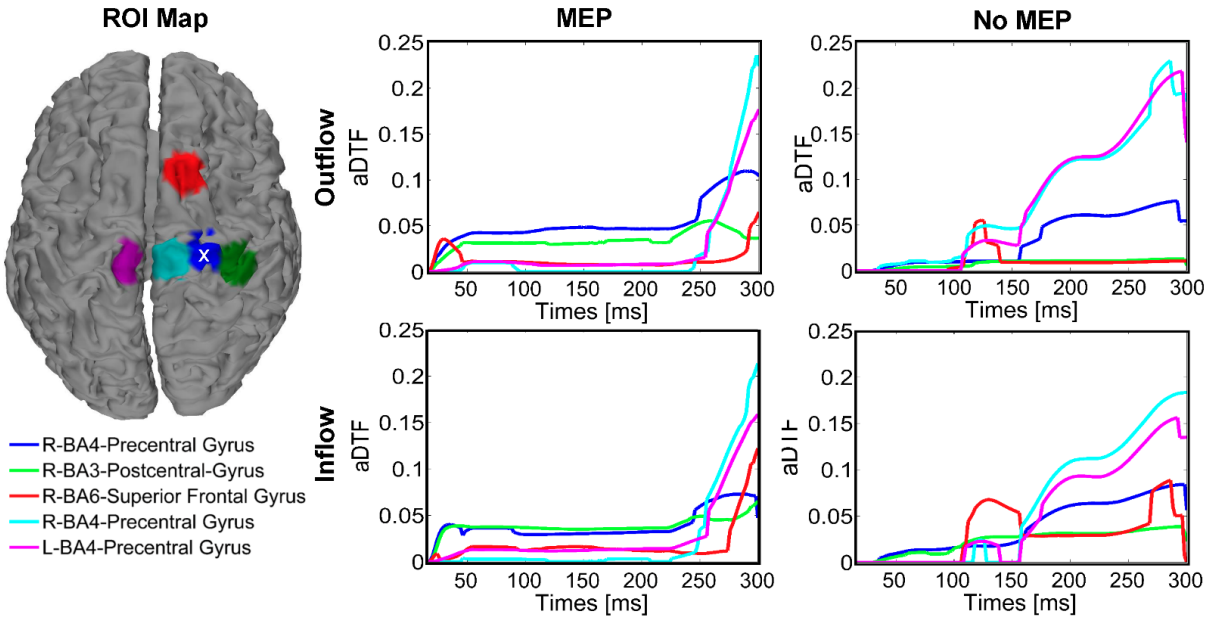

Figure 7: Information transfer amongst TMS-evoked regions of interest (ROIs) for right primary motor cortex stimulation. Five ROIs were selected (left) using the Minimum Norm estimates for each latency. Time varying connectivity as measured by the adaptive directed transfer function was calculated using the evoked activity from 1-80Hz for each of the five ROIs for trials containing MEPs (middle column) and trials without MEPs (right column), including both outflow (top row) and inflow (bottom row) patterns.

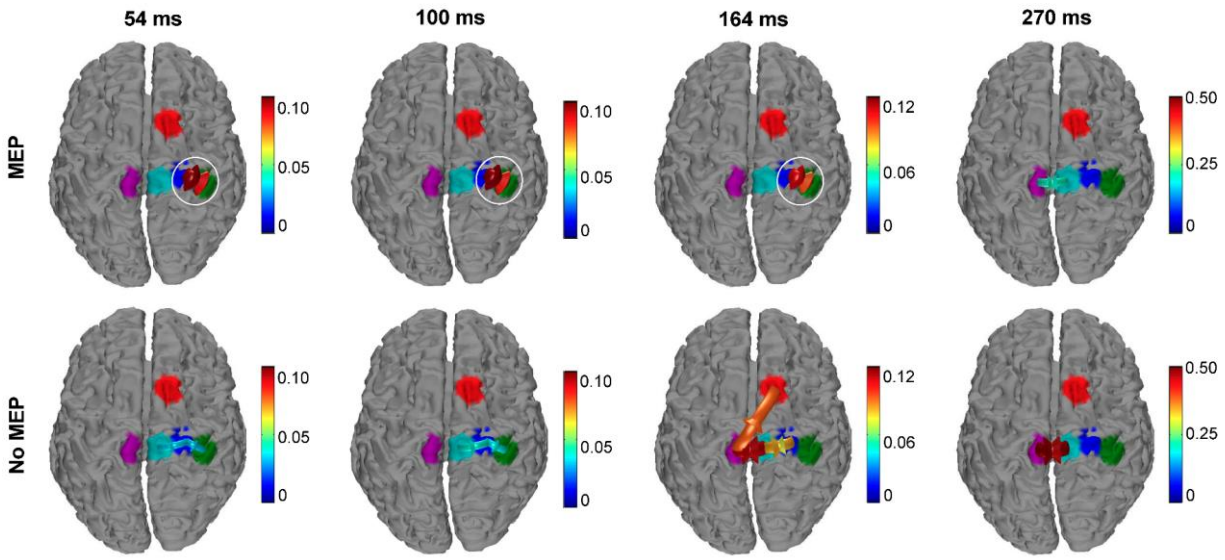

Figure 8: Connectivity patterns amongst TMS-evoked regions of interest (ROIs) for right primary motor cortex stimulation. Arrows indicate significant connectivity between ROIs at the 54ms, 100 ms, 164 ms, and 270 mslatencies. The color of the arrow indicates the strength of the connection. White circles emphasize differences in connectivity patterns amongst trials with MEPs (top) and without MEPs (bottom).

5 Conclusions and future works

This thesis collects the experiences made during my PhD and summarizes the works done in the fields of signal processing of biomedical data, with a special focus on TMS EEG data, and those related to the characterization of the brain imaging in both studies regarding healthy subjects and clinical studies.

The first study can be considered an interesting example of asymmetric hyperexcitability that could represent a mechanism of brain functional plasticity in a chronic disorder, such as symmetric arrested hydrocephalus.

The second study presented suggest that in AD and SIVD the motor cortex is functionally rearranged and its excitability is enhanced, supporting the idea that cortical hyperexcitability can promote cortical plasticity. While this study can highlight the functional involvement of cortical areas in motor control in SIVD, the present value of TMS as a clinical tool in the field is reduced as the neurophysiological profile identified did not lead to a clear distinction between vascular and neurodegenerative dementia. In my opinion, however also the electrophysiological similarities should be seen with interest as, according to the emerging principles of brain functional plasticity and connectivity they seem to highlight to common compensatory mechanisms realized by different type of injured brains, shading light on possible rehabilitative strategies able to modulate brain excitability.

In the third study by using EEG-TMS co-registration, was clearly demonstrated that the sensorimotor system in mild AD is strongly hyperexcitable. If these changes have some role in maintaining substantially intact the sensorimotor performance in mild AD patients need to be confirmed by further studies but could be here preliminary interpreted as a compensatory mechanism allowing the preservation of sensorimotor programming and execution over a long period despite disease progression.

The fourth study confirms the hypothesis that bidirectional neural interface could be of primary interest to redirect cortical areas deprived of their original function because of amputation toward restorative neuroplasticity.

In the fifth study the results suggest that a multimodal approach is helpful for advanced study of the characteristics of excitability and connectivity morpho/functional physiological and pathological aging. Indeed, it allows identifying anomalies in the connections between different brain areas of being possibly causative mechanisms involved in the pathogenesis of Alzheimer's disease.

From the sixth study clearly emerge that EEG co-registrated with TMS is a unique toolbox to evaluate not only the connectivity between areas as results of an inductive procedure but actually to measure the strength of connections existing between the activated areas. This is crucial to guarantee innovative paradigms of rehabilitation in stroke patients and amputees.

In addition, future works will regard the possibility to combine Brain Machine Interfaces (BMIs) with invasive and non-invasive brain stimulation (NIBS) to provide even better understanding of mechanisms underlying brain recovery and to improve efficacy of BMIs in stroke neurorehabilitation.

Nowadays, BMIs are being used as prostheses in order to replace lost function, but in future they may be used as tools to manipulate brain plasticity.

Brain plasticity that arise from closed-loop stimulation suggests an additional application in the case of incomplete injuries to enhance surviving descending pathways and promote rehabilitation. Crucial in this perspective will be the on line evaluation of brain areas connections to enhance the efficacy of neurorehabilitation therapy. These technologies in combination with the application of appropriate brain connectivity evaluation techniques that can follow the dynamical nature of TEPs through the computation may allow the formation of new neural circuits that restore functions with applications in a wide range of neurological injuries.

References List

Arnold, Tom, Mark J. Bertus, and Jonathan Godbey. "A simplified approach to understanding the Kalman filter technique." *The Engineering Economist* 53.2 (2008): 140-155.

Astolfi, L., Cincotti F., D. Mattia, C. Babiloni, F. Carducci, Basilisco A., P.M. Rossini, S. Salinari, L. Ding, Y. Ni, B. He, F. Babiloni, "Assessing cortical functional connectivity by linear inverse estimation and directed transfer function: simulations and application to real data." *Clinical Neurophysiology* 116.4 (2005a): 920-932.

Astolfi, L., et al. "Time-varying cortical connectivity by high resolution EEG and directed transfer function: simulations and application to finger tapping data." Engineering in Medicine and Biology Society, 2004. IEMBS'04. 26th Annual International Conference of the IEEE. Vol. 2. IEEE, 2004.

Astolfi, Laura, et al. "Estimation of effective and functional cortical connectivity from neuroelectric and hemodynamic recordings." Neural Systems and Rehabilitation Engineering, IEEE Transactions on 17.3 (2009): 224-233.

Astolfi, Laura, et al. "Estimation of the cortical connectivity by high-resolution EEG and structural equation modeling: simulations and application to finger tapping data." Biomedical Engineering, IEEE Transactions on 52.5 (2005b): 757-768.

Babiloni, F., et al. "Estimation of the cortical functional connectivity with the multimodal integration of high-resolution EEG and fMRI data by directed transfer function." Neuroimage 24.1 (2005b): 118-131.

Babiloni, F., et al. "Improved Estimation of Human Cortical Activity and Connectivity with the Multimodal Integration of Neuroelectric and Hemodynamic Data." *Engineering in Medicine and Biology Society, 2005. IEEE-EMBS 2005. 27th Annual International Conference of the*. IEEE, 2006.

Beaulieu, Christian. "The basis of anisotropic water diffusion in the nervous system–a technical review." *NMR in Biomedicine* 15.7-8 (2002): 435-455.

Bergquist, A. J., et al. "Neuromuscular electrical stimulation: implications of the electrically evoked sensory volley." *European journal of applied physiology* 111.10 (2011): 2409-2426.

Bestmann, Sven, et al. "Mapping causal interregional influences with concurrent TMS–fMRI." *Experimental brain research* 191.4 (2008): 383-402.

Boly, Mélanie, et al. "Brain connectivity in disorders of consciousness." *Brain connectivity* 2.1 (2012): 1-10.

Bonato, C., C. Miniussi, and P. M. Rossini. "Transcranial magnetic stimulation and cortical evoked potentials: a TMS/EEG co-registration study." *Clinical Neurophysiology* 117.8 (2006): 1699-1707.

Bortoletto, Marta, et al. "The Contribution of TMS-EEG Coregistration in the Exploration of the Human Cortical Connectome." *Neuroscience & Biobehavioral Reviews* (2014).

Bozzali, Marco, et al. "White matter integrity assessed by diffusion tensor tractography in a patient with a large tumor mass but minimal clinical and neuropsychological deficits." *Functional neurology* 27.4 (2012): 239.

Brown, Harriet, Karl Friston, and Sven Bestmann. "Active inference, attention, and motor preparation." *Frontiers in psychology* 2 (2011).

Burke, David, Simon C. Gandevia, and Brian McKeon. "The afferent volleys responsible for spinal proprioceptive reflexes in man." *The Journal of physiology* 339.1 (1983): 535-552.

Carey, James R., et al. "Serial treatments of primed low-frequency rTMS in stroke: Characteristics of responders vs. nonresponders." *Restorative neurology and neuroscience* 32.2 (2014): 323-335.

Casali, Adenauer G., et al. "A theoretically based index of consciousness independent of sensory processing and behavior." Science translational medicine 5.198 (2013): 198ra105-198ra105.

Casali, Adenauer G., et al. "General indices to characterize the electrical response of the cerebral cortex to TMS." *Neuroimage* 49.2 (2010): 1459-1468.

Casula, Elias P., et al. "Low-frequency rTMS inhibitory effects in the primary motor cortex: Insights from TMS-evoked potentials." *NeuroImage* 98 (2014): 225-232.

Chen, Robert, ed. *Cortical Connectivity: Brain Stimulation for Assessing and Modulating Cortical Connectivity and Function*. Springer Science & Business Media, 2012.

Chen, Wei-Hung, et al. "Low-frequency rTMS over lateral premotor cortex induces lasting changes in regional activation and functional coupling of cortical motor areas." *Clinical Neurophysiology* 114.9 (2003): 1628-1637.

Collins, David F. "Central contributions to contractions evoked by tetanic neuromuscular electrical stimulation." *Exercise and sport sciences reviews* 35.3 (2007): 102-109.

Conturo, Thomas E., et al. "Tracking neuronal fiber pathways in the living human brain." *Proceedings of the National Academy of Sciences* 96.18 (1999): 10422-10427.

Dayan, E., Censor, N., Buch, E. R., Sandrini, M., & Cohen, L. G. (2013). Noninvasive brain stimulation: from physiology to network dynamics and back. *Nature neuroscience*, *16*(7), 838-844.

Delorme, A., & Makeig, S. (2004). EEGLAB: an open source toolbox for analysis of single-trial EEG dynamics including independent component analysis. *Journal of neuroscience methods*, *134*(1), 9-21.

Denslow, Stewart, et al. "Cortical and subcortical brain effects of transcranial magnetic stimulation (TMS)-induced movement: an interleaved TMS/functional magnetic resonance imaging study." *Biological psychiatry* 57.7 (2005): 752-760.

Di Lazzaro, V., et al. "Generation of I waves in the human: spinal recordings." *Supplements to Clinical neurophysiology* 56 (2003): 143.

Di Lazzaro, Vincenzo, and Ulf Ziemann. "The contribution of transcranial magnetic stimulation in the functional evaluation of microcircuits in human motor cortex." Frontiers in neural circuits 7 (2013).

Di Pino, G., et al. "A neurally-interfaced hand prosthesis tuned inter-hemispheric communication." *Restorative neurology and neuroscience* 30.5 (2012): 407.

Dougherty, Robert F., et al. "Functional organization of human occipital-callosal fiber tracts." *Proceedings of the National Academy of Sciences of the United States of America* 102.20 (2005): 7350-7355.

Douglas, Rodney J., Kevan AC Martin, and David Whitteridge. "A canonical microcircuit for neocortex." Neural computation 1.4 (1989): 480-488.

Driver, Jon, et al. "Concurrent brain-stimulation and neuroimaging for studies of cognition." *Trends in cognitive sciences* 13.7 (2009): 319-327.

Eichler, Michael. "A graphical approach for evaluating effective connectivity in neural systems." *Philosophical Transactions of the Royal Society of London B: Biological Sciences* 360.1457 (2005): 953-967.

Esser, S. K., et al. "A direct demonstration of cortical LTP in humans: a combined TMS/EEG study." Brain research bulletin 69.1 (2006): 86-94.

Ferrarelli, Fabio, et al. "Reduced evoked gamma oscillations in the frontal cortex in schizophrenia patients: a TMS/EEG study." *The American journal of psychiatry* 165.8 (2008): 996-1005.

Ferreri F., D. Ponzo, L. Vollero, Guerra, A, G. Di Pino, S. Petrichella, A. Benvenuto, M. Tombini, L. Rossini, L. Denaro, S. Micera, G. Iannello, E. Guglielmelli, V. Denaro, P.M. Rossini. "Does an intraneural interface short-term implant for robotic hand control modulate sensorimotor cortical integration? An EEG-TMS co-registration study on a human amputee." *Restorative neurology and neuroscience* 32, no. 2 (2014): 281-292.

Ferreri, F., Vecchio, F., Vollero, L., Guerra, A., Petrichella, S., Ponzo, D., Määttä, S., Mervaala E., Könönen, M., Ursini F., Pasqualetti P., Iannello G., Rossini P.M., & Di Lazzaro V., (2016). Sensorimotor cortex excitability and connectivity in Alzheimer's disease: A TMS-EEG Co-registration study. Human brain mapping. 37:2083–2096

Ferreri, Florinda, et al. "Human brain connectivity during single and paired pulse transcranial magnetic stimulation." *Neuroimage* 54.1 (2011): 90-102.

Ferreri, Florinda, et al. "Human brain cortical correlates of short-latency afferent inhibition: a combined EEG–TMS study." *Journal of neurophysiology* 108.1 (2012): 314-323.

Ferreri, Florinda, et al. "Motor cortex excitability in Alzheimer's disease: a transcranial magnetic stimulation study." *Annals of neurology* 53.1 (2003): 102-108.

Fletcher, E. M., C. L. Kussmaul, and G. R. Mangun. "Estimation of interpolation errors in scalp topographic mapping." *Electroencephalography and clinical neurophysiology* 98.5 (1996): 422-434.

Fox, Peter, et al. "Imaging human intra-cerebral connectivity by PET during TMS." *Neuroreport* 8.12 (1997): 2787-2791.

Friston, Karl, Jérémie Mattout, and James Kilner. "Action understanding and active inference." *Biological cybernetics* 104.1-2 (2011): 137-160.

Fuggetta, Giorgio, et al. "Acute modulation of cortical oscillatory activities during short trains of high-frequency repetitive transcranial magnetic stimulation of the human motor cortex: A combined EEG and TMS study." *Human brain mapping* 29.1 (2008): 1-13.

Fuggetta, Giorgio, et al.. "Modulation of cortical oscillatory activities induced by varying single-pulse transcranial magnetic stimulation intensity over the left primary motor area: a combined EEG and TMS study." *Neuroimage* 27.4 (2005): 896-908.

Gandolla, Marta, et al. "Re-thinking the role of motor cortex: context-sensitive motor outputs?." *NeuroImage* 91 (2014): 366-374.

Gazzaniga, Michael S. "Cerebral specialization and interhemispheric communication." *Brain* 123.7 (2000): 1293-1326.

Gerloff, Christian, et al. "Multimodal imaging of brain reorganization in motor areas of the contralesional hemisphere of well recovered patients after capsular stroke." *Brain* 129.3 (2006): 791-808.

Giambattistelli, Federica, et al. "The spontaneous fluctuation of the excitability of a single node modulates the internodes connectivity: A TMS-EEG study." Human brain mapping 35.4 (2014): 1740-1749.

Gibson, James J. *The Ecological Approach to Visual Perception: Classic Edition*. Psychology Press, 2014.

Granger, Clive WJ. "Investigating causal relations by econometric models and cross-spectral methods." *Econometrica: Journal of the Econometric Society* (1969): 424-438.

Grefkes, Christian, and Gereon R. Fink. "Reorganization of cerebral networks after stroke: new insights from neuroimaging with connectivity approaches." *Brain* (2011): awr033.

Grefkes, Christian, and Nick S. Ward. "Cortical Reorganization After Stroke How Much and How Functional?." *The Neuroscientist* 20.1 (2014): 56-70.

Grefkes, Christian, et al. "Cortical connectivity after subcortical stroke assessed with functional magnetic resonance imaging." *Annals of neurology* 63.2 (2008): 236-246.

Groppa, Sergiu, et al. "Subcortical substrates of TMS induced modulation of the cortico-cortical connectivity." *Brain stimulation* 6.2 (2013): 138-146.

Guerra, Andrea, Sara Petrichella, Luca Vollero, David Ponzo, Patrizio Pasqualetti, Sara Määttä, Esa Mervaala, Mervi Könönen; Federica Bressi; Giulio Iannello, Paolo Maria Rossini, Florinda Ferreri. "Neurophysiological features of motor cortex excitability and plasticity in Subcortical Ischemic Vascular Dementia: a TMS mapping study." *Clinical Neurophysiology* (2014).

Guerra, Andrea, et al. "Transcranial magnetic stimulation studies in Alzheimer's disease." *International Journal of Alzheimer's Disease* 2011 (2011).

Guerra, Andrea, Giuseppe Curcio, Patrizio Pasqualetti, Federica Bressi, Sara Petrichella, Federica Scrascia, David Ponzo, Mervi Könönen, Federica Bressi, Giulio Iannello, Paolo Maria Rossini, Florinda Ferreri. "Unilateral cortical hyperexcitability in congenital hydrocephalus: A TMS study." *Neurocase* 20, no. 4 (2014): 456-465.

Guillery, R. W., and S. Murray Sherman. "Thalamic relay functions and their role in corticocortical communication: generalizations from the visual system." Neuron 33.2 (2002): 163-175.

Hallett, Mark. "Transcranial magnetic stimulation: a primer." *Neuron* 55.2 (2007): 187-199.

Hamalainen, M. S., & Sarvas, J. (1989). Realistic conductivity geometry model of the human head for interpretation of neuromagnetic data. *Biomedical Engineering, IEEE Transactions on*, *36*(2), 165-171.

Hampson, Michelle, and Ralph E. Hoffman. "Transcranial magnetic stimulation and connectivity mapping: tools for studying the neural bases of brain disorders." *Frontiers in systems neuroscience* 4 (2010).

Harrison, L. M., O. David, and K. J. Friston. "Stochastic models of neuronal dynamics." *Philosophical Transactions of the Royal Society B: Biological Sciences* 360.1457 (2005): 1075-1091.

Harrison, L., William D. Penny, and Karl Friston. "Multivariate autoregressive modeling of fMRI time series." *NeuroImage* 19.4 (2003): 1477-1491.

Hatsopoulos, Nicholas G., and Aaron J. Suminski. "Sensing with the motor cortex." *Neuron* 72.3 (2011): 477-487.

He, B., Musha, T., Okamoto, Y., Homma, S., Nakajima, Y., & Sato, T. (1987). Electric dipole tracing in the brain by means of the boundary element method and its accuracy. *Biomedical Engineering, IEEE Transactions on*, (6), 406-414.

Horvath, Jared C., et al. "Transcranial magnetic stimulation: a historical evaluation and future prognosis of therapeutically relevant ethical concerns." *Journal of medical ethics* 37.3 (2011): 137-143.

Huber, Reto, et al. "Human cortical excitability increases with time awake." *Cerebral cortex* 23.2 (2013): 1-7.

Huber, Reto, et al. "Measures of cortical plasticity after transcranial paired associative stimulation predict changes in electroencephalogram slow-wave activity during subsequent sleep." *The Journal of Neuroscience* 28.31 (2008): 7911-7918.

Hummel, Friedhelm C., and Christian Gerloff. "Interregional long-range and short-range synchrony: a basis for complex sensorimotor processing." *Progress in brain research* 159 (2006): 223-236.

Ilmoniemi, Risto J., and Dubravko Kičić. "Methodology for combined TMS and EEG." *Brain topography* 22.4 (2010): 233-248.

Ilmoniemi, Risto J., et al. "Neuronal responses to magnetic stimulation reveal cortical reactivity and connectivity." *Neuroreport* 8.16 (1997): 3537-3540.

Innocenti, Giorgio M. "General organization of callosal connections in the cerebral cortex." *Sensory-motor areas and aspects of cortical connectivity*. Springer US, 1986. 291-353.

Iramina, Keiji, et al. "Effects of transcranial magnetic stimulation on EEG activity." *Magnetics, IEEE Transactions on* 38.5 (2002): 3347-3349.

Iwahashi, M., et al. "Differences in evoked EEG by transcranial magnetic stimulation at various stimulus points on the head." *Engineering in Medicine and Biology Society, 2008. EMBS 2008. 30th Annual International Conference of the IEEE*. IEEE, 2008.

Jacobs KM, Donoghue JP. (1991). Reshaping the cortical motor map by unmasking latent intracortical connections. *Science*, *251*(4996), 944-7

Johnson, Jeffrey S., et al. "Task-dependent changes in cortical excitability and effective connectivity: a combined TMS-EEG study." *Journal of neurophysiology* 107.9 (2012): 2383-2392.

Julkunen, Petro, et al. "Combining transcranial magnetic stimulation and electroencephalography may contribute to assess the severity of Alzheimer's disease." *International Journal of Alzheimer's Disease* 2011 (2011).

Julkunen, Petro, et al. "Navigated TMS combined with EEG in mild cognitive impairment and Alzheimer's disease: a pilot study." *Journal of Neuroscience Methods* 172.2 (2008): 270-276.

Kahkonen, S., et al. "Alcohol reduces prefrontal cortical excitability in humans: a combined TMS and EEG study." Neuropsychopharmacology 28.4 (2003): 747-754.

Kähkönen, Seppo, et al. "Distinct differences in cortical reactivity of motor and prefrontal cortices to magnetic stimulation." Clinical Neurophysiology 115.3 (2004): 583-588.

Kähkönen, Seppo, et al. "Prefrontal transcranial magnetic stimulation produces intensity-dependent EEG responses in humans." Neuroimage 24.4 (2005): 955-960.

Kandel, Eric R. "The brain and behavior." *Principles of neural science* 4 (2000).

Keller, Corey J., et al. "Mapping human brain networks with cortico-cortical evoked potentials." *Philosophical Transactions of the Royal Society B: Biological Sciences* 369.1653 (2014): 20130528.

KIM, DAE-SHIK, and MINA KIM. "Combining functional and diffusion tensor MRI." *Annals of the New York Academy of Sciences* 1064.1 (2005): 1-15.

Kitajo, K., Hanakawa, T., Ilmoniemi, R. J., & Miniussi, C. (2015). A contemporary research topic: manipulative approaches to human brain dynamics. *Frontiers in human neuroscience*, *9*.

Klimesch, Wolfgang, Paul Sauseng, and Simon Hanslmayr. "EEG alpha oscillations: the inhibition–timing hypothesis." *Brain research reviews* 53.1 (2007): 63-88.

Koch, Martin A., David G. Norris, and Margret Hund-Georgiadis. "An investigation of functional and anatomical connectivity using magnetic resonance imaging." *Neuroimage* 16.1 (2002): 241-250.

Komssi, S., & Kähkönen, S. (2006). The novelty value of the combined use of electroencephalography and transcranial magnetic stimulation for neuroscience research. *Brain research reviews*, *52*(1), 183-192.

Kujirai, T., et al. "Corticocortical inhibition in human motor cortex." *The Journal of physiology* 471.1 (1993): 501-519.

Le Bihan, Denis, et al. "Diffusion tensor imaging: concepts and applications." *Journal of magnetic resonance imaging* 13.4 (2001): 534-546.

Le Bihan, Denis. "Looking into the functional architecture of the brain with diffusion MRI." *Nature Reviews Neuroscience* 4.6 (2003): 469-480.

Leis, A. Arturo, et al. "Control of Ia afferent input to triceps surae (soleus) locomotor nucleus precedes agonist muscle activation during gait." *Journal of Electromyography and Kinesiology* 5.2 (1995): 95-100.

Levit-Binnun, Nava, et al. "Differences in TMS-evoked responses between schizophrenia patients and healthy controls can be observed without a dedicated EEG system." *Clinical Neurophysiology* 121.3 (2010): 332-339.

Liew, Sook-Lei, et al. "Non-invasive brain stimulation in neurorehabilitation: local and distant effects for motor recovery." *Frontiers in human neuroscience* 8 (2014).

Lioumis, Pantelis, et al. "Reproducibility of TMS—Evoked EEG responses." Human brain mapping 30.4 (2009): 1387-1396.

List, Jonathan, et al. "Relationship between excitability, plasticity and thickness of the motor cortex in older adults." *Neuroimage* 83 (2013): 809-816.

Litvak, Vladimir, et al. "Artifact correction and source analysis of early electroencephalographic responses evoked by transcranial magnetic stimulation over primary motor cortex." *Neuroimage* 37.1 (2007): 56-70.

Lowe, S. L., et al. "Ante mortem cerebral amino acid concentrations indicate selective degeneration of glutamate-enriched neurons in Alzheimer's disease." *Neuroscience* 38.3 (1990): 571-577.

Lowe, S. L., et al. "Gamma-aminobutyric acid concentration in brain tissue at two stages of Alzheimer's disease." *Brain* 111.4 (1988): 785-799.

Mäki, Hanna, and Risto J. Ilmoniemi. "The relationship between peripheral and early cortical activation induced by transcranial magnetic stimulation." *Neuroscience letters* 478.1 (2010): 24-28.

Massimini, M., et al. "Cortical reactivity and effective connectivity during REM sleep in humans." *Cognitive neuroscience* 1.3 (2010): 176-183.

Massimini, M., G. Tononi, and R. Huber. "Slow waves, synaptic plasticity and information processing: insights from transcranial magnetic stimulation and high-density EEG experiments." *European Journal of Neuroscience* 29.9 (2009): 1761-1770.

Massimini, Marcello, et al. "Breakdown of cortical effective connectivity during sleep." *Science* 309.5744 (2005): 2228-2232.

Massimini, Marcello, et al. "Triggering sleep slow waves by transcranial magnetic stimulation." *Proceedings of the National Academy of Sciences* 104.20 (2007): 8496-8501.

Mäki, Hanna, and Risto J. Ilmoniemi. "The relationship between peripheral and early cortical activation induced by transcranial magnetic stimulation." *Neuroscience letters* 478.1 (2010): 24-28.

Miniussi, Carlo, and Gregor Thut. "Combining TMS and EEG offers new prospects in cognitive neuroscience." *Brain topography* 22.4 (2010): 249-256.

Miniussi, Carlo, and Paolo Maria Rossini. "Transcranial magnetic stimulation in cognitive rehabilitation." *Neuropsychological rehabilitation* 21.5 (2011): 579-601.

Miniussi, Carlo, et al. "Efficacy of repetitive transcranial magnetic stimulation/transcranial direct current stimulation in cognitive neurorehabilitation." *Brain Stimulation* 1.4 (2008): 326-336.

Miniussi, Carlo, Justin A. Harris, and Manuela Ruzzoli. "Modelling non-invasive brain stimulation in cognitive neuroscience." *Neuroscience & Biobehavioral Reviews* 37.8 (2013): 1702-1712.

Moseley, Michael E., et al. "Diffusion-weighted MR imaging of anisotropic water diffusion in cat central nervous system." *Radiology* 176.2 (1990): 439-445.

Murphy, M., Riedner, B. A., Huber, R., Massimini, M., Ferrarelli, F., & Tononi, G. (2009). Source modeling sleep slow waves. *Proceedings of the National Academy of Sciences*, *106*(5), 1608-1613.

Nägga, Katarina, N. Bogdanovic, and Jan Marcusson. "GABA transporters (GAT-1) in Alzheimer's disease." *Journal of neural transmission* 106.11-12 (1999): 1141-1149.

Nardone, R., et al. "Transcranial magnetic stimulation (TMS)/repetitive TMS in mild cognitive impairment and Alzheimer's disease." *Acta Neurologica Scandinavica* 129.6 (2014): 351-366.

Nikouline, V., Jarmo Ruohonen, and Risto J. Ilmoniemi. "The role of the coil click in TMS assessed with simultaneous EEG." Clinical Neurophysiology 110.8 (1999): 1325-1328.

Niskanen, Eini, et al. "New insights into Alzheimer's disease progression: a combined TMS and structural MRI study." *PLoS One* 6.10 (2011): e26113.

Ohyama, Masashi, et al. "Preserved benzodiazepine receptors in Alzheimer's disease measured with C-11 flumazenil PET and I-123 iomazenil SPECT in comparison with CBF." *Annals of nuclear medicine* 13.5 (1999): 309-315.

Pallanti, S., and A. Marras. "Transcranial Magnetic Stimulation in Alzheimer's Disease: A Review of Investigational and Therapeutic Findings." *J Alzheimers Dis Parkinsonism* 5.187 (2015): 2161-0460.

Paradiso, Michael A., Mark F. Bear, and Barry W. Connors. "Neuroscience: exploring the brain." *Hagerstwon, MD: Lippincott Williams & Wilkins* (2007): 718.

Pascual-Leone, Alvaro, et al. "Characterizing brain cortical plasticity and network dynamics across the age-span in health and disease with TMS-EEG and TMS-fMRI." *Brain topography* 24.3-4 (2011): 302-315.

Paus, T., P. K. Sipila, and A. P. Strafella. "Synchronization of neuronal activity in the human primary motor cortex by transcranial magnetic stimulation: an EEG study." *Journal of Neurophysiology* 86.4 (2001): 1983-1990.

Paus, Tomáš. "Inferring causality in brain images: a perturbation approach." *Philosophical Transactions of the Royal Society B: Biological Sciences* 360.1457 (2005): 1109-1114.

Pellegrino, G., et al. "Inter-hemispheric coupling changes associate with motor improvements after robotic stroke rehabilitation." *rehabilitation* 2 (2012): 3.

Pennisi, Giovanni, et al. "Transcranial magnetic stimulation in Alzheimer's disease: a neurophysiological marker of cortical hyperexcitability." *Journal of neural transmission* 118.4 (2011): 587-598.

Penny, Will, Zoubin Ghahramani, and Karl Friston. "Bilinear dynamical systems." *Philosophical Transactions of the Royal Society of London B: Biological Sciences* 360.1457 (2005): 983-993.

Pepin, Jean Louis, et al. "Motor cortex inhibition is not impaired in patients with Alzheimer's disease: evidence from paired transcranial magnetic stimulation." *Journal of the neurological sciences* 170.2 (1999): 119-123.

Petrichella, S., Johnson Nessa, He Bin, "The Influence of Corticospinal Activity on TMS-Evoked Activity and Connectivity in Healthy Subjects: A TMS-EEG Study''. *Plos One, 2017.*

Petrichella S., Vollero L., Ferreri F., Guerra A., Määtta, S., Könönen M., Di Lazzaro V., Iannello G., Channel interpolation in TMS EEG: a quantitative study towards an accurate topographical representation, *38th Annual International Conference of the IEEE Engineering in Medicine and Biology Society (EMBC'16)*, Orlando, Florida, USA on August 17-20.

Petrichella, Sara, Vollero L., Ferreri F., Di Lazzaro V., Iannello G. "TRS-TMS: An EEGLAB plugin for the reconstruction of onsets in EEG-TMS datasets." *Bioinformatics and Bioengineering (BIBE), 2013 IEEE 13th International Conference on*. IEEE, 2013.

Pfefferbaum, Adolf, Elfar Adalsteinsson, and Edith V. Sullivan. "Replicability of diffusion tensor imaging measurements of fractional anisotropy and trace in brain." *Journal of Magnetic Resonance Imaging* 18.4 (2003): 427-433.

Rogasch, Nigel C., and Paul B. Fitzgerald. "Assessing cortical network properties using TMS–EEG." *Human brain mapping* 34.7 (2013): 1652-1669.

Rosanova, Mario, et al. "Natural frequencies of human corticothalamic circuits." *The Journal of Neuroscience* 29.24 (2009): 7679-7685.

Rossini, P. M., et al. "Non-invasive electrical and magnetic stimulation of the brain, spinal cord, roots and peripheral nerves: Basic principles and procedures for routine clinical and research application. An updated report from an IFCN Committee." *Clinical Neurophysiology* 126.6 (2015): 1071-1107.

Rossini, Paolo M., et al. "Double nerve intraneural interface implant on a human amputee for robotic hand control." *Clinical neurophysiology* 121.5 (2010): 777-783.

S. Luck & E. Kappenman (2008). *Oxford Handbook of Event-Related Potential Components*. New York, Oxford University Press

Sack, Alexander T., et al. "Optimizing functional accuracy of TMS in cognitive studies: a comparison of methods." *Journal of Cognitive Neuroscience* 21.2 (2009): 207-221.

Sandrini, Marco, Carlo Umiltà, and Elena Rusconi. "The use of transcranial magnetic stimulation in cognitive neuroscience: a new synthesis of methodological issues." *Neuroscience & Biobehavioral Reviews* 35.3 (2011): 516-536.

Sarasso, Simone, et al. "Quantifying cortical EEG responses to TMS in (un) consciousness." *Clinical EEG and neuroscience* 45.1 (2014): 40-49.

Sato, Sumire, Til Ole Bergmann, and Michael R. Borich. "Opportunities for concurrent transcranial magnetic stimulation and electroencephalography to characterize cortical activity in stroke." *Frontiers in human neuroscience* 9 (2015).

Schulz, Hannah, et al. "Now I am ready—now I am not: the influence of pre-TMS oscillations and corticomuscular coherence on motor-evoked potentials." *Cerebral cortex* 24.7 (2014): 1708-1719.

Scola, Elisa, et al. "A diffusion tensor MRI study of patients with MCI and AD with a 2-year clinical follow-up." *Journal of Neurology, Neurosurgery & Psychiatry* 81.7 (2010): 798-805.

Shafi, Mouhsin M., et al. "Exploration and modulation of brain network interactions with noninvasive brain stimulation in combination with neuroimaging." *European Journal of Neuroscience* 35.6 (2012): 805-825.

Siebner, Hartwig R., et al. "Consensus paper: combining transcranial stimulation with neuroimaging." *Brain stimulation* 2.2 (2009): 58-80.

Skudlarski, Pawel, et al. "Measuring brain connectivity: diffusion tensor imaging validates resting state temporal correlations." Neuroimage 43.3 (2008): 554-561.

Soekadar, Surjo R., et al. "Brain–machine interfaces in neurorehabilitation of stroke." *Neurobiology of disease* (2014).

Soekadar, Surjo R., Niels Birbaumer, and Leonardo G. Cohen. "Brain–computer interfaces in the rehabilitation of stroke and neurotrauma." *Systems neuroscience and rehabilitation*. Springer Japan, 2011. 3-18.

Speer, Andrew M., et al. "Intensity-dependent regional cerebral blood flow during 1-Hz repetitive transcranial magnetic stimulation (rTMS) in healthy volunteers studied with H 2 15 O positron emission tomography: I. Effects of primary motor cortex rTMS." *Biological psychiatry* 54.8 (2003): 818-825.

Stančák, Andrej, Carl H. Lücking, and Rumyana Kristeva-Feige. "The size of corpus callosum and functional connectivities of cortical regions in finger and shoulder movements." *Cognitive brain research* 13.1 (2002): 61-74.

Tallon-Baudry, Catherine, et al. "Stimulus specificity of phase-locked and non-phase-locked 40 Hz visual responses in human." *The Journal of Neuroscience* 16.13 (1996): 4240-4249.

Thut, G., et al. "Effects of single-pulse transcranial magnetic stimulation (TMS) on functional brain activity: a combined event-related TMS and evoked potential study." *Clinical neurophysiology* 114.11 (2003): 2071-2080.

Thut, Gregor, and Alvaro Pascual-Leone. "A review of combined TMS-EEG studies to characterize lasting effects of repetitive TMS and assess their usefulness in cognitive and clinical neuroscience." *Brain topography* 22.4 (2010): 219-232.

Thut, Gregor, and Alvaro Pascual-Leone. "Integrating TMS with EEG: How and what for?." *Brain topography* 22.4 (2010): 215-218.

Tiitinen, Hannu, et al. "Separation of contamination caused by coil clicks from responses elicited by transcranial magnetic stimulation." Clinical neurophysiology 110.5 (1999): 982-985.

Tombini, Mario, et al. "Combined analysis of cortical (EEG) and nerve stump signals improves robotic hand control." *Neurorehabilitation and neural repair* 26.3 (2012): 275-281.

Vollero, Luca, Sara Petrichella, and Giulio Innello. "Optimal weighted averaging of event related activity from acquisitions with artifacts." *38th Annual International Conference of the IEEE Engineering in Medicine and Biology Society (EMBC'16)*, Orlando, Florida, USA on August 17-20.

Wagner, Timothy, Antoni Valero-Cabre, and Alvaro Pascual-Leone. "Noninvasive human brain stimulation." *Annu. Rev. Biomed. Eng.* 9 (2007): 527-565.

Wahl, Mathias, et al. "Human motor corpus callosum: topography, somatotopy, and link between microstructure and function." *The Journal of neuroscience* 27.45 (2007): 12132-12138.

Ward, Nick. "Assessment of cortical reorganisation for hand function after stroke." *The Journal of physiology* 589.23 (2011): 5625-5632.

Wilke, C., Ding, L., & He, B. (2008). Estimation of time-varying connectivity patterns through the use of an adaptive directed transfer function. *Biomedical Engineering, IEEE Transactions on*, *55*(11), 2557-2564.

Wokke, M. E., Talsma, L. J., & Vissers, M. E. (2014). Biasing neural network dynamics using non-invasive brain stimulation. *Frontiers in systems neuroscience*, *8*.

Wolpert, Daniel M., Zoubin Ghahramani, and Michael I. Jordan. "An internal model for sensorimotor integration." *Science-AAAS-Weekly Paper Edition* 269.5232 (1995): 1880-1882.

Zanon, Marco, et al. "Cortical connections between dorsal and ventral visual streams in humans: evidence by TMS/EEG co-registration." *Brain topography* 22.4 (2010): 307-317.

Zanon, Marco, et al. "Long-range neural activity evoked by premotor cortex stimulation: a TMS/EEG co-registration study." *Frontiers in human neuroscience* 7 (2013).

Ziemann, U. "Non-invasive brain stimulation and brain plasticity." *the 6th International Symposium on Navigated Brain Stimulation in Neurosurgery*. 2014.

Ziemann, U. L. F., John C. Rothwell, and Michael C. Ridding. "Interaction between intracortical inhibition and facilitation in human motor cortex." *The Journal of physiology* 496.3 (1996): 873-881.

Ziemann, Ulf. "Transcranial magnetic stimulation at the interface with other techniques a powerful tool for studying the human cortex." *The Neuroscientist* 17.4 (2011): 368-381.